



University
of Glasgow

Al-Budairi, Hassan Dakhil (2012) *Design and analysis of ultrasonic horns operating in longitudinal and torsional vibration*. PhD thesis.

<http://theses.gla.ac.uk/3851/>

Copyright and moral rights for this thesis are retained by the author

A copy can be downloaded for personal non-commercial research or study, without prior permission or charge

This thesis cannot be reproduced or quoted extensively from without first obtaining permission in writing from the Author

The content must not be changed in any way or sold commercially in any format or medium without the formal permission of the Author

When referring to this work, full bibliographic details including the author, title, awarding institution and date of the thesis must be given

**DESIGN AND ANALYSIS OF ULTRASONIC
HORNS OPERATING IN LONGITUDINAL AND
TORSIONAL VIBRATION**

Hassan Dakhil Al-Budairi

A thesis for the degree of Doctor of Philosophy (PhD)

Submitted to the School of Engineering,
College of Science and Engineering,
University of Glasgow

December 2012

DECLARATION

I declare that this thesis is a record of the original work carried out by myself under the supervision of Prof. Margaret Lucas in the School of Engineering at the University of Glasgow, United Kingdom, during the period of April 2009 to August 2012. The copyright of this thesis therefore belongs to the author under the terms of the United Kingdom Copyright acts. Due acknowledgement must always be made of the use of any material contained in, or derived from, this thesis. The thesis has not been presented elsewhere in consideration for a higher degree.

Signature _____

Printed name __Mr. Hassan Dakhil Al-Budairi __

Signature _____

Printed name _Prof. Margaret Lucas _____

I. Abstract

Combining modes of vibration, such as longitudinal and torsional vibration, is advantageous in many ultrasonic applications such as ultrasonic drilling, welding, and motors. In this work we present a novel approach to the design a longitudinal-torsional (LT) ultrasonic horn which adapts the front mass in a traditional Langevin transducer. Different approaches, such as degeneration of longitudinal vibration and coupling between longitudinal (L) and torsional (T) modes, have been used to generate the LT mode of vibration. The degeneration approach creates a non-uniform section, by cutting and twisting a number of slots along the path of the L wave such that part of the wave converts into T wave whilst the remaining part propagates unchanged through the section; these two parts are recombined near the output surface to form LT vibration. The mode coupling approach uses two set of vibration generators, usually piezoelectric elements, where one set generates L vibration whilst the second set generates T vibration. An exponential cross-sectional horn uses to combine the two modes where the area reduction factor is selected such that these modes resonate at the same frequency. However, many limitations prevent the wide usage of these methods in ultrasonic applications. These limitations are the complex design and excitation, possible coupling with surrounding modes, instability in operating at different boundaries, difficulty in securing the structure without influencing the vibrational response and the low produced torsionality, which is the ratio of torsional to longitudinal response at the output face.

The new approach is based on combining the principles of these methods to overcome the previously stated limitations, the slotting technique is incorporated into the exponential cross-sectional path and the horn produced is utilised as the front mass of a Langevin transducer. A set of design and performance criteria are used to optimise the transducer and includes applicable design; methods of securing the transducer; and the excitation features of LT transducer such that it can operate without the effects of surrounding modes of vibration and can produce high response and torsionality at the output surface. A methodology which combines mathematical and experimental modelling is used to optimise LT transducer design. The mathematical modelling, which includes finite element (FE) and analytical methods, is performed to optimise the geometry and to predict electromechanical parameters, modal parameters and the dynamic behaviour of LT transducer. The experimental modelling is used to validate the mathematical results and to characterise the fabricated prototypes under different operating conditions.

The dimensions of the initial design of the L mode Langevin transducer are derived from the principles of the wave equation. This transducer has a set of piezoceramic components sandwich between a cylindrical back mass and an exponential front mass connected by a pre-stressed bolt. The dimensions are used to create the FE model, using the FE software package ABAQUS, where different shapes of cut at different dimensions and at various angle of twist along the front mass are introduced and examined by a modal analysis procedure to the front mass. An optimised model is then utilised in a size scaling study to confirm the suitability of using this approach for different ultrasonic applications.

The dimensions of the optimised design are also used in the analytical study, based on Mason's electric equivalent circuit approach, to predict the electromechanical parameters where a one-dimensional equivalent circuit approach is created separately for each part whilst the combination vibrational motion in the front mass is represented by two, longitudinal and torsional, equivalent circuits. The complete equivalent network of the LT transducer is then solved using the mathematical software package MATHEMATICA. The analytical model is also extended to validate some of particular FE findings such as the distribution of the response amplitude and the location of the longitudinal nodal plane along the transducer's structure.

Two optimised models of different sizes are fabricated and characterised through different testing techniques including electrical impedance analysis, experimental modal analysis (EMA) and experimental harmonic analysis. Optimisation of the pre-stressing of the transducer is performed by applying different torques to the pre-stressed bolt and measuring the electrical impedance spectra where the results are compared to analytical findings. EMA is then used to describe the natural characteristics of the structures where the results are used to accurately extract the modal parameters and to validate the predictions of the FE and analytical model. Different levels of harmonic excitation are used to characterise the fabricated prototypes where the results are compared to the findings of the mathematical modelling.

A case study of the design of the LT drill is presented to validate the design approach for real ultrasonic applications. A similar methodology is applied and the resulting LT drill is tested for both unloaded and loaded operating conditions. The results obtained show that this new approach can be easily and successfully applied to ultrasonic applications to produce a torsional to longitudinal amplitude response of 0.8 which is measured on a fabricated prototype.

II. Acknowledgments

First of all, I would like to express my gratitude to Allah (God) for providing me the blessings to complete this work. Then, I am truly indebted and thankful to the following colleagues, friends and family who have contributed their advice and support towards the development of this research.

I would like to express my special thanks of gratitude to my supervisor, Professor Margaret Lucas, who gave me this great opportunity to discover the amassing ultrasonic world. She continuously encouraged and challenged me through my research programme and never accepted less than my best efforts that enabled me to know more and more about so many things.

The Iraqi Ministry of Higher Education and Scientific Research, for funding this research.

The members of Dynamics Group, in particularly Dr. Patrick Harkness, for giving me their precious time, generous friendship and kind feedback throughout the years of study.

The technical staff, Mr. Brain Robb and his colleagues, for their expertise, extensive help and assistance in the workshop and their kindness and patience concerning my many job requests.

Staff at the School of Engineering, University of Glasgow, for their assistance, help and accommodating my demanding needs on resources throughout my studies.

Most especially to my big family, my lovely mother, father and brothers, and to my small family, my wonderful wife Alyaa and my little angel, Sama, for their understanding and support. Words alone cannot express what I owe them for their encouragement and patient love that inspired me to complete this work.

III. Table of contents

I. Abstract.....	v
II. Acknowledgments	vii
III. Table of contents	viii
IV. List of table captions.....	xiii
V. List of figure captions	xiii
VI. List of symbols.....	xix
VII. Abbreviations.....	xxi
Chapter 1 Introduction	1
1.1 Generating of ultrasonic waves.....	2
1.2 Ultrasonic transducers.....	4
1.3 Modes of vibration	7
1.3.1 Longitudinal –torsional mode of vibration	8
1.3.1.1 Degeneration of longitudinal vibration approach	8
1.3.1.2 Coupling between longitudinal and torsional modes approach	9
1.4 Objectives.....	10
1.5 The research goals.....	11
1.6 Scope of work	11
Chapter 2 Literature review	13
2.1 Background	13
2.2 Introduction to LT mode of vibration	13
2.3 Producing of LT vibration.....	14
2.4 Application of LT vibration	17
2.4.1 Ultrasonic welding	18
2.4.2 Ultrasonic motors	18
2.4.3 Ultrasonic rock drilling	20
2.4.4 Ultrasonic dissection	21
2.4.5 Other applications	21

2.5 Modelling of LT Ultrasonic vibration.....	22
2.6 Analytical modelling method.....	22
2.7 Numerical modelling methods.....	24
2.8 Conclusions.....	24
 Chapter 3 Transducer design and numerical modelling.....	 26
3.1. Introduction.....	26
3.2. Design parameters of power ultrasonic transducers.....	27
3.2.1. Driving frequency and wavelength.....	27
3.2.2. Selection of piezoelectric components.....	29
3.2.3. Selection of metal parts.....	30
3.2.4. Transducer securing feature.....	31
3.3. Performance criteria.....	31
3.3.1. Frequency separation between vibrational modes.....	32
3.3.2. Torsionality.....	32
3.3.3. Characteristic frequencies.....	32
3.3.4. Electrical input power.....	33
3.3.5. Mechanical output power.....	33
3.3.6. Coupling factor.....	34
3.3.7. Mechanical quality factor.....	34
3.4. Design of a longitudinal-torsional transducer.....	35
3.4.1. Experimental tensile test.....	37
3.4.2. Addition of slots to the front mass.....	40
3.5. Numerical modelling of the LT transducer.....	41
3.5.1. Definition of material properties.....	42
3.5.2. Defining of metal materials.....	42
3.5.3. Defining of piezoceramic materials.....	42
3.5.3.1. Elasticity of piezoelectric material.....	44
3.5.3.2. Piezoelectric properties of the piezoelectric material.....	46
3.5.3.3. Permittivity of the piezoelectric material.....	48
3.5.4. Discretisation of the domain.....	51
3.5.5. Create analysis steps.....	52
3.5.6. Interaction between parts.....	52

3.5.7. Imposing boundary conditions	54
3.5.8. Preloading the transducer	54
3.5.9. Solving the system's equations	55
3.5.10. Post processing the solution	56
3.6. Frequency extraction procedure	56
3.7. Dynamic analysis procedure	61
3.8. Electrical analysis procedure.....	62
3.9. Generalisation of transducer design	62
3.10. Summary	64
 Chapter 4 Analytical modelling of LT transducer	 65
4.1 Introduction	65
4.2 Theory of wave motion in an elastic solid	66
4.2.1 Theory of one-dimensional wave propagation.....	67
4.2.2 Higher order wave equation	69
4.2.3 Solution of the one-dimensional wave equation	69
4.3 General wave equation and equivalent circuit approach.....	72
4.4 Alternative equivalents models	77
4.5 Equivalent circuit of longitudinal-torsional (LT) Transducer circuit	77
4.5.1 Exponential slotted section	81
4.6 Piezoceramic transducer losses	95
4.7 Modelling of pre-stress effect	97
4.8 Modelling of external loads	97
4.9 Mathematica script	98
4.10 Summary	99
 Chapter 5 Experimental analysis and results	 100
5.1 Introduction	100
5.2 Fabrication of LT transducer.....	102
5.2.1 Preparation of transducer parts.....	103
5.2.2 Assembly of transducer parts	104
5.3 Pre-loading of LT transducers.....	105
5.4 Experimental analysis of fabricated transducers.....	108

5.4.1 Electrical impedance analysis	108
5.4.1.1 Evaluation of FE model	110
5.4.1.2 Evaluation of the analytical model.....	111
5.4.2 Experimental modal analysis	114
5.4.2.1 Excitation signals	115
5.4.2.2 Boundary conditions	115
5.4.2.3 Measurement instruments	116
5.4.2.4 Data processing	116
5.4.2.5 FRF curve fitting	118
5.4.3 Evaluation of FE model for transducer 1	118
5.4.4 Evaluation of the FE model for transducer 2	120
5.5 Evaluation of the analytical model for transducer 1	121
5.6 Power harmonic analysis	124
5.7 Evaluation of the analytical model.....	127
5.8 Dynamic evaluation of the analytical and FE models.....	128
5.9 Summary	130
 Chapter 6 Case study: design of LT ultrasonic drill	 132
6.1 Introduction	132
6.2 FE model of LT drill	133
6.3 Analytical model of LT drill	135
6.4 Evaluation the analytical model of LT drill	136
6.5 Evaluation of the FE model of the LT drill.....	137
6.6 Power harmonic characterisation	138
6.6.1 Free boundary condition	138
6.6.2 Load boundary condition	139
6.7 Conclusions	141
 Chapter 7 Conclusions and suggestions for future work	 142
7.1 Conclusions	142
7.2 Suggestions for future work	144
7.2.1 Design a driving system and investigate the effect of excitation method on LT drill performance.....	144

7.2.2 Design of the LT drill bit144

7.2.3 Investigate other LT ultrasonic applications144

Appendix I: Publications.....146

Appendix II: References147

IV. List of table captions

Table 1-1 Comparison between magnetostrictive and piezoelectric transducers.	6
Table 3-1 Properties of the recommended materials[73].	31
Table 3-2 Dimensions of piezoceramic components.	36
Table 3-3 Experimental results for the modulus of elasticity.	38
Table 3-4 Materials properties of the transducer parts.	38
Table 3-5 Conversion of matrix to tensor notation.	44
Table 3-6 Piezoelectric material data conversion sheet for Sonox P8.	49
Table 3-7 Piezoelectric material data conversion sheet for PIC 181.	50
Table 3-8 Dimensions for the profiles of the cuts.	57
Table 4-1 Acoustical impedance of back mass and bolt section of region 2.	79
Table 4-2 Equivalent acoustical impedances of different assumptions for region 2.	79
Table 5-1 Dimensions of fabricated transducers.	103
Table 5-2 Pre-stressing calculations of transducer 1.	107
Table 5-3 Pre-stressing calculation of transducer 2.	107
Table 5-4 Analytical and experimental data of transducers 1 and 2.	113
Table 6.1 FE predicting of modes of vibration for LT drill.	134

V. List of figure captions

Figure 1-1 Classification and applications of sound waves over a typical ranges of frequencies [4].	2
Figure 1-2 Magnetostrictive effect (left) and the inverse magnetostrictive effect (right) [7, 8].	3
Figure 1-3 Direct piezoelectric effect (left) and the inverse piezoelectric effect (right) [11].	4

Figure 1-4 Conventional Langevin transducer [12].	5
Figure 1-5 Mode shapes, from a finite element model of a rod.	7
Figure 1-6 Schematic of the degeneration of L vibration approach in a sandwich transducer.	9
Figure 1-7 Schematic of the coupling between modes approach in a sandwich transducer.	10
Figure 2-1 A longitudinal-torsional stepped waveguide (left) and its oscillation amplitude (referred as 2ξ) in micrometres as a function of frequency in kilocycles per second (right) [17].	15
Figure 2-2 Principles of traveling waves in an ultrasonic motor [44].	19
Figure 2-3 Principles of longitudinal-torsional ultrasonic motor [45].	19
Figure 3-1 The principle of half wavelength synthesis [13].	29
Figure 3-2 Variation of admittance magnitude and phase angle with frequency [13].	33
Figure 3-3 Variation of resonance frequencies of longitudinal transducer with the modulus of elasticity of the back mass material.	37
Figure 3-4 Tensile test specimen (left) and Tensile test setup (right).	38
Figure 3-5 Profile of the front mass.	40
Figure 3-6 Initial model of the ultrasonic transducer.	41
Figure 3-7 Extension and shear deformation of isotropic material	43
Figure 3-8 Extension and shear deformation of anisotropic material[80].	43
Figure 3-9 Meshing technique for transducer model.	52
Figure 3-10 Multi contact nodes.	53
Figure 3-11 Preloading the bolt.	55
Figure 3-12 Resonance frequency reduction for different pre-stress bias.	55
Figure 3-13 Different slotted cross-sections from (a) rectangular, (b) trapezoidal and (c) quarter circle cuts.	57
Figure 3-14 Convergence of resonance frequencies and the size of the output file for a different number of elements.	58
Figure 3-15 Frequency spacing and torsionality of a rectangular cut for different depths of cut.	60
Figure 3-16 Frequency spacing and torsionality of a trapezoidal cut for different depths of cut.	60

Figure 3-17 Frequency spacing and torsionality of a quarter circle cut for different depths of cut.	61
Figure 3-18 Dimensions of the optimum transducer model relative to the piezoceramic thickness.	63
Figure 3-19 Torsionality for different sizes of transducers.	64
Figure 3-20 Frequency spacing ratio of LT-F and LT-T modes for different sizes of transducer.	64
Figure 4-1 Normal stresses acting on a differential element of a uniform rod.	68
Figure 4-2 Reflection and transmission at an interface between different mediums.	71
Figure 4-3 Analogue of uniform cross-section of acoustical structure to equivalent T-circuit of one-dimensional acoustic wave.	73
Figure 4-4 Analogue of exponential cross-section of acoustical structure to equivalent T-circuit of one-dimensional acoustic wave.	75
Figure 4-5 Mason equivalent circuit of a piezoelectric disc operation in the thickness mode.	76
Figure 4-6 Schematic representation of the piezoelectric transducer and the different regions.	78
Figure 4-7 Representation of forces and torsional moment directions (a) and a cross-sectional area (b) of the slotted section (region 5).	82
Figure 4-8 Variation of the torsional conversion coefficient along the axial direction of the horn.	84
Figure 4-9 Variation of torsional conversion coefficient with helix angle and position.	85
Figure 4-10 The complete equivalent network of the transducer based on Mason's model.	87
Figure 4-11 Simplifying the left side of the equivalent network.	89
Figure 4-12 Simplifying the right side of the equivalent network.	91
Figure 4-13 The equivalent network after simplification.	92
Figure 4-14 Transfer the total acoustical impedance to the electrical branch.	93
Figure 4-15 The current loops of the equivalent network.	94
Figure 4-16 Current loops analysis of the L-circuit.	94
Figure 4-17 Current loops analysis of the T-circuit.	95

Figure 4-18 Flowchart for computing the equivalent network of the transducer.	98
Figure 5-1 Validation and updating of finite element model.	102
Figure 5-2 Components of transducer 1.	104
Figure 5-3 Components of transducer 2.	104
Figure 5-4 Exploded schematic of transducer assembling.	105
Figure 5-5 Preload setup of transducer 1.	109
Figure 5-6 Agilent 4294A Impedance analyser.	109
Figure 5-7 Experimental electrical impedance magnitude of transducer 1 for different applied torque.	110
Figure 5-8 Experimental electrical impedance magnitude of transducer 2 for different applied torque.	110
Figure 5-9 F_r , F_a and k_{eff} of transducer 1 for different applied torques.	110
Figure 5-10 F_r , F_a and k_{eff} of transducer 2 for different applied torques.	110
Figure 5-11 Experimental and FE impedance spectra magnitude (left) and the phase diagram (right) for transducer 1.	111
Figure 5-12 Experimental and analytical impedance spectra magnitude (left) and the phase diagram (right) for transducer 1.	112
Figure 5-13 Experimental and analytical impedance spectra magnitude (left) and the phase diagram (right) for transducer 2.	112
Figure 5-14 Experimental and corrected analytical impedance spectra magnitude (left) and the phase diagram (right) for transducer 1.	113
Figure 5-15 Experimental and corrected analytical impedance spectra magnitude (left) and the phase diagram (right) for transducer 2.	114
Figure 5-16 Corrected analytical and FE prediction of LT frequencies for different sizes of transducer, resonance frequency (left) and anti-resonance frequency (right).	114
Figure 5-17 EMA setup for transducer 1 (left) and grid points along the transducer (right).	119
Figure 5-18 Normalised modal peaks functions of EMA for transducer 1.	119
Figure 5.19: Normalised mode shapes of EMA and FE of transducer 1.	120
Figure 5-20 Normalised modal peaks functions of EMA for transducer 2.	121
Figure 5-21 Normalised mode shapes of EMA and FE for transducer 2.	121

Figure 5-22 Normalised amplitude for (a) analytical model L-T mode, (b) FE model L-T, T and F modes, and (c) experimental measurement of L-T, T and F modes.	123
Figure 5-23 Burst response of current [68].	124
Figure 5-24 Experimental harmonic analysis data for transducer 1.	125
Figure 5-25 Experimental harmonic analysis data of transducer 2.	126
Figure 5-26 Input current (left) and power (right) at different excitation levels for transducer 1.	127
Figure 5-27 Input current (left) and power (right) at different excitation levels for transducer 2.	127
Figure 5-28 Peaks response of (a) L (b) T and (c) torsionality for varied excitation for transducer 1.	129
Figure 5-29 Peaks response of (a) L (b) T and (c) torsionality for varied excitation for transducer 2.	130
Figure 6-1 FE model of the horn (left) and the normalised distribution of vibration amplitude along the horn (right).	133
Figure 6-2 FE model of LT drill.	134
Figure 6-3 Equivalent electrical network for LT drill.	135
Figure 6-4 Fabricated LT drill.	136
Figure 6-5 Electrical impedance spectrum (left) and phase difference (right) of analytical and experimental analysis.	136
Figure 6-6 EMA testing of LT drill (left) and modal peaks function (right). .	137
Figure 6-7 Normalised mode shapes of EMA (upper) and FE (lower) of LT drill.	138
Figure 6-8 Peaks amplitude of L and T responses (left) and torsionality (right) for LT transducer (without horn).	139
Figure 6-9 Peaks amplitude of L and T responses (left) and torsionality (right) for LT drill (with horn).	139
Figure 6-10 LT drill loaded to sandstone material (left) and bone surrogate material (right).	140
Figure 6-11 Amplitude peaks of L response (left) and T response (right) for sandstone load.	140
Figure 6-12 Torsionality values for sandstone load.	140

Figure 6-13 Amplitude peaks of L response (left) and T response (right) for
bone surrogate load.140

Figure 6-14 Torsionality values for bone surrogate load.141

VI. List of symbols

C or D	Elastic stiffness constant of piezoelectric material.
c	Velocity of the stress wave.
C_o	Electrical capacitance.
d_{ij}	Piezoelectric constant.
E	Yong's modulus of elasticity.
e	Piezoelectric charge constant.
F or P	Mechanical force.
\hat{F}_m	Output mechanical force mean value.
f	Frequency.
G	Shear modulus of elasticity.
g	Piezoelectric voltage constant.
H_o	Magnetic field.
I	Current.
I_o	Area moment of inertia.
\hat{I}	Current mean value.
i, j, k, l, p, q	Directional notations.
k	Wave number.
k_{ij}	Electromechanical coupling coefficient of piezoelectric material.
k_{eff}	Effective electromechanical coupling coefficient of the transducer.
l	Length.
M	Torsional moment.
N	Transformation coefficient.
N_L	Conversion coefficient of longitudinal vibration.
N_T	Conversion coefficient of torsional vibration.
n	Ratio of small end to large end radii of exponential horn.
n_o	Number of piezoelectric components.
P_e	Electrical power.

\hat{P}_e	Effective electrical power.
\hat{P}_m	Effective harmonic vibration power.
Q_m	Mechanical Quality factor.
Q_e	Piezoelectric constant factor.
Q_k	Dielectric constant factor.
q_e	Electrical charge.
r	Radius.
S	Cross-sectional area.
s	Elastic compliance.
T or σ	Total elastic stress.
T_o	Mechanical torque.
t	Time.
u	Displacement.
v	Velocity.
V	Voltage.
\hat{V}	Voltage mean value.
V_o	Volume.
\hat{v}_m	Output velocity mean value.
x, y or z	Position.
$\langle z \rangle$	Area weighted integral.
Z	Acoustical impedance
Z_e	Electrical impedance.
Z_o	Characteristic acoustical impedance.
α	Mass proportional damping coefficient.
β	Stiffness proportional damping coefficient.
γ	Area decay coefficient for exponential horn.
σ	Total stress.
ε	Total elastic strain.
ε^T	Relative permittivity evaluated at constant stress.
ε^S	Relative permittivity evaluated at constant strain.
λ	Wavelength.

ρ	Density.
ϑ	Bolt thread angle.
φ_e	Phase difference between input voltage and current.
φ_m	Phase difference between force and velocity.
$\tan \delta_m$	Mechanical loss tangent.
$\tan \delta_e$	Dielectric loss tangent.
$\tan \delta_k$	Electromechanical loss tangent.
ν	Poisson's ratio.
θ	Helix angle.
ω	Angular frequency.
μ	Friction coefficient.

VII. Abbreviations

EMA	Experimental modal analysis.
FE	Finite element.
FRF	Frequency response function.
L	Longitudinal vibration mode.
T	Torsional vibration mode.
F	Flexural vibration mode.
LT	Longitudinal-torsional vibration.
PZT	Lead Zirconate Titanate.

Chapter 1 Introduction

Sound waves define a sequence of compression and rarefaction and is the means by which acoustic energy propagates in an elastic medium. The number of repeated sequences per unit time is called the frequency which can be used to classify the sound waves as shown in Figure 1-1. The ability of the human ear to detect sound is used as the threshold limits along the frequency axis, where the sound wave frequency lower and upper limits are called infrasound and ultrasound, respectively. Ultrasonics (from ultrasound) is a term which refers to the application of sound waves in transporting mechanical energy at a frequency greater than the upper threshold limit (typically considered to be 20kHz). It is also used as a shorthand term for any piece of equipment employing ultrasonic waves.

Nowadays, a wide range of applications use ultrasonic principles which can be categorised, according to the rate of energy transfer (or power intensity), into low or high power ultrasonic applications. In low power ultrasonics, the propagated waves do not alter the physical properties of the propagation medium and are usually applied in frequencies above 100kHz with power intensity ranging from 0.1 - 0.5W/cm². These are widely used in non-destructive testing and medical diagnostic applications. High power ultrasonics (sometimes referred to as macrosonics or simply power ultrasonics) requires a power intensity generally higher than 10W/cm² so that the sound waves induce a permanent change in the propagation medium. Power ultrasonics is normally applied in a frequency range of 20kHz to 100kHz such as that typically used in ultrasonic cutting, ultrasonic welding, and many other ultrasonic applications [1-3].

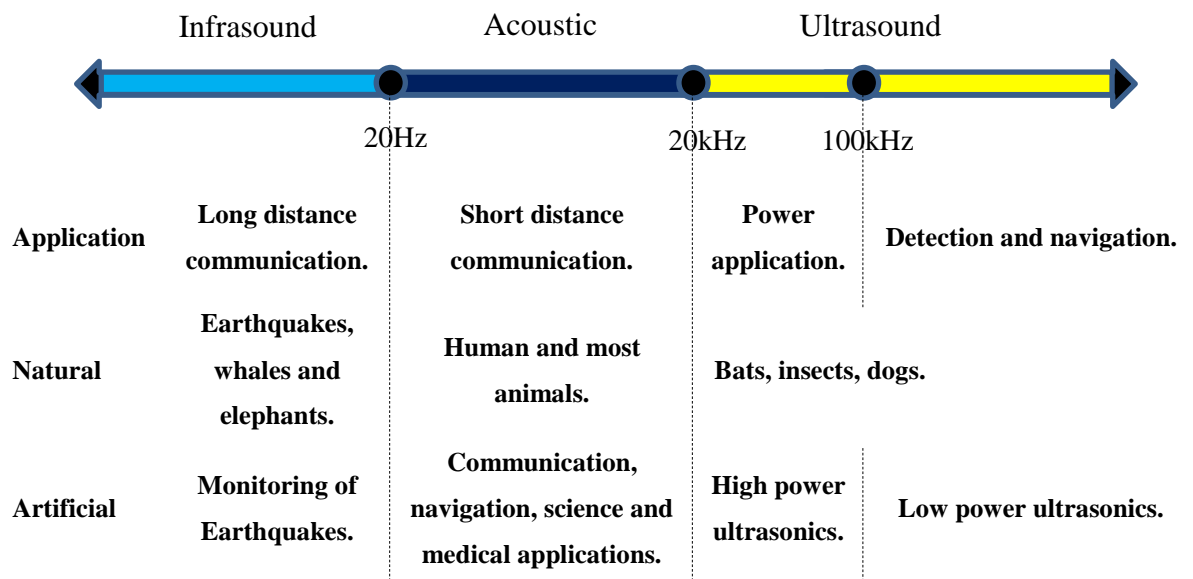


Figure 1-1 Classification and applications of sound waves over a typical ranges of frequencies [4].

1.1 Generating of ultrasonic waves

The most common methods used to produce waves in ultrasonic applications are: mechanical, magnetostrictive and piezoelectric methods. The mechanical method is the earliest known method for producing ultrasonic frequencies up to 30kHz by using Galton's whistle. This is operated by blowing a jet of high pressure gas into a tube. The tube has an internal piston to vary the frequency by varying the resonance cavity length. Galton's whistle, also known as a silent or dog whistle, is utilised for dog training purposes [5].

The magnetostrictive method uses naturally occurring ferromagnetic materials, which can convert magnetic energy into kinetic energy (or the reverse), such as iron, cobalt and nickel. These materials contain natural distortions and unaligned regions that possess a magnetic polarity called domains. When a magnetic field, H_o , is applied to a ferromagnetic material, the domains will rotate to align themselves with the direction of the applied field. This rotation leads to a change in the geometric dimensions of the material and therefore produces a deformation, ΔL . This property was first discovered by Joule in 1842, who noticed a change in the length of a sample of nickel when it's magnetic state change. He called this phenomenon Joule or magnetostrictive effect whilst the reciprocal effect, in which the applied magnetic field is changed due to a mechanical compression, F_C , or tension, F_T , force, is called the inverse magnetostrictive or Villari effect. These effects are presented in Figure 1-2 [6, 7].

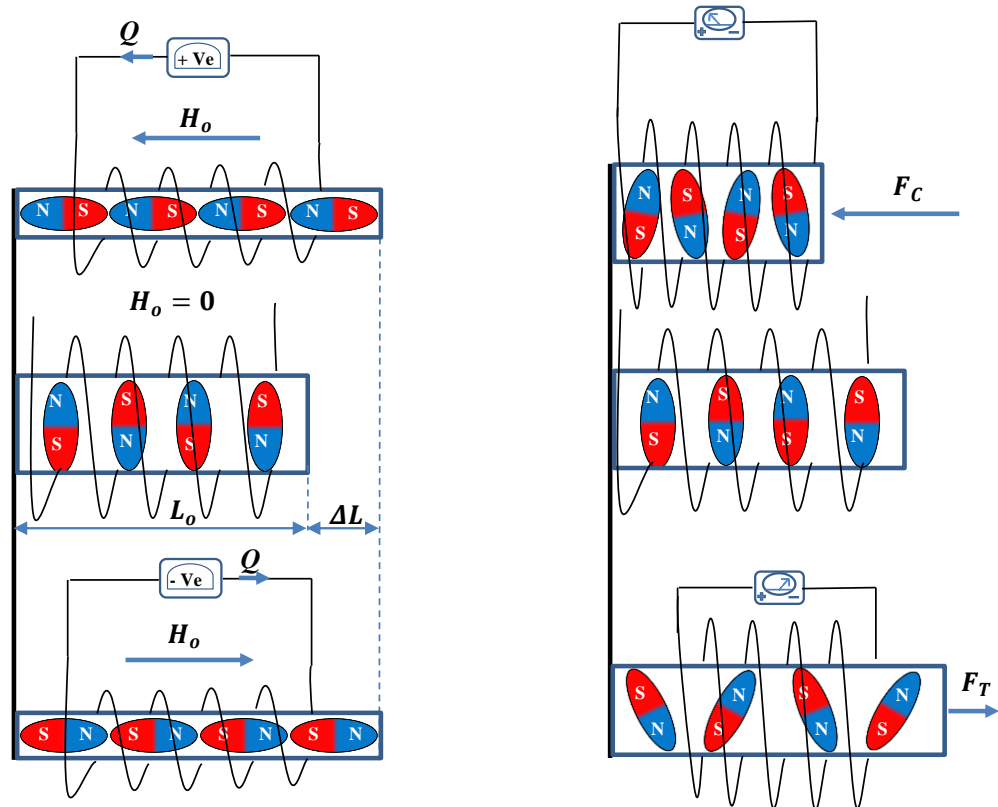


Figure 1-2 Magnetostrictive effect (left) and the inverse magnetostrictive effect (right) [7, 8].

The piezoelectric method uses piezoelectricity (from the Greek: piezein 'press or squeeze' and electricity) which is a property of certain classes of crystalline materials which consist of polarised molecules. When a mechanical compression, F_C , or tension, F_T , force is applied to one of these materials, the crystalline structure produces a potential difference, and therefore a charge, Q_e , proportional to the applied force. This behaviour is called the direct piezoelectric effect. Conversely, the inverse piezoelectric effect occurs when an electrical field is applied across the material. The polarised molecules will align themselves with the electrical field, which induces electric dipoles within the molecular or crystalline structure of the material. This molecular realignment causes a change in material dimensions. Piezoelectric materials include natural materials such as quartz and Rochelle salts or manufactured materials, which exhibit better performance, such as Lead Zirconate Titanate (PZT) and Barium Titanate. The first demonstration of the direct piezoelectric effect was in 1880 by Curie whilst the inverse piezoelectric effect was mathematically derived from the fundamentals of thermodynamic principles by Lippmann in 1881. These effects are shown in Figure 1-3, where the poling axis represents the direction of piezoelectric effect [9, 10].

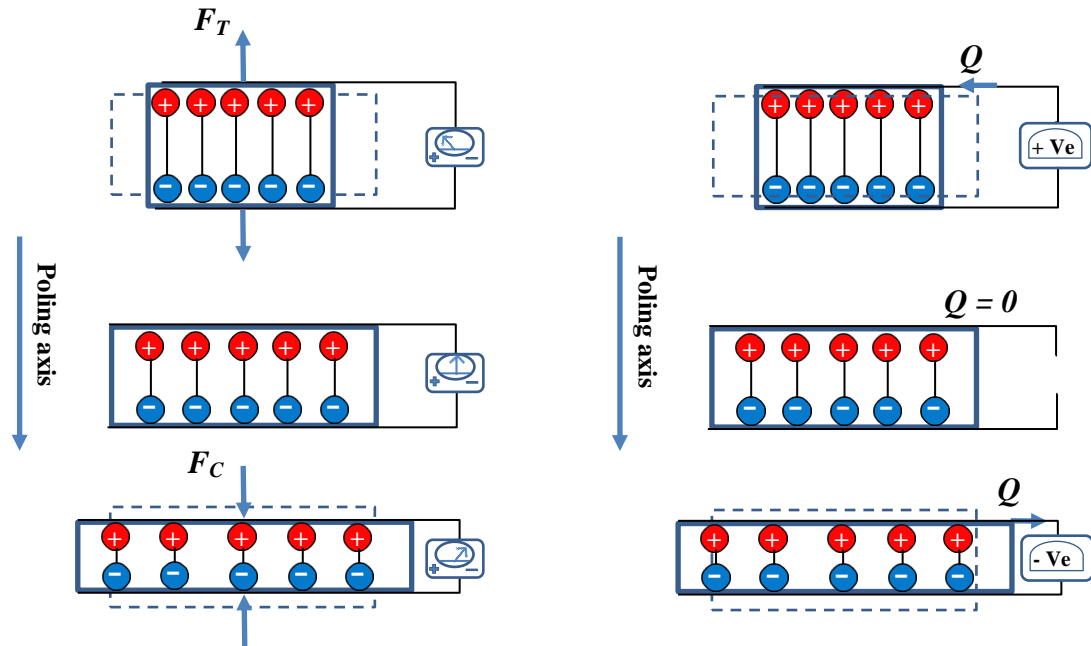


Figure 1-3 Direct piezoelectric effect (left) and the inverse piezoelectric effect (right) [11].

1.2 Ultrasonic transducers

In ultrasonic power transduction, the magnetostrictive effect and indirect piezoelectric effect are employed to convert alternating current energy to acoustical energy at high frequencies. Therefore, an ultrasonic power transducer can be either magnetostrictive or piezoelectric.

A simple form of a magnetostrictive transducer consists of a core of ferromagnetic material bonded by a conducting wire. When an electrical current is pulsed into the wire at a certain frequency, a magnetic field is produced and causes a reorientation of the core's domains which align themselves along the direction of the applied field. This reorientation changes direction at each half cycle of the input pulse and causes a reciprocal deformation of the core material. Therefore the frequency will be double that of the pulses frequency.

The most common type of piezoelectric transducer, which is called a Langevin transducer and is sometimes referred to as a sandwich or stacked transducer, consists of the piezoelectric element(s) that are sandwiched between electrodes and are pre-stressed by front and back masses (layers) as shown in Figure 1-4. The piezoelectric element(s) generates an acoustic wave in both the front and back directions, however the function of the back mass being to encourage wave propagation in the forward direction. This is achieved by using a back mass of higher acoustic impedance than the front mass, which transmits the acoustic energy to the load.

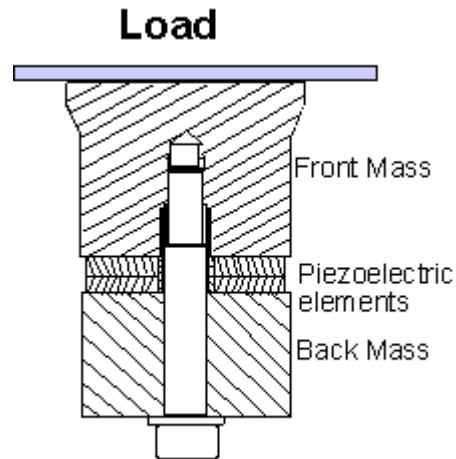


Figure 1-4 Conventional Langevin transducer [12].

Similar to a magnetostrictive transducer, piezoelectric transducers are excited by an electrical current that is pulsed to the piezoelectric element(s) through the electrodes which causes the elements to vibrate at the same frequency as the applied pulses. However, it has been shown that piezoelectric transducers present better characteristics than the magnetostrictive transducers in different fields of ultrasonic applications which are listed in Table 1-1.

Table 1-1 Comparison between magnetostrictive and piezoelectric transducers.

Magnetostrictive transducer	Piezoelectric transducer
1- The overall efficiency of converting electrical energy to mechanical energy is low and in some cases it is only 50-60%.	1- Efficient devices where most of electrical energy is converted to mechanical energy and the overall efficiency can reach up to 90%.
2- Large size devices which may require special cooling methods to keep components within acceptable operating temperatures.	2- They are relatively small and lightweight devices which do not require significant cooling. Reliable for long-term operation.
3- Requires expensive and large electronic components that are able to withstand the high operating temperatures.	3- Stable over a broad range of temperature, but may be affected by long use at high temperatures.
5- Affected by the surrounding electromagnetic fields which limit its usage for such environment.	4- Not affected by external electromagnetic fields.
4- Requires large generator enclosures which may limit the flexibility of usage for many applications.	4- Simple, reliable, and very robust. Can be used in different fields of industry, medicine, and aerospace applications.
5- Typical operating frequency is less than 30kHz which limits use in high frequency applications.	5- Can be designed for a wide range of frequencies based on the requirements of application.

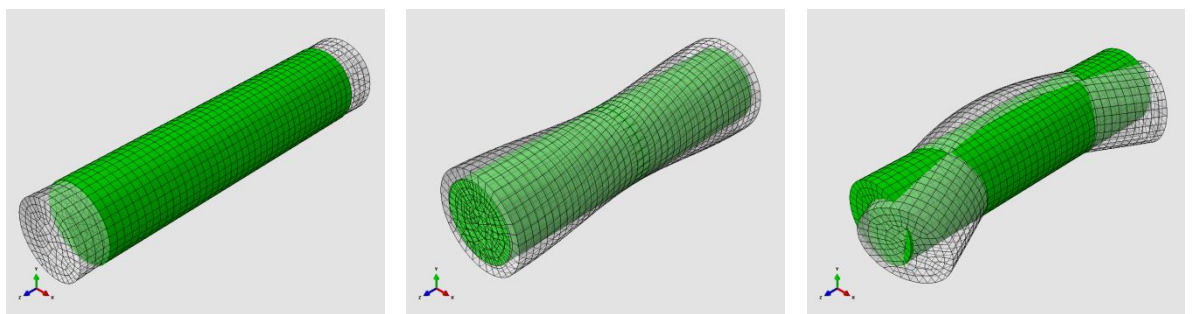
In addition to the above points, the configuration of the Langevin transducer has many other advantages which can be summarised as follows [11, 13]:

- 1- It is possible to apply a mechanical pre-stress to the piezoelectric elements by means of a central bolt or peripheral sleeve. This will decrease the electrical impedance of the transducer, increase the generated dynamic stress amplitude and increase the maximum power intensity considerably. It also prevents piezoelectric element(s) fracture in the expansion half-cycle and improves the mechanical contact between transducer parts which, in turn, decreases mechanical losses.
- 2- The additional mass will increase the mechanical strength and the mechanical quality factor of the transducer.
- 3- Piezoelectric materials have poor thermal capacity which is compensated by the metal masses which act as heat sinks. Therefore, the Langevin configuration enables the transducer to be driven at a higher frequency where elevated temperatures can occur.
- 4- The metal masses give flexibility to the design of variable shapes and dimensions.

- 5- The metal masses replace the required expensive piezoelectric material to achieve the required wavelength of the frequency, so that the transducer cost will decrease.
- 6- The metal masses help guide the majority of the generated acoustic energy towards the application direction rather than it dividing equally in both directions.

1.3 Modes of vibration

When a piezoelectric element is pulsed by an electrical current, it generates a vibrational wave of small amplitude which is insufficient for many ultrasonic applications. To overcome this limitation, transducers employ the mode shape of the structural geometry to amplify this amplitude. In pre-stressed sandwich transducers, the front and back masses are used to modify the resonance length of the structure so that the transducer will vibrate at resonance. Based on the required application, the selection of the mode of vibration is considered and then other design parameters of the transducer parts are decided. In general, ultrasonic transducers employ one mode of vibration which can be longitudinal (L) mode, torsional (T) mode or flexural (F) mode as shown in Figure 1-5. However, it is also possible to combine these modes of vibration to produce a new shape of motion. Possible combinations are longitudinal-torsional (LT), longitudinal-flexural (LF) and torsional-flexural (TF) modes of vibration which have proven to be useful in many modern applications [14].



(a) Longitudinal mode.

(b) Torsional mode.

(c) Flexural mode.

Figure 1-5 Mode shapes, from a finite element model of a rod.

1.3.1 Longitudinal –torsional mode of vibration

The longitudinal-torsional (LT) mode of vibration (sometimes referred to as the LT composite mode of vibration) is employed in many ultrasonic applications such as ultrasonic cutting, ultrasonic welding, ultrasonic motors and ultrasonic drilling. In this mode, the particles of the propagation medium vibrate in a spiral motion along the propagation direction. This spiral motion of the LT mode of vibration produces elliptical orbits in ultrasonic motor which has been shown to improve the produced torque. Also the elliptical motion increases the strength and uniformity of bonding in ultrasonic welding and enhances the drilling quality of ultrasonic drills [15, 16].

There are different approaches which can be used to generate LT vibrations in ultrasonic applications. However, two main approaches are widely used to produce this mode in ultrasonic horns (sometimes referred to as waveguides or resonators). These approaches are degeneration of L vibration, and coupling between L and T modes of vibration.

1.3.1.1 Degeneration of longitudinal vibration approach

In this approach, ultrasonic horns enable transformation of L motion which is excited by the piezoelectric stack into both L and T motion at the forward end, which is the working end of the horn. This can be obtained by geometrical modifications to the horn, which could be the front mass of a transducer or a part attached to the L mode transducer. These geometrical modifications create a non-uniform cross-section that twists along the horn axis and produces a spiral wave path as shown in Figure 1-6.

The non-uniform twisted section can be created in a bar by placing a number of grooves along its length and then physically twisting the bar. It can also be created by machining a number of twisted grooves along a bar to produce spiral wave paths. Another method to produce this section is by twisting a rectangular cross-sectional bar about its lengthwise axis which can also produce the required wave path. When these horns are mechanically connected to L wave generators, they produce the desired LT vibration at their working tips.

This approach is simple in implementation, requires a single source of vibration and has good resonance stability for various boundary conditions. However, it produces low torsionality, which defines the ratio of T to L response amplitude at the output surface of the horn. The only possibility to produce high torsionality is to excite the horn at a non-

resonance frequency, but this will produce a low response amplitude which is insufficient for ultrasonic applications [17].

Other disadvantages of this approach are: the slotted section reduces the flexural stiffness of the horn which gives a possibility of unwanted modal coupling between the desired and surrounding modes, especially F modes. Also, creating slots on the horn can produce, when attached to a transducer, a long and heavy ultrasonic system which is impractical for use in many applications such as medical devices [18, 19].

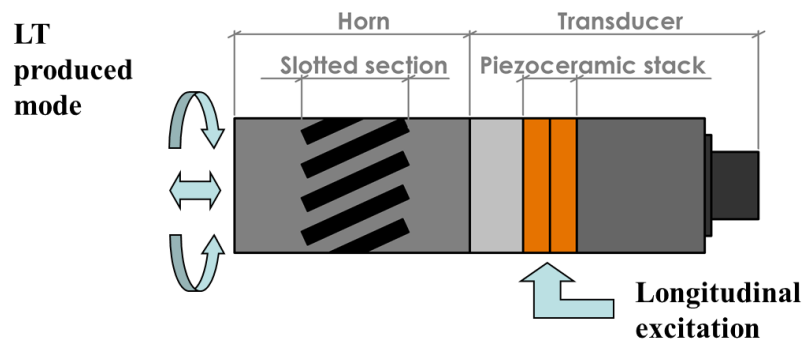


Figure 1-6 Schematic of the degeneration of L vibration approach in a sandwich transducer.

1.3.1.2 Coupling between longitudinal and torsional modes approach

This approach can be utilised in ultrasonic sandwich transducers by using two sets of piezoelectric component(s) of different poled directions; set one is poled in the L direction whilst set two is poled in the T direction to generate L and T waves, respectively. These waves subsequently combine in the front mass horn which is designed such that the whole transducer is resonant in the L and T modes at the same frequency. An exponential cross-sectional decay horn is used successfully for this purpose as shown in Figure 1-7 [20].

This approach yields high torsionality and can be designed to control the amplitude of each response separately which is an important advantage for many applications. However, it has limitations in terms of complexity in both mechanical design and electrical excitation. This approach also requires more expensive tangentially-poled piezoceramic discs and, as might be expected, it can prove difficult to maintain frequency matching between the two resonances under different load conditions. Furthermore, as the transducer needs to be secured to a housing by clamping at the zero vibrational response location (nodal plane), this approach produces two nodal planes (for L and T modes) and therefore it is difficult to create a clamping feature that does not influence the vibrational response [18, 21].

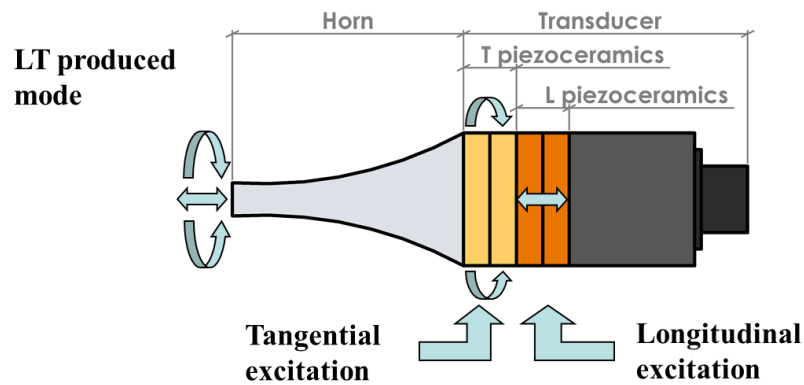


Figure 1-7 Schematic of the coupling between modes approach in a sandwich transducer.

1.4 Objectives

The objective of this work is to create a new approach to the design LT transducers which can overcome the limitations in the above-mentioned approaches. The proposed approach should have simplicity in design, fabrication and excitation features, and is also required to produce high torsionality with stable resonance conditions and a good frequency separation between the desired LT mode and surrounding modes. Finally an easy clamping feature is essential for casing purposes. A combination of the principles of degeneration and coupling approaches is proposed to produce this design. A slitting-twisting technique is introduced into an exponential cross-sectional horn which acts as the front mass in a Langevin longitudinal transducer. This configuration reduces the boundaries between transducer parts and therefore decreases the mechanical losses.

This research concentrates on optimising a number of geometrical design parameters based on a set of transducer performance criteria. The design parameters include shape, dimensions and twist angle of the created slots whilst the performance criteria include torsionality, frequency spacing between modes, ratio of L response between front and back masses and the location of the nodal plane along the structure.

The initial dimensions of a longitudinal Langevin transducer with an exponential front mass are calculated based on the wave equation and acoustical relationships between transducer parts. A finite element (FE) model is then created for different cut shapes, dimensions and various twist angles along the front mass. A modal analysis procedure is performed to optimise the cut geometries based on the performance criteria. The FE model is also used to perform a size scaling study to generalise the design for different ultrasonic applications.

The optimum design is evaluated analytically, based upon the equivalent electrical circuit method, to explore design aspects which cannot be covered by the FE model such as the electrical impedance spectra and the effective coupling between electrical and mechanical energy. The method is expanded to validate some FE results such as the distribution of response amplitude and the location of the L nodal plane of the desired mode along the transducer structure. Finally, a number of prototypes are fabricated and experimentally investigated to validate the modelling findings and characterise the fabricated transducers for different operating conditions.

1.5 The research goals

The LT mode of vibration has many applications in power ultrasonic devices; therefore the current work aims to design a LT ultrasonic transducer which has the following advantages:

- 1- The transducer can produce high torsionality.
- 2- The operating mode has sufficient frequency separation from the surrounding modes to prevent any possible modal coupling during operating.
- 3- The design improves transducer efficiency by minimising boundary losses.
- 4- The design can be scaled to suit different ultrasonic applications.
- 5- The fabrication processes are simple enough to ensure reasonable cost of fabrication.

1.6 Scope of work

The following work is organised as follows:

Chapter 2 is a scientific literature review where a general overview of different transducers is presented. An introduction to LT transducers and the methods of producing this mode in ultrasonic application is then discussed, reviewing a number of applications that can benefit from this combination of motions. Finally the modelling approaches for LT systems are demonstrated followed by a discussion of their advantages and limitations.

Chapter 3 presents the FE model approach to the LT transducer. The principles of transducer design and optimisation criteria are highlighted; first the design and characterisation of the wave equation and the acoustical relationships between the longitudinal Langevin transducer parts are used to calculate the initial dimensions. Second, the FE model of the initial design is created where the modelling steps for materials and

boundary definitions besides discretisation and analysis configurations are discussed in detail. An FE modal analysis procedure is then used to optimise this design where different cross-sectional cuts of different depths and at various twist angles are introduced in the front mass. The FE model is also employed in a numerical size scaling study to generalise the geometric dimensions for different ultrasonic applications. Finally, the linear dynamic behaviour of the transducer is simulated where the output response and torsionality are predicted for different levels of harmonic excitation. An attempt is also made to calculate the electrical impedance spectra from the FE model over a range of frequencies.

Chapter 4 introduces the analytical model of the optimum design based on the equivalent electrical circuit method. This modelling procedure is used to explore the aspects which are not covered by the FE model and to validate some FE findings prior to fabrication. The principles of the equivalent electrical circuit method, based on Mason's model, are presented where the equation of wave motion in a solid elastic medium is used to create the system equations. MATHEMATICA is then used to solve these equations where a program code is written to calculate the electromechanical parameters such as the electrical impedance spectra and the voltage/current phase difference of the transducer.

Chapter 5 presents the fabrication process of two different sizes of LT transducer and the experimental testing methods of these prototypes. The fabrication process is divided into preparation and assembly steps where a detailed demonstration of each step is presented. The test methods, which included electrical impedance analysis, experimental modal analysis (EMA) and dynamic behaviour analysis, are introduced and the test results are compared to the model findings.

In chapter 6, a case study of designing a LT drill is presented where the developed methodologies of LT transducers, which presented in previous chapters, are employed and the resulting design of drill is fabricated and tested for different operating conditions. The test results are also compared to the model results for validating and characterisation purposes.

Chapter 7 presents the conclusions of this work, and makes suggestions for future work.

Chapter 2 Literature review

2.1 Background

Langevin transducers predominantly employ a single mode of vibration of the structural geometry to amplify the vibration generated in the piezoelectric element(s). The mode of vibration is selected based on the required application and the front and back masses are modified to obtain the resonance length of the selected mode. Although transducers can employ longitudinal (L), torsional (T) or flexural (F) modes of vibration, the L mode is used most often due to its simplicity in design and excitation, as well as, its high efficiency in converting electrical energy to mechanical energy [17, 20, 22, 23]. It is also possible to combine these modes of vibration to produce a new shape of motion. The possible combinations are longitudinal-torsional (LT), longitudinal flexural (LF) and torsional-flexural (TF) mode of vibration, which have proven to be useful in many modern ultrasonic applications [14].

2.2 Introduction to LT mode of vibration

Longitudinal-torsional (LT) vibration is utilised in many industrial applications to enhance performance. Applications such as ultrasonic cutting, ultrasonic drilling, ultrasonic welding and ultrasonic motors can benefit from this combination of vibrational motion. It is found that by combining torsional (T) vibration and longitudinal (L) vibration in the process of cutting glass, the required torque can be reduced by about 40-50%. Also, the introduction of T motion into L vibration in ultrasonic drilling can greatly improve the drilling process. Also, it is reported that the elliptical motion, which is obtained through this vibrational coupling, can increase the torque in ultrasonic motors and enhance the strength and uniformity of bonding in ultrasonic welding [15-17, 24].

Up until the middle of the 20th century, ultrasonic systems using LT vibration were proposed and studied, but were not widely used. In 1965 Rozenberg concluded that the

main reason for this was the lack of at least an approximate method to model such systems. Experimental modelling, based on a trial and error method, was the only approach used to optimise LT systems. Although this approach was complex, and it involved the fabrication of a large number of samples, it was the only acceptable approach. This was due to the fact that it provided a means for finding the best LT systems for practical applications and it produced a set of data which could be used to develop a procedure for modelling LT systems [17].

Over the last two decades, there has been enhanced interest in LT vibration for applications to ultrasonic welding, ultrasonic motors and ultrasonic drilling. Publications from researchers, such as Tsujino [25-31] and Shuyu [20, 32-34], have been focused on improvements to LT systems by simplifying the excitation methods, developing analytical representations and improving their response. The analytical approaches are developed based on the wave equation in elastic solids, and on equivalent circuit approaches, to calculate the design parameters of these systems. Other researchers employed advanced numerical methods to simulate and analyse LT systems [15, 16, 35, 36]. Many patents are filed which aim to improve the performance and the capability of different medical and dental applications through the introduction of LT vibration. Applications such as ultrasonic tissue dissection and ultrasonic scalpel/coagulation devices are reported [18, 19, 21, 37].

In the following sections, the methods of producing LT vibration in ultrasonic applications are presented. Then ultrasonic applications which can benefit from this combination of motion are reviewed. Finally, the modelling approaches which are used to study LT vibration are presented with details about their advantages and limitations.

2.3 Producing of LT vibration

Different approaches are used to produce LT vibration in ultrasonic systems. The first approach is based on the degeneration of L vibration into LT motion through geometrical modifications of the wave path. The earliest proposed vibrational system using this approach was in 1959 by Sirotyuk. This was investigated for industrial applications by Rozenburg in 1969. In this system, the second stage of a stepped horn is marked with gradually deepening grooves. These grooves form a helix, with a smoothly diminishing pitch, so that they emerge at small angles at the tip of the horn stem relative to the output face. This type of non-uniform cross-section causes initiation of torsional vibration

components when the horn is excited by L vibration through a transducer. The frequency characteristic of the system (the transducer and the horn) is displayed in Figure 2-1. This shows that it has two close resonance frequencies for L and T modes of vibration. Therefore, in order to produce the LT vibration, the system is excited at a frequency within the range between the resonance frequencies of these modes.

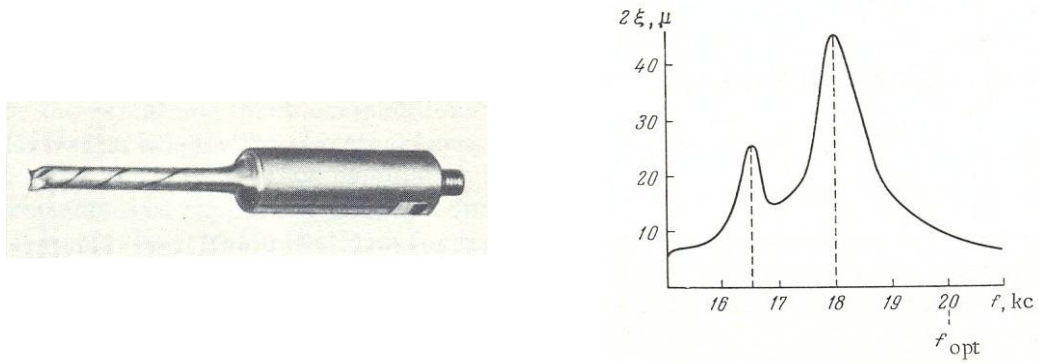


Figure 2-1 A longitudinal-torsional stepped waveguide (left) and its oscillation amplitude (referred as 2ξ) in micrometres as a function of frequency in kilocycles per second (right) [17].

Another type of LT stepped horn was designed by using an ordinary drill bit as the second stage. This does not feature a smooth variation in the pitch of the helical grooves. This is excited at a frequency near to the L and T resonance frequencies, and it produced a high torsionality of 156%, but had a low response which was insufficient for ultrasonic applications. Different sizes of these two types of horn were fabricated and investigated for output torsionality. The results showed that the torsionality depended mainly upon the slope of the grooves, relative to the axis of the horn, and on the depth of these grooves. It was found that the torsionality increases with increasing depth of groove and reduction of the slope within certain limits [17].

Another method of creating LT vibration in uniform horns was proposed by Mitskevich in 1969 and used by Kellsatel in 1981. Once again, the degeneration was obtained by the creation of a non-uniform cross-section along the length of a uniform bar, and then by twisting the bar along its lengthwise axis. The non-uniform cross-section can be created by placing a number of grooves along the bar, which is then physically twisted to spiral these grooves. It can also be made by twisting a bar of rectangular cross-section about its axis to produce a spiral wave path. The twisted bar is then mechanically connected at one end to a transducer which produces L motion, so as to produce a combination of LT vibration at the output end [18].

The degeneration approach was significantly improved by Tsujino, through the introduction of a specific component (converter) along a longitudinally excited waveguide. The convertor is originally incorporated at the L node, and it is divided into two regions. The first region is dominated by the L wave and represents the solid core of the convertor, this permits part of the excited L vibration to pass unchanged to the output surface of the waveguide. The second region is concentric to the solid core, but contains helical slits. This means that the remainder of the excited vibration must follow a spiral path and thus takes on a torsional aspect. The two parts of the wave are then recombined close to the output surface to generate the desired LT motion [25, 28, 38].

In general, the degeneration approach can be applied readily and requires only a single generator. It also has good design and fixture features and can obtain resonance stability over different boundary conditions. However, it also produces low torsionality and there is a possibility of unwanted coupling between the desired and the surrounding modes of vibration. This is partially because the slitted section reduces the flexural stiffness of the horn [39, 40].

Attempts have been made to combine rotational motion with longitudinal vibration in cutting tips of surgical devices. These attempts used electric motors to provide the rotation to the tip. However, this requires a complex arrangement for attaching and securing the motors [18, 21].

The second approach is based on coupling L and T modes of vibration through the use of two sets of piezoelectric components, with different polarisation directions, in a sandwich transducer model. The first set is poled in the thickness direction to generate the L vibration whilst the second set is poled in the tangential direction to generate the T vibration. These sets are excited by two separate ultrasonic generators which give the possibility of controlling each response separately. This is considered as an advantage for many ultrasonic applications, which require different amplitudes of response during the operating process. However it presents a complexity in the excitation of these sets of piezoelectrics [18].

The excitation method is simplified by Shuyu's work in 1996 where he derived a relationship between the eigenvalues and the decay coefficient of an exponential horn. This is used to adjust the resonance frequencies of the L and T modes. The exponential horn is used as a front mass in a sandwich transducer and the decay coefficient is selected such that the L and T modes of the whole transducer resonate at the same frequency. Therefore

only one ultrasonic generator is required to excite both sets of piezoelectric components [20].

This approach can produce high torsionality at the output surface of the transducer. However it requires the use of an expensive type of piezoelectric component, which is polarised in the tangential direction. This type of piezoelectric component has a much lower coupling coefficient between electrical and mechanical energy in comparison to the longitudinally poled components, this is because the polarisation is along the circumferential where large sectors of the component are difficult to polarise [32]. Therefore the overall transducer efficiency will decrease. Also, the transducer needs to be secured to the housing by clamping it at the minimum vibration response location (nodal plane) but this coupling method produces two nodal planes (for L and T modes). Therefore it is difficult to create a clamping configuration that does not influence the vibration response. Finally, the resonance condition of these modes will be modified due to the change in boundary conditions [41].

An alternative method that can be used to excite the exponential waveguide is to use more than one L mode transducer. The first transducer is attached to the large end of the waveguide causing it to vibrate in the L direction, whereas the other L transducers are attached to the sides of the waveguide so that a T mode can be obtained by modulating the excitation of these transducers. If the exponential waveguide has the same resonance frequency for L and T vibrations, then these transducers can be excited by one generator. However the geometry of such system is usually quite large and complex resulting in low output of T vibration [18].

2.4 Application of LT vibration

It has been shown that the idea of exploiting LT vibration in industrial applications dates back to 1969 when Rozenburg studied the application of LT systems of vibration in cutting and welding processes. However, the construction of these systems proved rather complicated. Later, developments in the design of sandwich piezoelectric transducers have allowed for a wide exploration of this combination in different applications. Applications such as ultrasonic cutting, welding, motors and drilling have attracted more attention [2]. In some applications, LT systems need to be small, uniaxial, light weight and relatively low power for special purposes such as in medical applications. Additionally, there is also a need for relatively large systems with high ultrasonic power for industrial applications

such as ultrasonic welding, and some medical applications, such as ultrasonic bone cutting [19].

2.4.1 Ultrasonic welding

Ultrasonic vibrations are used effectively for welding processes where no adhesive or solder are required. The conventional ultrasonic welding system of L vibration normal to the welding surface is traditionally used when the vibration stress induced in the welding specimen is in one dimension. However, it is found that the use of combined vibrations, such as LT vibration, will induce two dimensional vibration stresses which improve the welding characteristics. This improvement descends from the temperature rise due to two dimensional combined vibrations. It is also found that the use of LT vibration in ultrasonic welding leads to an increase in the welding area and produces more uniform bonding over the traditional L method. Thick metal plate specimens can be welded continuously, with a uniform welding strength that is independent of welding positions and directions through the use of LT vibration systems [26, 42].

LT vibration systems are also used in ultrasonic plastic welding, packaging and wire bonding where the degeneration of L vibration through a convertor is mainly used to produce the desired LT vibration. Single and multiple slits in sections along the convertor are used in order to reduce the stresses and to improve the vibration characteristics [28, 30].

2.4.2 Ultrasonic motors

Ultrasonic motors are required to have high torque characteristics at small dimensions. Compared to a conventional electromagnetic motor, they have several distinctive features such as simple structure, low velocity, high efficiency and no electromagnetic noise. Also they have a quick response and good control characteristics at start and stop due to the low inertia of the moving pieces [38].

In general, the simple form of an ultrasonic motor consists of a rotor and stator(s) where a generated elliptical vibration on the stator(s) surface transfers through a friction force to the rotor and causes the rotation. A traveling wave ultrasonic motor uses bending travelling waves in a piezoelectric ring or disc to generate the elliptical vibration in the stator(s), as shown in Figure 2-2. This type is widely applied in auto-focusing lens systems in cameras.

However, this type of motor produces low torque output [27, 35]. Alternatively, the LT composite mode of vibration is used to produce a high torque output, this approach is employed in two different types of ultrasonic motors. The first type is called a hybrid piezoelectric motor which was first proposed in 1980. This type uses two piezoelectric transducers as stators; the first transducer is longitudinally operated to generate the L motion, whilst the other transducer is tangentially operated to generate the T motion, as shown in Figure 2-3. These motions superimpose on the rotor part through the frictional force between the contact surfaces. In order to match the resonance of the L and T vibrations, an additional mass is added to the stator(s) to influence the eigenfrequencies of these modes [43]. An alternative matching method uses a compression force, which is applied between the stator(s) and the rotor to change the resonance conditions of the L mode so that it coincides with the T mode of vibration [24, 35].

The second type of ultrasonic motor uses a LT vibration convertor which is driven by the longitudinal vibration transducer only. The convertor consists of a cylindrical structure with diagonal slits cut along its circumference which is adjusted to the nodal plane of L vibration mode. This type is used due to its simple design and high production of torque along with the simple excitation requirements [19, 27, 38].

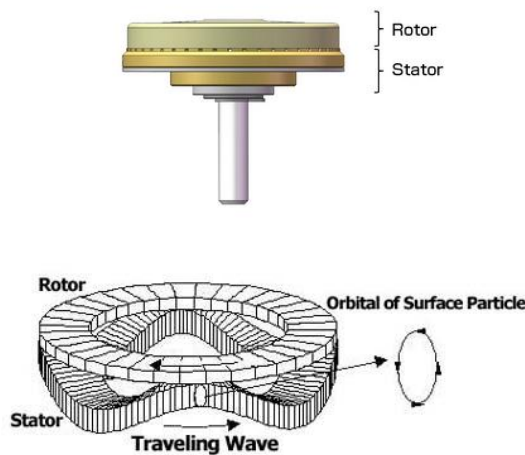


Figure 2-2 Principles of traveling waves in an ultrasonic motor [44].

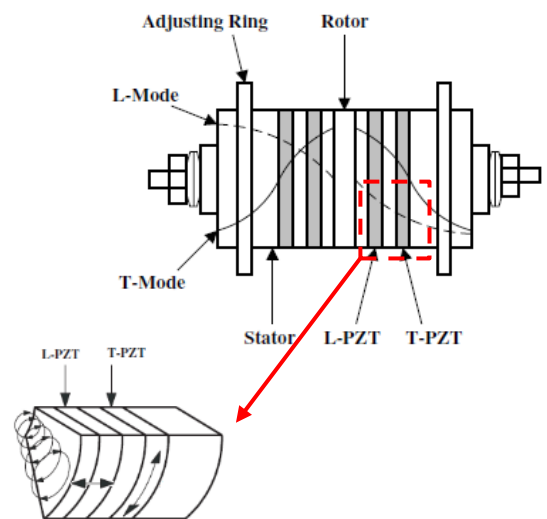


Figure 2-3 Principles of longitudinal-torsional ultrasonic motor [45].

2.4.3 Ultrasonic rock drilling

In general, drilling of rocks requires two stages: rupture of the material with a drill bit, and the removal of the produced cuttings (chips). The traditional technique of rotary drilling involves the breaking of rock, caused by the impact forces of the applied load and the shear forces of the bit rotation, whilst the chip removal can be done by fluids or via the helical augers of the drill bit in a dry drilling. Therefore, this technique requires large axial force and holding torques which may need a rigid platform. It also consumes high electrical power at the beginning of drilling along with the possibility of drill bit wear, which reduces the penetration rate and requires an increase in the applied load during drilling. These limitations prevent the use of this technique in some applications such as planetary drilling in which there has been a growing interest. Alternatively, the ultrasonic technique is considered to be a very promising technology for rock drilling and planetary sampling explorations. A generation of ultrasonic drills have been developed and successfully tested on a range of rocks [46].

Ultrasonic drills can be categorised into percussive (or free-mass) and LT drills. The simplest percussive drill consists of a L transducer, a tuned booster, a free-mass and a drill bit. The L vibrations excited by the transducer are amplified by the booster and transferred through impacts to the free-mass, which is placed between the booster tip and the bit base. Free-mass oscillations convert the ultrasonic energy into stress pulses which then propagate sonically to the bit/rock interface. The fracture of the rock occurs due to the high velocity of bit impacts on it, whilst the removal of cuttings is achieved through different methods such as fluid, pneumatic and coring methods [15, 36].

Incorporation of the T motion to the L vibration by means of incorporated motors has shown to improve the cutting removal and the rate of the drill's penetration. In the drilling of strong brittle materials, the rotary percussive drilling is more efficient in terms of required applied load and power consumption [47, 48]. However, the drilling system requires the integration of independent driving capacities for the drill and the motor(s). This leads to increases in the degree of complexity and the required power. Therefore, this is not preferable for planetary explorations.

In LT drills, the coupling between modes is achieved by means of two discrete transducers or two sets of piezoelectric elements to provide the LT vibration. However, as mentioned in section 2.3, it is preferable to avoid the multiplicity of ultrasonic generators. The desired LT vibration can also be obtained through eigenmode coupling and mode degenerating

methods. The eigenmode coupling differs from the coupling between modes in that the coupling occurs due to geometric modifications of the resonator so that the L and T modes are resonant at the same (or, more accurately, close) frequencies. A ring of diagonal slots on the body of a step horn and a helical flute along the stem of the horn are used to investigate the effectiveness of the eigenmode coupling and the degeneration methods in ultrasonic step horns, respectively. The findings show that the eigenmode coupling method can produce higher torsionality, but it is not associated with high L output. Therefore, the mode degeneration method is more applicable for applications that require a strong LT motion [16, 49].

2.4.4 Ultrasonic dissection

The ability to separate collagenous tissue, bone and other connective or supportive tissues using precise control, with very little heat generation, whilst avoiding damage to the surrounding tissues, are the main advantages of ultrasonic tissue dissections. The ultrasonic dissection is also safer than other methods because the energy is absorbed into the target tissue without transmission into neighbouring regions [19]. The first application of ultrasonic vibration in the separation of tissues was done by Balamuth in 1979. He presented a variety of surgical instruments equipped with vibration tips for different applications in the dissection of biological tissue. Later on, many devices and methods reported the difference in the use of L and flexural (F) vibration in dissection applications. However, all of these methods have not accomplished the objective of rapid and precise removal of tissues which are normally resistant to L or F vibration. Different configurations for introducing T motion into the L vibration of the dissection tips have been reported. These configurations showed a significant enhancement in the dissection of the resistant tissues. Configurations that make use of rotating motors, modification of the wave path by creating and twisting of grooves and combinations of L and T piezoelectric generators in the transducer are used successfully and showed high improvement in tissue dissection devices [18, 21, 37, 50].

2.4.5 Other applications

Ultrasonic systems are also utilised to machine holes in ceramic materials, where the traditional method of laser, water jet and wire electrical discharge are inconvenient due to

their large and complex structures. The disadvantages of ultrasonic machining which included lower removal rates and lower machining accuracy are shown to be resolved by employing the LT vibration. Asami [51, 52] presented a simple and miniaturised LT system which consisted of a hollow stepped horn, with a diagonal slit convertor, that is mechanically connected to a L mode transducer so as to degenerate the L vibration into LT motion. The investigation showed that the LT vibration system can be used successfully to machine holes in brittle materials with high accuracy.

2.5 Modelling of LT Ultrasonic vibration

Up until the 1980s, the applicability of LT systems was limited due to the lack of an effective method to accurately predict the performance of such a system. Prior to that time, analytical and experimental treatments were involved in the analysis of ultrasonic horns. However, the analytical model was not suitable for the analysis of the combination of vibration behaviour in design of LT horns. The experimental method, which was used to select the optimum ultrasonic horn, runs into difficulty when it is applied for the LT design of horns. This is because it requires fabricating a large number of prototypes which have no use if they are not successful. Nevertheless, this method was the only acceptable method which provided a means of finding the best LT horn for practical applications. It also produces a set of data that could be used to develop a method for calculating LT systems [17].

Nowadays mathematical modelling, which includes analytical and numerical methods, is intensively used, along with the experimental modelling methods, to design, develop and test the performance of LT systems. Analytical methods, involve the use of the wave equation and the relationships that describe wave propagation within elastic mediums are used to obtain the analytical expressions. However, many systems possess complex functionality that makes it hard to track their behaviour by using these formulas. Numerical methods are used alternatively to simulate and analyse these systems. Each of these two methodologies comes with advantages and limitations which can be presented as follows:

2.6 Analytical modelling method

The analytical modelling method is a mathematical representation of the system, where its behaviour and changes can be described through a set of equations. In ultrasonics, the

wave equation is used to study the wave motion along the model. In the early 1940s the one-dimensional wave equation in elastic solid media was used extensively for the design and improvement of ultrasonic horns [53, 54]. However, it was found that the analytical solution of the wave equation in piezoelectric materials is difficult to derive through direct solution methods [55].

In 1948, Mason demonstrated that in the one-dimensional analysis of piezoelectric materials, most of the difficulties in deriving the solutions could be overcome by borrowing ideas from electric network theory. Mason's equivalent circuit method became widely used and other equivalent approaches are also derived based on similar principles. Several examples of the one-dimensional modelling of piezoelectric transducers can be found in the literature [56-60].

Multi-dimensional wave equations are also used in the modelling of piezoelectric materials. The first proposed two-dimensional model was suggested in 1985 by Hutchens [61]. However such models are usually expensive in terms of solution time and are also often unrealistic for modelling purposes if dynamic behaviour is to be considered. Most multi-dimensional models treat piezoelectric materials solely and are not conducive to multi-layer transducer modelling [62].

For the case of a LT transducer, Shuyu used the equivalent circuit approach to model the coupling between modes approach [34] and the degeneration of L mode approach [32] in a sandwich transducer. The solution is the superimposition of the one-dimensional wave equations for L and T vibrations where two branches of Mason's equivalent circuit are used to solve the equations of wave motion for the LT models.

An analytical modelling is normally inaccurate when compared with reality due to simplifications in the modelling. It is applicable for a system of relatively simple geometry, whereas there will be difficulties finding the solution for complex geometries. It also presents a difficulty when finding the solution for multiple materials, as well as complex loading and boundary conditions. The analytical model requires detailed knowledge of the system and the solution techniques. The analyst is usually responsible for determining the modelling parameters. Nevertheless, analytical models are inexpensive in terms of the required solving time and can provide an abstract description of the system. This modelling strategy can be used to explore different aspects of the system that may not be possible through other modelling methods.

2.7 Numerical modelling methods

Numerical modelling methods, such as the finite element (FE) method, are also a mathematical method that uses a numerical time-stepping procedure to find an approximate solution for the equations that governing the system's behaviour. The process of creating a numerical model based on FE consists of: idealising the system geometry, defining material properties and boundary conditions, discretising the system into a finite element model and then analysing based on the required results. Therefore, the accuracy of FE results depends heavily on the accuracy of performing these steps.

The FE method was first applied to piezoelectric materials by several authors in the late 1960s and early 1970s. Authors such as Allik and Hughes formulated FE models for three dimensional piezoelectric mediums [63]. This formulation was developed and computerised to analyse a complicated three-dimensional piezoelectric transducer in 1974 [64]. In the following years, the FE method gained increasingly popularity for the modelling of piezoelectric systems. However, it was not widely used until 1986 when piezoelectric elements were included in a commercial finite element software package [65]. During that time, most piezoelectric FE analyses were either modal or time-harmonic. However, with the advent of computing and the development of various FE codes, it became possible to perform different types of analysis such as large scale transient analysis for piezoelectric systems.

Numerical solutions have several advantages over analytical solutions. Firstly, the equations are more intuitive and the basic procedures are the same regardless of the complexity of the system. Therefore more realistic models of greater complexity can be investigated. The main drawback of numerical methods is their expensiveness in terms of time consumption and computing requirements. Other disadvantages such as overestimation of parameters and difficulties in representing some aspects, such as nonlinearities and losses, can be minimised through modelling assumptions.

2.8 Conclusions

LT vibration systems have been used in ultrasonic applications since the late 1950s and the early 1960s. Then, due to the lack of an effective method to predict the system behaviour, and the difficulties associated with experimental methods, their improvement has been limited. Two decades later, the developments of numerical methods and measurement

techniques have significantly helped to create different LT systems. Many studies are published based on a combination of FE predictions and experimental validation. Furthermore, an analytical method, which is based on the equivalent electrical circuit method, was developed early in the 1990s to predict the electromechanical parameters of LT systems that could not be accurately predicted by FE models. However, the literature does not offer an adequate methodology to combine FE and analytical models in order to cover most design parameters prior to fabrication. This methodology can help to avoid the high possibility of mismatch between the predicted behaviour and the measured behaviour when only one type of mathematical model is used. FE and analytical methods use different calculation approaches, so it is possible to validate some of the findings prior to fabrication.

In terms of generating LT vibration, it is found that the literature studies used either degeneration or coupling between modes in their approach to produce this vibration in ultrasonic systems. However, the limitations of these approaches were the main reasons that many of these studies have not been implemented on a sufficient scale. The current study aims to focus equally on the advantages and limitations of these methods. By combining the advantages of these approaches it is found that many of the limitations can be removed. Furthermore, this study also aims to develop a generalised approach for the design of LT systems that can fit a wide range of ultrasonic applications.

Chapter 3 Transducer design and numerical modelling

3.1. Introduction

The demands on piezoelectric transducers have increased significantly over the past few decades as different ultrasonic applications have been introduced or developed. These include ultrasonic cutting, ultrasonic welding and ultrasonic drilling. The design of ultrasonic transducers can be described as the process of finding the optimal design variables. These include the variables that determine the material and dimensions of the mechanical (acoustical) and piezoelectric elements, which minimise or maximise a certain number of objectives such as the input power and the output amplitude. These objectives are also subject to specific requirements such as resonance frequency, limitation of input voltage, applied pre-stress and geometric constraints [13].

Transducers were originally designed through the use of one-dimensional analytical models and experimental prototypes [66]. Analytical models simplify the transducer by using the solution of the wave equation to calculate the geometric dimensions. The principle of wave propagation through different media is used to select the appropriate materials for transducer parts. Experimental prototypes employ a trial and error method to characterise and validate the analytical model. However, these approaches have the following disadvantages:

- 1- The solution of the wave equation in the analytical model is complex and sometimes requires unrealistic assumptions.
- 2- The experimental approach is expensive in terms of the number of fabricated prototypes and the required time and equipment for the test.
- 3- The experimental approach is not a reproducible process.
- 4- The overall characteristics of piezoelectric transducers are affected by various factors. These include the lateral dimensions of the front and back masses, the inherent properties of piezoelectric materials, and the electrical and mechanical boundary conditions, which may not be considered in the initial model.

Numerical analysis based on the finite element (FE) method was first introduced for the modelling of piezoelectric materials using three-dimensional (3D) wave equation in 1970 [67]. FE uses a process of numerical analysis that breaks a system into discrete elements in order to solve or simulate the problem. It aims to obtain an approximate solution or estimation for different problems. The use of FE in analysis, design and product refinement has developed in parallel with advances in computing power where many FE codes have been developed to provide accurate results for complicated problems.

FE analysis of a system is classified as an approximate solution technique because it considers perfect parameters of material properties and boundary conditions. In reality these parameters contain flaws or imperfections. However, the level of inaccuracy within the approximation can be minimised by considering parameters that simulate the real system. FE requires large amounts of computation memory and time, especially for the analysis of high frequency three-dimensional problems, however the development in computer processing makes these requirements achievable [68].

In this chapter, the principles of Langevin transducer design, which uses an exponential horn as the front mass, are presented. Initially, the basic concepts of ultrasonic power transducer devices are reviewed. Next, the optimisation parameters of the intended design are described. Then the numerical modelling steps and the solution techniques are presented. Finally, some of the results are discussed and the preferred design is selected.

3.2. Design parameters of power ultrasonic transducers

Ultrasonic transducers are used to transfer high frequency electrical energy into high frequency mechanical vibration. Normally, power ultrasonic transducers are designed to operate in a frequency range between 20-100kHz to obtain higher output intensities.

The design parameters of piezoelectric transducers are different depending on the application. However, there are some common parameters that are shared between most applications. These parameters, along with the special requirements of the proposed design, are now summarised.

3.2.1. Driving frequency and wavelength

The driving frequency is selected based on the requirements of the application. Most ultrasonic transducers are designed to be driven at a resonance frequency f so as to maximise vibration amplitudes. In the case of longitudinal mode transducers it is common

to use the resonance frequency of the first longitudinal vibration mode (the fundamental mode) where the highest amplitude can be obtained.

When designing ultrasonic resonators, the resonance frequency is used to calculate the wavelength λ as follows:

$$\lambda = \frac{c}{f} \quad 3.1$$

where c is the wave velocity of longitudinal vibration which depends on the acoustic properties of the resonator. For a resonator of uniform cross section that is composed of homogeneous material, the wave velocity is found by:

$$c = \sqrt{\frac{E}{\rho}} \quad 3.2$$

where E and ρ are the Young's modulus of elasticity and the density of the resonator material, respectively. However, for a non-uniform cross-sectional resonator, such as an exponential resonator, the wavelength can be calculated by [69, 70]:

$$\lambda = \frac{c}{2\pi f} \sqrt{(2\pi)^2 + (\ln n)^2} \quad 3.3$$

where n is the ratio of the small end to the large end radius.

The wavelength is used to calculate the length of the resonator. In general, this can be equal to a quarter wavelength, half a wavelength or one wavelength. However, the half wavelength resonators are the most used in ultrasonic applications.

The ultrasonic transducer is a combination of different parts; and therefore different materials. The above equations cannot be applied directly to calculate the overall length. Instead, the transducer model is divided into sections, where these equations can be applied to each section individually.

Similar to ultrasonic resonators, most ultrasonic transducers are designed with the half wavelength pattern. This has the advantage that it is easily combinable with other half wavelength parts such as boosters, horns and tools. This advantage is necessary to form the whole ultrasonic system without changing the eigenshape of each part, as shown in Figure 3-1. Another advantage of half wavelength synthesis is that, in the ideal case, there is no force acting at the interfaces between the individual parts. Therefore, the boundary conditions of each part in the whole synthesised system are the same as those of each separate part, free at both ends. Each part can then be initially developed according to the specified resonance frequency and then these parts are synthesised to produce the whole system [13].

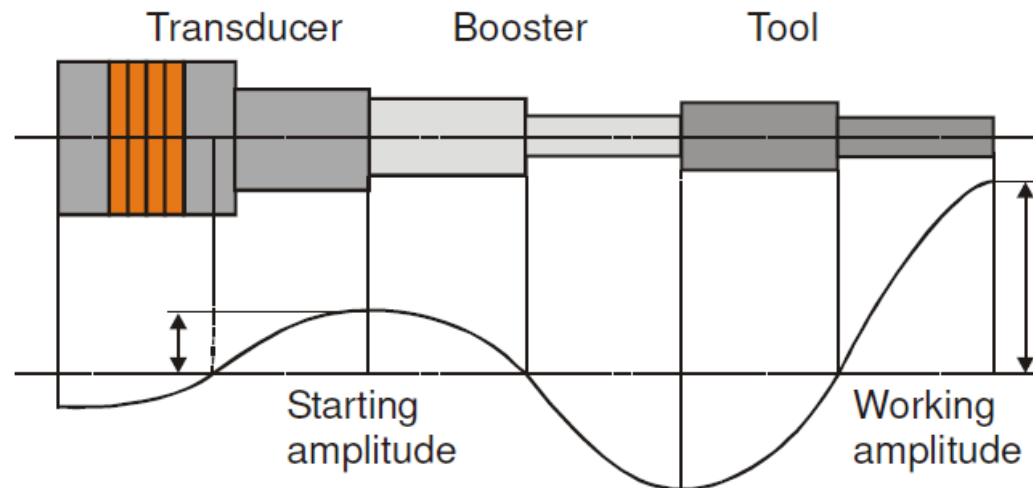


Figure 3-1 The principle of half wavelength synthesis [13].

3.2.2. Selection of piezoelectric components

Piezoelectric materials are categorised according to their chemical composition and the specific application conditions. For the effective design of a power ultrasonic transducer, the following criteria are required [71]:

- 1- The piezoelectric material can withstand a high electric driving voltage and mechanical loads.
- 2- It has low dielectric loss at high driving level and high permittivity.
- 3- It requires a high mechanical quality factor and high Curie temperature.
- 4- It has high coupling coefficient between the electrical and mechanical energy and stable properties (low dependency on time and temperature).

The dimensions of the piezoelectric components are selected based on the output acoustic power required, the operating mode of vibration and the type of transducer model. In the case of longitudinal mode power transducers, the thickness of piezoelectric components is normally less than one-tenth of the wavelength. This thickness limit is used to retain reasonably high coupling between electrical and mechanical energy and to improve the power handling capacity [59]. The displacement of each element is very small, therefore several components are connected mechanically in series so that the displacement of the whole stack assembly is equal to the summation of the individual displacements [11]. However, increasing the number of elements in the stack leads to an increase in the mechanical losses due to an increase in the size of the boundaries between these components. The lateral dimensions of the components are normally less than a quarter of wavelength to avoid coupling between the longitudinal and lateral modes. Also this

prevents the possible excitation of unwanted modes. The geometrical shape of the component is selected based on the geometry of the proposed transducer design and the method of applying pre-stress on the piezoelectric components. For a Langevin transducer, with a central pre-stressed bolt, a ring shape component is usually selected [72].

3.2.3. Selection of metal parts

The Langevin ultrasonic transducer has two types of materials: piezoelectric material, which represents the vibrational generator, and the metal material, which represent the vibrational transmitter. For effective transmission of acoustic energy between these materials, and to avoid the internal reflection of stress waves, the acoustic properties should be matched. The following equation can be used to satisfy this condition [72]:

$$Z_c = \sqrt{Z_f Z_b} \quad 3.4$$

where Z_c , Z_f and Z_b are the acoustical impedances of the piezoelectric materials and the front and back masses, respectively. These impedances are calculated by multiplying the characteristic acoustical impedance Z_o by the cross-sectional area of the transducer's parts. The characteristic acoustical impedance is a material property produced by multiplying the material density ρ by the wave velocity c .

Another condition for effective use of the acoustic energy is to guide most of generated vibration in the piezoelectric material towards the front mass rather than the back mass where the energy is not required and therefore represents an energy loss. In a longitudinal mode transducer, the acoustical energy that is generated in the piezoelectric material transmits to both front and back masses. Therefore, in order to minimise the energy loss, the back mass should have higher acoustical impedance than the front mass, so that most of the energy will be guided toward the front mass. A list of recommended materials for ultrasonic applications which can satisfy these two conditions is shown in Table 3-1. The wave velocity and the characteristic acoustical impedance are presented for each material.

The fatigue strength is another important parameter that should be considered in the selection of the metal parts. These parts will be subjected to very high cyclic loading and this can initiate cracks and fatigue failure. Therefore high fatigue strength is essential.

Table 3-1 Properties of the recommended materials[73].

No.	Material	Wave velocity (m/s)	Characteristic acoustical impedance (N.s/m ³)
1	Grade 5 Titanium alloy (Ti-6Al-4V)	4900	39.2 x10 ⁶
2	Aluminium alloy (AlCuMGPb 2011)	5000	14.25 x10 ⁶
3	Aluminium alloy (AlCuMg2 2024)	5100	14.28 x10 ⁶
4	Tool Steel	5250	41.2 x10 ⁶

3.2.4. Transducer securing feature

Ultrasonic transducers should be secured into housing for safe operation and easy adaptation to different arrangements of ultrasonic systems. For the Langevin transducer, the securing feature is normally a flange adapted from the main parts of the transducer. As the vibrational amplitude varies along the transducer, it is important to secure it at a position where it will have the minimum influence on vibrational amplitude. The nodal plane, which is the plane of zero vibrational amplitude, represents the best selection as a securing location. For a traditional symmetrical transducer, the nodal plane is located at the middle of the piezoelectric components. This presents a number of difficulties as a location for the securing feature. This is because the piezoelectric materials are composite materials which have low machinability. Also the maximum stress occurs at the nodal plane and this can lead to increase in temperature which can lead to destruction of the piezoelectric component. It is also important to ensure that the location of securing feature does not change the boundary conditions for the design of the transducer. Therefore, in the current modelling, the length of the back mass is modified such that the nodal plane can be shifted from the piezoceramic section to the front mass.

3.3. Performance criteria

The optimisation of transducer design is based on performance criteria which are, like the design parameters, a combination of specific application criteria and general ultrasonic transducer design criteria. For the proposed design, the following criteria are used:

3.3.1. Frequency separation between vibrational modes

The proposed transducer should have sufficient frequency separation between the operating frequency and all other undesired resonances. Otherwise, the supplied power may accidentally jump to a secondary resonance; especially during the transient starting conditions or under highly loaded conditions. Such a jump could cause poor or erratic performance and could overstress the transducer. Poor frequency separation may also cause non-uniform or asymmetric transducer vibration amplitudes, which may lead to early transducer failure. Frequency separation between modes can be estimated by modal analysis where the resonance frequencies of the desired vibrational mode and the nearest (surrounding) modes are determined. It is generally considered that the ratio of the frequency difference between the desired mode and the neighbouring mode to the frequency of the desired mode should not be less than 10%. However, during operation the frequency separation of neighbouring modes is effected by other parameters such as device loading and temperature changes due to self-heating of the piezoceramic material and heating of the working ultrasonic tool.

3.3.2. Torsionality

Torsionality is defined as the ratio of torsional to longitudinal response at the output surface of the transducer. The proposed design is intended to produce high torsionality through the conversion of generated L vibration into a combination of L and T vibration at the output surface. It is also important to ensure that it maintains constant torsionality over a wide range of excitations for different boundary conditions (free and loaded). The required torsionality can vary depending on the application. In ultrasonic drilling, for example, a torsionality of 1, where the torsional response is equal to the longitudinal response, is desirable.

3.3.3. Characteristic frequencies

Piezoelectric transducers are a combination of electrical and mechanical parts. Subsequently there are three pairs of characteristic frequencies. The first pair is series f_s and parallel f_p frequencies at which the infinite and zero electrical admittance of a lossless transducer model will occur, respectively. The second pair is the frequencies f_m and f_n at which the electrical admittance becomes maximum and minimum, respectively. Finally,

the third pair is the resonance frequency f_r and the anti-resonance frequency f_a at which the phase angle between the input voltage and current is zero which is shown in Figure 3-2. In the initial modelling stages of ultrasonic transducers, these frequencies are approximately equal, this means $f_s \approx f_m \approx f_r$ and $f_p \approx f_n \approx f_a$ [13].

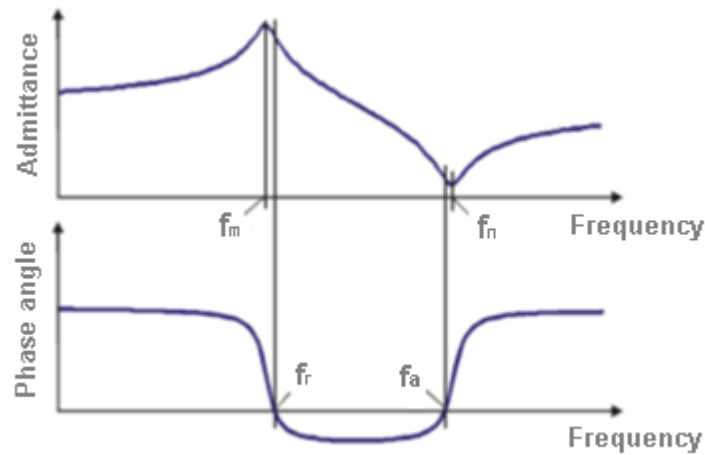


Figure 3-2 Variation of admittance magnitude and phase angle with frequency [13].

3.3.4. Electrical input power

The input electrical power P_e to an ultrasonic transducer operating at resonance is calculated by:

$$P_e = V I \quad 3.5$$

where V and I are the AC input voltage and the current respectively. However, it is often not possible to drive a transducer exactly at resonance; this will show a capacitive or inductive behaviour. Therefore, the mean power (effective power) \hat{P}_e equation is used and in the case of harmonic excitation, it is determined as:

$$\hat{P}_e = \frac{1}{2} \hat{V} \hat{I} \cos \varphi_e \quad 3.6$$

where \hat{V} and \hat{I} are the mean values of the input voltage and the current respectively, and φ_e is the phase difference between the input voltage and current.

3.3.5. Mechanical output power

Through an analogy with the definition of electrical power, the harmonic vibration effective power \hat{P}_m can be calculated by:

$$\hat{P}_m = \frac{1}{2} \hat{F}_m \hat{v}_m \cos \varphi_m \quad 3.7$$

where \hat{F}_m and \hat{v}_m are the mean values of the output force and the velocity respectively, and φ_m is the phase difference between the output force and velocity.

3.3.6. Coupling factor

The electromechanical coupling factor k_{ij} is an indicator of the efficiency of energy conversion in the piezoelectric component. The first subscript indicates the perpendicular direction to the electrical poles, whilst the second subscript denotes the direction along which the mechanical energy is developed. The value quoted in the piezoelectric supplier's specifications is typically the maximum theoretical value. Although the highest value is usually desirable for the efficient design of a piezoelectric transducer, it does not represent the overall efficiency of the transducer, this is due to the fact that it does not consider the loss or the recovery of unconverted energy in the transducer [11, 74].

An accurate measurement for the efficiency of energy conversion in a piezoelectric component is called the effective coupling coefficient k_{eff} . This is the ratio of useable energy that is delivered by the component to the total energy that it consumes. Although it is difficult to find the effective coupling coefficient based on this definition, it is possible to calculate it by using the characteristic frequency values as follows:

$$k_{eff}^2 = \frac{f_p^2 - f_s^2}{f_p^2} \quad 3.8$$

where f_s and f_p are the series and parallel resonances of transducer, respectively. For an optimum design, the ratio of the effective coupling coefficient k_{eff} to the piezoelectric material coupling coefficient in the thickness mode k_t should be approached [12].

3.3.7. Mechanical quality factor

The mechanical quality factor Q_m is defined as the energy stored in the transducer to the energy supplied by the generator per cycle. It gives the rise of resonance amplitude where a higher quality factor corresponds to high transducer efficiency and large resonant amplitude. It can be used to calculate the mechanical loss factor $\tan \delta_m$ according to following relation:

$$\tan \delta_m = \frac{1}{Q_m} \quad 3.9$$

3.4. Design of a longitudinal-torsional transducer

The longitudinal-torsional (LT) Langevin transducer, for power ultrasonic applications, consists of: an exponential front mass, a stack of piezoelectric components sandwiched between metal electrodes, a hollow cylindrical back mass and a pre-stressed bolt. The following steps are used to design such a transducer.

The first step is to choose an initial value for the operating frequency f , in order to produce high amplitude and to minimise the effect of heat generation on the transducer's performance. The initial value is chosen as 20kHz which represents, theoretically, the low ultrasonic threshold.

The second step is to select materials for the transducer parts. There are different configurations of materials, which are selected based on the application, and the acoustic matching for electromechanical conversion. For power ultrasonic applications, several manufacturers supply Lead Titanate Zirconate (PZT) material with desirable properties [59]. The properties of PZT can be optimised to suit specific applications through the appropriate adjustment of the chemical composition at the fabrication stage. It is also a hard material which is chemically inert and completely insensitive to humidity or other atmospheric influences [11].

Two types of piezoceramic ring shape components, with different dimensions, are selected in the current work. The first type is Sonox P8 from CeramTec GmbH. This is characterised by its ability to withstand high electrical driving and intense mechanical load. It also offers low dielectric losses and has a high permittivity (between 900-1400) as well as high mechanical quality factor (between 500-2000) and a high Curie temperature [71].

The second type is PIC 181 from PI Piezotechnology. This modified PZT material is characterised by its extremely high mechanical quality factor and its high Curie temperature. It is specialised for high power applications, showing good stability over time, as well as high dielectricity and good elastic properties [75]. These two types are used to design different sizes of the proposed transducer. The geometric dimensions of the rings are listed in Table 3-2.

Table 3-2 Dimensions of piezoceramic components.

	Inner diameter (mm)	Outer diameter (mm)	Thickness (mm)	Dielectric loss factor $\tan \delta$	Relative permittivity $\epsilon_{33}^T/\epsilon_0$	Mechanical quality factor Q_m
Sonox P8	16	38	5	0.002	1000	1000
PIC 181	5.2	12.7	1.5	0.003	1200	2000

The elastic, piezoelectric and dielectric properties of piezoceramic materials are characterised by the fundamental constants which are obtained from a series of measurements on samples of various orientations [10]. According to the selected experimental technique, these samples are also subjected to many other considerations such as their size and shape. It is difficult to fulfil the criteria that are stipulated for these tests to be carried out successfully. Therefore, the manufacturer supplied data is considered in this work [71, 75].

For the metal parts, a grade 5 Titanium alloy (also known as Ti-6Al-4V or for simplicity Ti-6-4) is used for the exponential front mass and the pre-stressed bolt. This is because it has high tensile strength, high toughness even at extreme temperatures, light weight and good acoustic properties. Low carbon steel is used for the back mass due to its high density and therefore high characteristic acoustical impedance. Finally, a copper alloy C101 is used for the electrodes due to the high electrical conductivity.

The elastic properties of the titanium alloy Ti-6-4 can be obtained from the literature with reasonable accuracy. However, there is wide range of data for steel. For example the Young's modulus of low carbon steel can vary, depending on the composition and manufacturing process, between 68.9 - 213GPa [76]. If this range is used to define the elastic properties of the back mass material for the longitudinal transducer in the FE model, the resonance frequencies of the desired L mode and two surrounding modes, F and T, can considerably vary as shown in Figure 3-3. Therefore, it is important to obtain accurate values for the elastic properties of materials prior to the creation and analysis of the FE model.

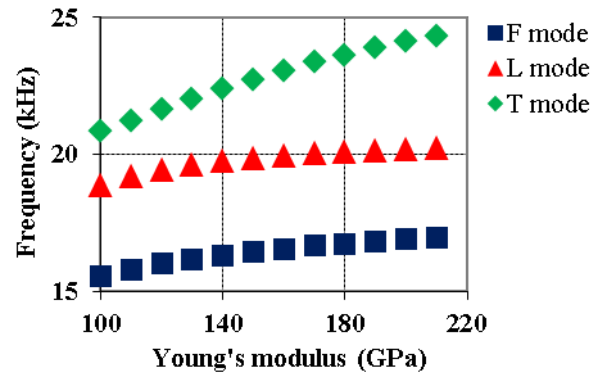


Figure 3-3 Variation of resonance frequencies of longitudinal transducer with the modulus of elasticity of the back mass material.

3.4.1. Experimental tensile test

A tensile test is conducted by pulling a specimen, of a predefined geometry, along an axis until failure occurs in the specimen. The applied force and the extension displacement of the specimen are measured during the pulling process. The measured quantities are used to derive a stress-strain curve for the material, which is used to extract the modulus of elasticity (also called Young's modulus of elasticity or tensile modulus). This modulus is a measure of the stiffness of a material in its elastic region and it is defined as the ratio of the uniaxial stress to the uniaxial strain. It is used in FE codes to characterise the elasticity of isotropic materials.

There are several techniques that can be used to apply the pulling load and measure the extension of the specimen. These depend on the specimen type and the required accuracy of the results. In the current work, the tensile test set-up and the specimen geometry of a rounded dog bone shape are considered according to the BSI 10002-1 standard [77]. The tensile test procedure is implemented by testing 4 specimens of each material (the titanium alloy and the low carbon steel) through the use of a computerised tensile test machine (Zwick Roell Z250) with an extensometer (Epsilon 3542), as is shown in Figure 3-4. The strain rate of the test is chosen according to the standard and the average value of the test results for each material is considered in the FE model in accordance with Table 3-3.

The material properties of the transducer's parts are shown in Table 3-4, where the density of the titanium alloy and the low carbon steel are extracted experimentally. The copper electrodes are normally thin sheet. Therefore their properties, and the Poisson's ratios of all metal parts, are taken from reference [76].

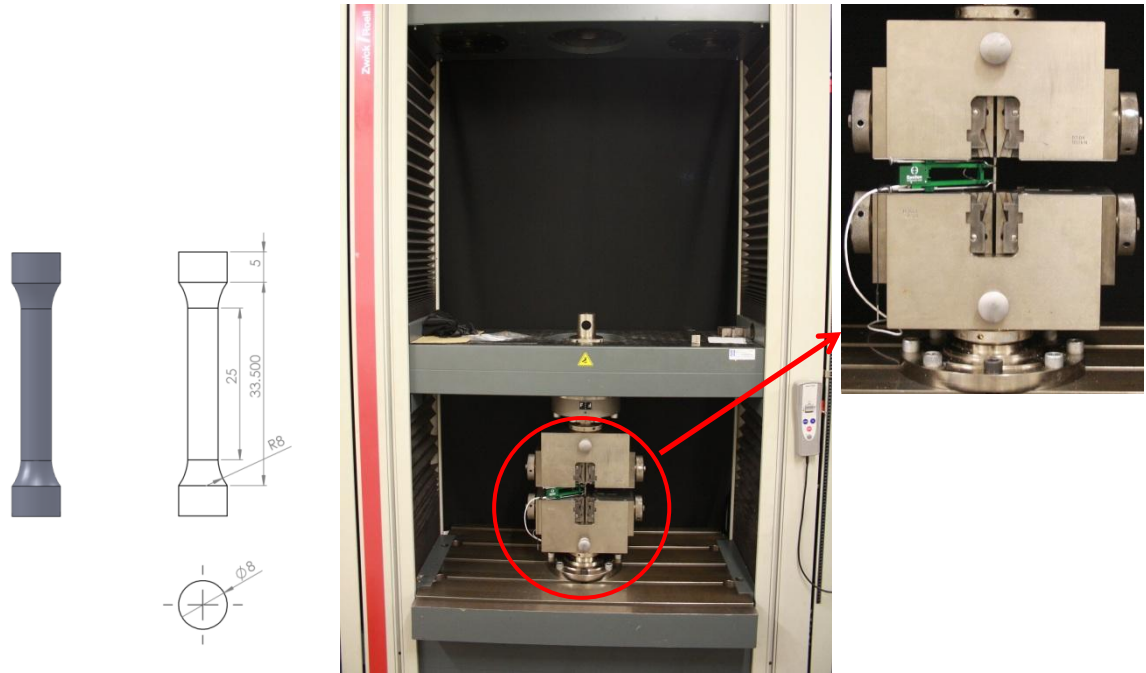


Figure 3-4 Tensile test specimen (left) and Tensile test setup (right).

Table 3-3 Experimental results for the modulus of elasticity.

No.	E (low carbon steel) GPa.	Average value	% error	E (titanium alloy Ti-6-4) GPa.	Average value	% error
1	174.46	179.18	2.6	115.46	110.40	4.5
2	171.29		4.4	107.56		2.5
3	186.88		4.2	106.16		3.8
4	184.09		2.7	112.43		1.8

Table 3-4 Materials properties of the transducer parts.

No.	Part	Material	Young's modulus (GPa)	Density (kg/m ³)	Poisson's ratio	Wave velocity (m/s)
1	Piezoelectric rings	P8	73	7700	-	3080
		PIC 181	70.4	7800	-	3005
2	Electrodes	Copper C101	115	8900	0.31	3595
3	Back mass	Low carbon steel	179.18	7723	0.3	4816
4	Front mass	Titanium alloy	110.40	4418	0.342	5027
5	Pre-stressed bolt	Ti-6-4				

The third step is to calculate the dimensions of the different parts. The front mass is designed so that it is a quarter of the wavelength whilst the other quarter of the wavelength

consists of the back mass and the piezoceramic stack. The following relationship can be used to calculate their lengths [59, 72]:

$$\frac{Z_b}{Z_c} \tan\left(\frac{2\pi f l_b}{c_b}\right) \tan\left(\frac{2\pi f l_c}{c_c}\right) = 1 \quad 3.10$$

where Z_b , c_b , Z_c , c_c are the acoustical impedance and the wave velocity of the back mass and the piezoelectric components, respectively. The length of the back mass is l_b and the length of piezoelectric stack is l_c . Both of these are the unknown variables in this equation. Two P8 piezoceramic components are chosen for the initial design. Therefore, by using the dimensions in Table 3-2, the length of piezoceramic stack is 10mm. Equation 3.10 is then used to calculate the length of the back mass section. Finally the copper electrodes are chosen as 0.4mm thickness which is selected based on better conductivity and rigidity.

The lateral dimensions of the back mass, the base of the front mass and the electrodes are equal to the lateral dimensions of the piezoceramic rings, which are given in Table 3-2. However, the back mass inner diameter is equal to the outer diameter of the pre-stressed bolt which is required to be less than the inner diameter of the piezoceramic ring. This is necessary to create a gap between the pre-stressed bolt and the piezoceramic stack so that an electrical insulator layer can be inserted to prevent an electrical short between electrodes.

The front mass cross-section is shown in Figure 3-5. This consists of a base section, a middle exponential section and a front cylindrical section. The total length l_t is calculated as a quarter of the wavelength by using a combination of Equations 3.2 and 3.3. The base section l_{base} is an important securing feature for the transducer and its length is chosen as 15mm. This section is also used to hold the transducer during the pre-stressing process. The front end l_{front} is used to allow for the attachment of other resonator parts to the transducer and the length is taken as 5mm. These dimensions are considered initially, based on the required tuned length, and then optimised by modal analysis for the location of nodal plane. The reduction in the radius of the exponential section r_z along the decay section is calculated as follows:

$$r_z = r_o e^{-\gamma z} \quad 3.11$$

where r_o and γ are the radius at the large end and the exponential decay coefficient, respectively. This coefficient can be calculated as:

$$\gamma = \frac{\ln\left(\frac{r_o}{r_l}\right)}{l_e} \quad 3.12$$

where r_l is the radius of the small end of exponential section.

Finally the dimensions of the pre-stressed bolt are selected based on the empirical recommendations by MP Interconsulting (MPI). It is suggested that M12 is used for the current design [12, 72].

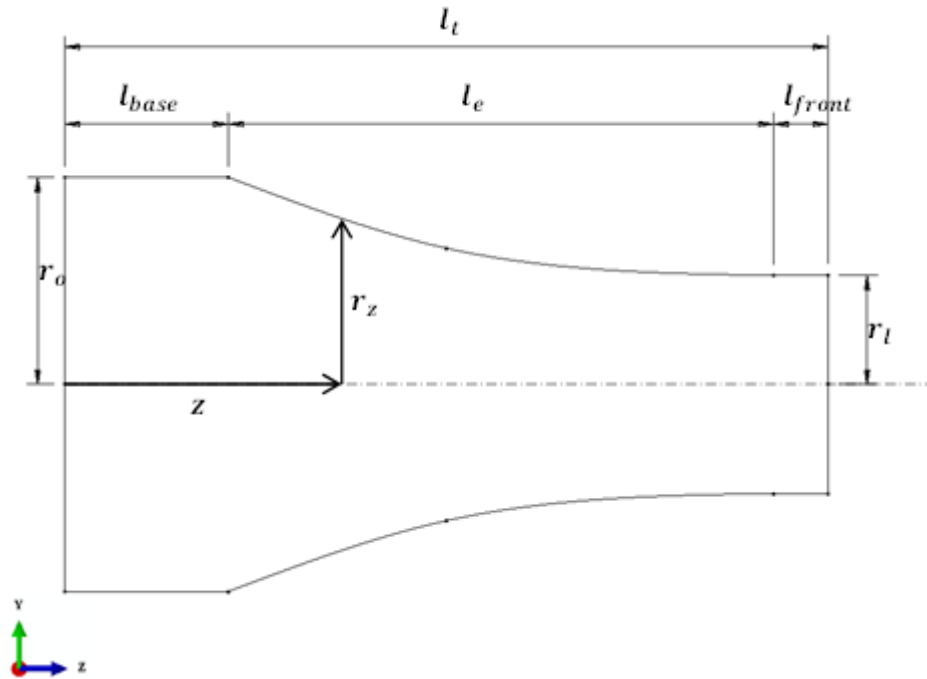


Figure 3-5 Profile of the front mass.

3.4.2. Addition of slots to the front mass

In the proposed design, the conversion of generated L vibration into a combination of LT vibration occurs in the front mass through the addition of geometric slots. This technique is implemented by cutting and extruding (with axial rotation) a number of slots along the decay section of the front mass. The conversion efficiency mainly depends on the number, dimensions and twist angle of these slots. Three different profile cuts are suggested, these are rectangular, trapezoidal and quarter circle cuts, which will be presented in section 3.6. An optimisation study is performed to study the effect of their dimensions and twist angle on the performance of the LT transducer. The parameters for the optimisation are the torsionality, the frequency separation between modes, the ratio of the longitudinal response at the front and back faces, and the location of the nodal plane along the transducer model.

3.5. Numerical modelling of the LT transducer

The calculated dimensions in section 3.4 are used to create the geometry for the initial design of a Langevin transducer using Abaqus/CAE v6.10-2, a commercial multi-disciplinary FE code. This code is used throughout the work to simulate the vibrational behaviour of the transducer. It is also used to study the linear dynamic behaviour of the transducer through harmonic excitation analysis.

The transducer parts are created and assembled as shown in Figure 3-6. The unslitted model is symmetric along the axial plane, so it would be possible to analyse it using a two-dimensional (2D) model, which would significantly reduce the computation power required. The introduction of the required slots to the front mass will remove this symmetry, it is therefore required that the transducer is analysed using a three-dimensional (3D) model. The 3D model is also necessary for studying the torsional behaviour as it cannot be represented in a 2D model.

The FE analysis of the transducer is a continuum problem in which all parts of the model are continuous at all points in space. The solution to such a continuum problem can be developed from the following general procedure steps:

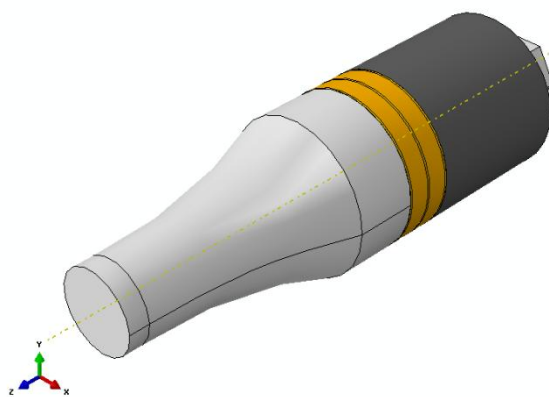


Figure 3-6 Initial model of the ultrasonic transducer.

3.5.1. Definition of material properties

In FE codes, a set of material properties is defined by specifying the relevant data of each property into the material module provided by the code. Selecting material properties mainly depends on the type of analysis required whilst the property behaviour is selected based on the type of material. This may be linear or nonlinear, as well as, isotropic or anisotropic. Abaqus material library provides general categories for different material modules where the relevant data can easily be specified. These categories include general properties such as material density, and elastic mechanical properties, as well as, electrical properties such as piezoelectricity and dielectricity.

When modelling a piezoceramic transducer, the required definition for materials can be classified into two types: metal and piezoelectric.

3.5.2. Defining of metal materials

For vibration and dynamic analysis, the properties required for metal parts are the mechanical elastic and the general mass properties. These properties are considered to be linear and isotropic, these are adequate assumptions for small elastic strain (normally less than 5%) [78].

For the mechanical elastic property, the required data is: the Young's modulus of elasticity, Poisson's ratio and the material density for the general mass property. These properties are listed in Table 3-4.

3.5.3. Defining of piezoceramic materials

In general, the analysis of piezoelectric materials requires a complete consideration of the mechanical, electromechanical and electrical aspects of these materials. This can be obtained by defining the elasticity, the piezoelectricity and the dielectricity (or permittivity) properties, respectively. Additionally, the general mass properties are also required for vibration and dynamic analysis.

As mentioned previously, the material property behaviour can be classified as isotropic or anisotropic. Isotropic behaviour assumes that the properties are directionally independent. For elastic properties, this means that the normal stresses produce normal strain whilst shear stresses produce shear strain only, as shown in Figure 3-7. In contrast, anisotropic properties are direction dependent. Therefore the normal stresses can produce both normal

and shear strain and the shear stresses also can produce normal and shear strain, as shown in Figure 3-8. There is another classification, named orthotropic behaviour, in which the material properties are dependent on three mutually perpendicular symmetry planes. Some engineering materials including certain piezoelectric materials, such as Rochelle salt, are orthotropic materials [79]. Within the orthotropic classification, there is a special case in which the material properties behave as isotropic only in two directions. This case is called transverse isotropic and means that the material has isotropic properties in one plane and different or anisotropic properties in the direction normal to this plane [79]. Some piezoceramic materials, such as PZT-4 and barium titanate, are considered to be transverse isotropic, here the anisotropic axis is normally assigned as the direction of polarisation in these materials.

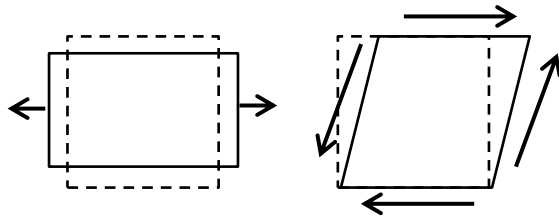


Figure 3-7 Extension and shear deformation of isotropic material

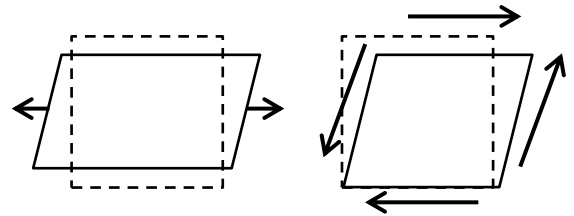


Figure 3-8 Extension and shear deformation of anisotropic material[80].

The coupling between the electrical and mechanical parts of piezoelectric materials requires a mathematical form to relate to the relevant data from the material properties. These properties can be described by tensor notation. This is a mathematical framework for formulating and solving physical problems. A tensor is classified by its order (also called degree or rank), which represents the dimensionality of the array required to represent this tensor. For example a scalar quantity, such as density, is represented by a single number and is therefore considered to be a zero order tensor. A tensor is usually denoted by indices that can be subscript and superscript, after a symbolic variable. The number of indices gives the order of the tensor. For example, the elastic stiffness constant for piezoelectric materials is a fourth order tensor C_{ijkl} , while the piezoelectric constant d_{ijk} is a third order tensor. For simplicity, it is possible to write this long notation from the tensor form into a compressed matrix array form in which the notation ij or kl is replaced by p or q respectively. Notations such as i, j, k, l take the values 1,2,3, whilst the notation p, q take the values 1,2,3,4,5,6. This compressed form is normally used by manufacturers to provide

elastic and piezoelectric data. However, Abaqus requires that the data is written in the tensor form. Therefore, in order to convert these forms, tensor notation is introduced in the place of the compressed matrix notation according to Table 3-5 [10, 78].

When the tensor form is used, a rectangular system identifies the geometry through the subscripts: x , y , and z . This system is normally replaced by notation using 1, 2, and 3 respectively. Also the shear components xy , xz , and yz are replaced by 4, 5 and 6 respectively. Finally, the direction of positive polarisation is normally aligned with the z -axis of the rectangular system (or direction 3) [74]. Then the anisotropic axis of the material properties behaviour will be consistent with the directions mentioned previously.

Table 3-5 Conversion of matrix to tensor notation.

<i>p</i> or <i>q</i>	<i>ij</i> or <i>kl</i>
1	11
2	22
3	33
4	12
5	13
6	23

3.5.3.1. Elasticity of piezoelectric material

The material elastic property is defined by the modulus of elasticity C_{ij} where the first subscript indicates the stress direction and the second subscript indicates the strain direction. It can also be defined by the elastic compliance s_{ij} , which is the reciprocal of C_{ij} . In this case, the first subscript indicates the strain direction while the second subscript indicates the stress direction.

For piezoelectric materials, the modulus of elasticity C_{ij} , or the elasticity compliance s_{ij} , can be evaluated under a constant electrical displacement C_{ij}^D or s_{ij}^D respectively, where the superscript D indicates a constant electrical displacement (open circuit). They can also be evaluated at a constant electrical field as C_{ij}^E or s_{ij}^E respectively. Here the superscript E indicates the constant electrical field (short circuit). The elastic modulus evaluated at short circuit conditions is less than its value when evaluated under an open circuit conditions because the mechanical stress of the piezoelectric material produces an electrical response which opposes the resultant strain [74, 81].

Abaqus considers the modulus of elasticity to be evaluated at a constant electrical field C_{ij}^E . It is defined in the tensor form, which is referred to as D_{ijkl} , rather than the simple form. A linear elastic model is provided by Abaqus to describe the stress-strain relationship. This is valid for small elastic strains as follows [78]:

$$\sigma_{ij} = D_{ijkl}\epsilon_{ij} \quad 3.13$$

Where σ_{ij} and ϵ_{ij} are the total stress and total elastic strain, respectively, and D_{ijkl} is the elastic stiffness parameter evaluated at a constant electrical field in the form of a fourth order elastic tensor. For a general orthotropic material, the elasticity tensor is given in a symmetric matrix form as follows:

$$[D] = \begin{bmatrix} D_{1111} & D_{1122} & D_{1133} & 0 & 0 & 0 \\ & D_{2222} & D_{2233} & 0 & 0 & 0 \\ & & D_{3333} & 0 & 0 & 0 \\ & & & D_{1212} & 0 & 0 \\ & \text{symmetric} & & & D_{1313} & 0 \\ & & & & & D_{2323} \end{bmatrix} \quad 3.14$$

where D_{ijkl} parameters are defined as follows [78]:

$$D_{1111} = E_1(1 - \nu_{23}\nu_{32})Y \quad 3.15a$$

$$D_{1122} = E_1(\nu_{21} - \nu_{31}\nu_{23})Y = E_2(\nu_{12} - \nu_{32}\nu_{13})Y \quad 3.15b$$

$$D_{1133} = E_1(\nu_{31} - \nu_{21}\nu_{32})Y = E_3(\nu_{13} - \nu_{12}\nu_{23})Y \quad 3.15c$$

$$D_{2222} = E_2(1 - \nu_{13}\nu_{31})Y \quad 3.15d$$

$$D_{2233} = E_2(\nu_{32} - \nu_{12}\nu_{31})Y = E_3(\nu_{23} - \nu_{21}\nu_{13})Y \quad 3.15e$$

$$D_{3333} = E_3(1 - \nu_{12}\nu_{21})Y \quad 3.15f$$

$$D_{1212} = G_{12} \quad 3.15g$$

$$D_{1313} = G_{13} \quad 3.15h$$

$$D_{2323} = G_{23} \quad 3.15i$$

$$Y = \frac{1}{1 - \nu_{12}\nu_{21} - \nu_{23}\nu_{32} - \nu_{31}\nu_{13} - 2\nu_{21}\nu_{32}\nu_{13}} \quad 3.15j$$

For orthotropic materials, nine constants are required to be calculated prior to defining the elastic tensor matrix. These are the elastic moduli (E_1, E_2, E_3), the Poisson's ratios ($\nu_{12}, \nu_{13}, \nu_{23}$) and the shear moduli (G_{12}, G_{13}, G_{23}). However, for transverse isotropic materials, where the mutual plane is considered to be in the z -direction, the following relations are considered to simplify the elastic matrix:

$$E_1 = E_2 \quad 3.16a$$

$$\nu_{13} = \nu_{23} \quad 3.16b$$

$$G_{12} = G_{13} = G_{23} \quad 3.16c$$

The manufacturers normally provide two elastic compliance parameters for a constant electrical field, these are s_{11}^E and s_{33}^E as well as the Poisson's ratio ν_{13} . Therefore the following relations and assumptions are used to calculate the required constants [9]:

$$E_1 = \frac{1}{s_{11}^E} \quad 3.17a$$

$$E_3 = \frac{1}{s_{33}^E} \quad 3.17b$$

$$s_{12}^E = 0 \quad 3.17c$$

$$\nu_{12} = \nu_{21} = 0 \quad 3.17d$$

$$\nu_{31} = \nu_{13} \frac{E_3}{E_1} \quad 3.17e$$

$$\nu_{32} = \nu_{23} \frac{E_3}{E_2} \quad 3.17f$$

$$G_{12} = \frac{1}{2(s_{11}^E - s_{12}^E)} \quad 3.17g$$

Therefore Equations 3.16a to 3.16c and 3.17a to 3.17g can be combined with equations 3.15a to 3.15j to calculate the stiffness parameters of the elastic tensor matrix in Equation 3.14.

3.5.3.2. Piezoelectric properties of the piezoelectric material

The piezoelectric property of the piezoelectric material defines the relationship between the mechanical deformation and the electrical field. There are three constants which are used to characterise the piezoelectric property for different applications. The first constant is a piezoelectric charge constant, d_{ij} , which relates the mechanical strain to the electrical field. The first subscript of d_{ij} indicates the direction of the applied electrical field while the second subscript indicates the direction of the induced strain.

The second constant is also named a piezoelectric charge constant and is denoted by e_{ij} . However, it relates the mechanical stress to the electrical field, where the first subscript of e_{ij} indicates the direction of the applied electrical field and the second subscript indicates the direction of the induced stress. These two parameters are normally used as important indicators for actuator applications because the induced strain (or stress) in applying an

electrical field is the product of the electrical field value and this constant. Therefore they have a high influence on the current design.

The third constant that is used to characterise the piezoelectricity, is the piezoelectric voltage constant g_{ij} . This relates the electrical field to the mechanical stress. The first subscript of g_{ij} indicates the direction of the applied mechanical stress and the second subscript indicates the direction of the generated electrical field. It is an important parameter to assess the suitability of material for sensing applications because the strength of the induced electrical field that is produced by a piezoelectric material in response to an applied physical stress is the product of the value of the applied stress and this parameter.

Abaqus provides linear relations between the mechanical and electrical fields in a matrix as follows [78]:

$$[d] = \begin{bmatrix} d_{111} & d_{122} & d_{133} & d_{112} & d_{113} & d_{114} \\ d_{211} & d_{222} & d_{233} & d_{212} & d_{213} & d_{214} \\ d_{311} & d_{322} & d_{333} & d_{312} & d_{313} & d_{314} \end{bmatrix} \quad 3.18$$

It is also possible to define the piezoelectric charge constant in stress form as:

$$[e] = \begin{bmatrix} e_{111} & e_{122} & e_{133} & e_{112} & e_{113} & e_{114} \\ e_{211} & e_{222} & e_{233} & e_{212} & e_{213} & e_{214} \\ e_{311} & e_{322} & e_{333} & e_{312} & e_{313} & e_{314} \end{bmatrix} \quad 3.19$$

For a piezoelectric material poled in the thickness direction (the z -direction or 3-direction), matrices in Equations 3.18 and 3.19 are simplified to the following formats:

$$[d] = \begin{bmatrix} 0 & 0 & 0 & 0 & 0 & d_{123} \\ 0 & 0 & 0 & 0 & d_{213} & 0 \\ d_{311} & d_{322} & d_{333} & 0 & 0 & 0 \end{bmatrix} \quad 3.20$$

$$[e] = \begin{bmatrix} 0 & 0 & 0 & 0 & 0 & e_{123} \\ 0 & 0 & 0 & 0 & e_{213} & 0 \\ e_{311} & e_{322} & e_{333} & 0 & 0 & 0 \end{bmatrix} \quad 3.21$$

Manufacturer data usually provides the charge constants in the strain form, d_{33} , d_{31} and d_{15} . In order to find the constant values for the above equations, the conversions in Table 3-5 are used along with the following relationships: $d_{123} = d_{15}$, $d_{213} = d_{123}$, $d_{311} = d_{31}$, $d_{322} = d_{311}$ and $d_{333} = d_{33}$.

It is possible to find the configuration of the stress format $[e]$ through the configuration of the strain format $[d]$ by using the following expression [10]:

$$[e] = [d][D] \quad 3.22$$

3.5.3.3. Permittivity of the piezoelectric material

The piezoelectric permittivity, or dielectric constant, is the dielectric displacement per unit electric field. The dielectric constant can be evaluated at either a constant stress ε_{ij}^T or at a constant strain ε_{ij}^S . The first subscript indicates the direction of the dielectric displacement whilst the second subscript indicates the direction of the electric field. These constants are sometimes provided in the form of relative dielectric constants. The relative dielectric constant is the ratio of dielectric constant to the absolute dielectric constant ε_0 which is equal to 8.85×10^{-12} farad/metre.

Abaqus defines the dielectric properties of piezoelectric materials in a matrix form of diagonal dielectric constants, evaluated at constant strain (fully constrained material), as follows:

$$[\varepsilon^S] = \begin{bmatrix} \varepsilon_{11}^S & 0 & 0 \\ 0 & \varepsilon_{22}^S & 0 \\ 0 & 0 & \varepsilon_{33}^S \end{bmatrix} \quad 3.23$$

Manufacturer data is usually provided as ε_{11}^S and ε_{33}^S (or in the relative form), however, this assumes that for a piezoelectric material poled in the thickness direction: $\varepsilon_{22}^S = \varepsilon_{11}^S$.

If permittivity data is given in a constant stress form $[\varepsilon^T]$, then it is possible to convert them into the permittivity at a constant strain form $[\varepsilon^S]$ through the following relationship [10, 82]:

$$[\varepsilon^S] = [\varepsilon^T] - [e]^t[d] \quad 3.24$$

where $[e]^t$ and $[d]$ are the transpose of the charge constants matrix in the stress form and the charge constants matrix in the strain form, respectively.

A conversion data sheet is created in Excel to convert the manufacturer piezoelectric material data into Abaqus format as shown in Table 3-6 for Sonox P8 and Table 3-7 for PIC 181. In the case of orthotropic materials, the material orientation must be assigned. For piezoelectric materials, the poling direction is defined, and finally, each created material is attributed to the model through the section module. The section contains information about the properties of a part or the region of a part.

Table 3-6 Piezoelectric material data conversion sheet for Sonox P8.

Piezoceramic material data conversion sheet

Sonox P8

1 Elasticity				[D] (N/m ²)			
I- input data	S_{11}^E	1.14E-11	m ² /N	III- Output	D_{1111}^E	9.54E+10	
	S_{33}^E	1.37E-11	m ² /N		D_{1122}^E	-7.73E+09	
	S_{12}^E	0.00E+00	m ² /N		D_{1133}^E	2.58E+10	
	ν_{13}	0.30			D_{2222}^E	9.54E+10	
	ν_{12}	0.00			D_{2233}^E	2.58E+10	
ν_{23}	0.30		D_{3333}^E		8.59E+10		
II- Calculation	E_1	8.77E+10	N/m ²		D_{1212}^E	4.39E+10	
	E_2	8.77E+10	N/m ²		D_{1313}^E	4.39E+10	
	E_3	7.30E+10	N/m ²		D_{2323}^E	4.39E+10	
	G_{12}	4.39E+10	N/m ²		Y	1.18E+00	
	G_{13}	4.39E+10	N/m ²				
	G_{23}	4.39E+10	N/m ²				
	ν_{21}	0.00					
	ν_{31}	0.25					
	ν_{32}	0.25					

2 Piezoelectricity				[d] (C/N)				[e] (C/N)			
I- input data	d_{33}	2.40E-10	C/N	III- Output	d_{111}	0.00E+00		e_{111}	0.00E+00		
	d_{31}	-9.50E-11	C/N		d_{112}	0.00E+00		e_{112}	0.00E+00		
	d_{15}	3.80E-10	C/N		d_{133}	0.00E+00		e_{133}	0.00E+00		
II- Calculation	d_{123}	3.80E-10	C/N		d_{112}	0.00E+00		e_{112}	0.00E+00		
	d_{213}	3.80E-10	C/N		d_{113}	0.00E+00		e_{113}	0.00E+00		
	d_{311}	-9.50E-11	C/N		d_{123}	3.80E-10		e_{123}	1.67E+01		
	d_{322}	-9.50E-11	C/N		d_{211}	0.00E+00		e_{211}	0.00E+00		
	d_{333}	2.40E-10	C/N		d_{222}	0.00E+00		e_{222}	0.00E+00		
					d_{233}	0.00E+00		e_{233}	0.00E+00		
					d_{212}	0.00E+00		e_{212}	0.00E+00		
					d_{213}	3.80E-10		e_{213}	1.67E+01		
			d_{223}		0.00E+00		e_{223}	0.00E+00			
			d_{311}		-9.50E-11		e_{311}	-2.15E+00			
			d_{322}		-9.50E-11		e_{322}	-2.15E+00			
			d_{333}		2.40E-10		e_{333}	1.57E+01			
			d_{312}		0.00E+00		e_{312}	0.00E+00			
			d_{313}		0.00E+00		e_{313}	0.00E+00			
			d_{323}	0.00E+00		e_{323}	0.00E+00				

3 Dielectricity				[ε] (F/m)			
I- input data	$\epsilon_{33}^S/\epsilon_0$	5.40E+02		III- Output	ϵ_{11}^S	7.08E-09	
	$\epsilon_{11}^S/\epsilon_0$	8.00E+02			ϵ_{22}^S	7.08E-09	
	ϵ_0	8.85E-12	F/m		ϵ_{33}^S	4.78E-09	
II- Calculation	ϵ_{11}^S	7.08E-09	F/m				
	ϵ_{22}^S	7.08E-09	F/m				
	ϵ_{33}^S	4.78E-09	F/m				

C Coulomb
F Farads

Table 3-7 Piezoelectric material data conversion sheet for PIC 181.

Piezoceramic material data conversion sheet PIC 181

1 Elasticity [D] (N/m ²)				
I- input data	S_{11}^E	1.18E-11	m ² /N	
	S_{33}^E	1.42E-11	m ² /N	
	S_{12}^E	0.00E+00	m ² /N	
	ν_{13}	0.30		
	ν_{12}	0.00		
	ν_{23}	0.30		
II- Calculation	E_1	8.47E+10	N/m ²	
	E_2	8.47E+10	N/m ²	
	E_3	7.04E+10	N/m ²	
	G_{12}	4.24E+10	N/m ²	
	G_{13}	4.24E+10	N/m ²	
	G_{23}	4.24E+10	N/m ²	
	ν_{21}	0.00		
	ν_{31}	0.25		
	ν_{32}	0.25		
III- Output	D_{1111}^E	9.22E+10		
	D_{1122}^E	-7.45E+09		
	D_{1133}^E	2.48E+10		
	D_{2222}^E	9.22E+10		
	D_{2233}^E	2.48E+10		
	D_{3333}^E	8.28E+10		
	D_{1212}^E	4.24E+10		
	D_{1313}^E	4.24E+10		
	D_{2323}^E	4.24E+10		
	Y	1.18E+00		
	2 Piezoelectricity [d] (C/N) [e] (C/N)			
	I- input data	d_{33}	2.65E-10	C/N
d_{31}		-1.20E-10	C/N	
d_{15}		4.75E-10	C/N	
II- Calculation	d_{123}	4.75E-10	C/N	
	d_{213}	4.75E-10	C/N	
	d_{311}	-1.20E-10	C/N	
	d_{322}	-1.20E-10	C/N	
	d_{333}	2.65E-10	C/N	
III- Output	d_{111}	0.00E+00		
	d_{122}	0.00E+00		
	d_{133}	0.00E+00		
	d_{112}	0.00E+00		
	d_{113}	0.00E+00		
	d_{123}	4.75E-10		
	d_{211}	0.00E+00		
	d_{222}	0.00E+00		
	d_{233}	0.00E+00		
	d_{212}	0.00E+00		
	d_{213}	4.75E-10		
	d_{223}	0.00E+00		
	d_{311}	-1.20E-10		
	d_{322}	-1.20E-10		
	d_{333}	2.65E-10		
	d_{312}	0.00E+00		
	d_{313}	0.00E+00		
	d_{323}	0.00E+00		
e_{111}	0.00E+00			
e_{122}	0.00E+00			
e_{133}	0.00E+00			
e_{112}	0.00E+00			
e_{113}	0.00E+00			
e_{123}	2.01E+01			
e_{211}	0.00E+00			
e_{222}	0.00E+00			
e_{233}	0.00E+00			
e_{212}	0.00E+00			
e_{213}	2.01E+01			
e_{223}	0.00E+00			
e_{311}	-3.59E+00			
e_{322}	-3.59E+00			
e_{333}	1.60E+01			
e_{312}	0.00E+00			
e_{313}	0.00E+00			
e_{323}	0.00E+00			
3 Dielectricity [ε] (F/m)				
I- input data	$\epsilon_{33}^T/\epsilon_0$	1.20E+03		
	$\epsilon_{11}^T/\epsilon_0$	1.50E+03		
	ϵ_0	8.85E-12	F/m	
III- Output	ϵ_{11}^S	1.28E-08		
	ϵ_{22}^S	1.28E-08		
	ϵ_{33}^S	6.38E-09		
II- Calculation	ϵ_{11}^S	1.28E-08	F/m	
	ϵ_{22}^S	1.28E-08	F/m	
	ϵ_{33}^S	6.38E-09	F/m	

C Coulomb
F Farads

3.5.4. Discretisation of the domain

The next step is to discretise (mesh) the domain or solution region into sub-regions (elements) which are connected at discrete points (nodes). A variety of elements options are provided by FE codes and the accuracy of the solution depends heavily on the type, shape and density of the elements in the domain. These three attributes depend on the type of problem, the geometry of the structure and the type of materials [78].

For linear stress analysis in Abaqus, the recommended element for accurate results is named (C3D20R) which is a continuum (solid) element in 3D (brick) form that has 20 nodes, one at each vertex of the brick shape, and one in the middle of each edge between the vertex nodes. In order to minimise the computing time, the reduced integration option, where the number of interpolation points between nodes is reduced, is used [78].

The fundamental variables that are calculated during any analysis are called the degrees of freedom (dof). For stress analysis, the dof are the translations, however some element families, such as beam and shell families, have rotational dof as well. The translations are calculated in the x , y , and z directions at each node. These calculations are then obtained at any other point in the element by geometric interpolation. The order of the interpolation between nodes is determined by the number of nodes of the elements. Abaqus offers two geometric orders, first and second order. First order elements use linear interpolation to approximate the solution, whilst second order elements use quadratic interpolation. For modal behaviour investigations, quadratic elements should be used to ensure real mode shapes is predicted [68, 78].

For piezoceramic materials, the element named C3D20RE is provided by Abaqus. This element has similar characteristics and translation dof as the C3D20R along with an additional dof for electrical potential variable [78].

The hexahedral element shapes are used for almost all of the elements. However the introducing slots into the front mass produces a complex geometry that prevents elements forming the hexahedral shape. Therefore, a tetrahedral element shape is used for the slotted section as shown in Figure 3-9.

During a finite element analysis, a dense mesh typically results in a more accurate solution. However, as the mesh is made finer, the computation time increases. Therefore a balance must be struck between accuracy of analysis and computing resources. A convergence test is conducted to ensure that a further refinement of the mesh size is not required to obtain convergence in the solution within a reasonable computing time.

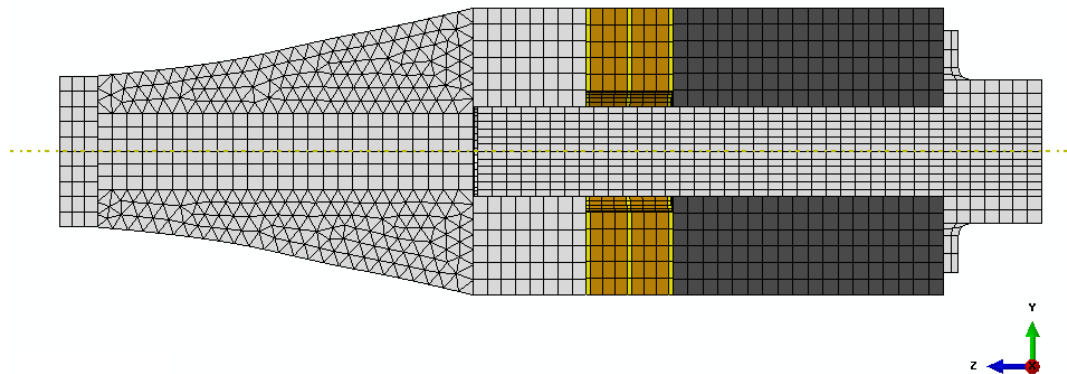


Figure 3-9 Meshing technique for transducer model.

3.5.5. Create analysis steps

The step module is used in Abaqus to choose an analysis, specify output requests, specify adaptive meshing, and specify analysis control. Within a model, it is possible to define a sequence of more than one analysis step. The step sequence provides a convenient way to track changes in the loading and boundary conditions of the model, as well as, changes in the way that the parts of the model interact with each other. It can deal with the removal or addition of parts, and any other changes that may occur in the model during the course of the analysis. In Abaqus, analysis steps are classified into two categories: general steps, where the response is nonlinear, and linear perturbation steps, which provide the linear response of the system about a base state. The base state defines the state of the system at the end of previous nonlinear step. If a linear perturbation is the first step then the base state is considered to be the default initial step that is provided by Abaqus code [78].

3.5.6. Interaction between parts

The Abaqus interaction module is used to define the contact conditions between the parts of the assembled model or between the model and its surroundings. The analysis code does not recognise any mechanical contact between the assemblies of parts unless that contact is specified in the interaction module. Mere physical proximity of two surfaces in the assembly is not enough to indicate any type of interaction. Abaqus provides two main algorithms to model mechanical contact interactions. These are a general contact algorithm

and a contact pair algorithm and can be used for 2D or 3D models. General contact defines all contacted surfaces in the model as one interaction module whilst the contact pair algorithm requires a definition for each contacted surface separately. This requires more parameters. Using the general contact algorithm, it is possible to have multiple contacts per node, this occurs when solid bodies meet at corners, as is shown in Figure 3-10. The contacts are between regions 1 and 2, and between 2 and 3, this requires that the corner points have two contact definitions. In addition, the general contact algorithm is usually faster than the contact pair algorithm. Finally, a penalty enforcement of contact constraint, with an automatically chosen stiffness, is used to prevent any penetration between surfaces.

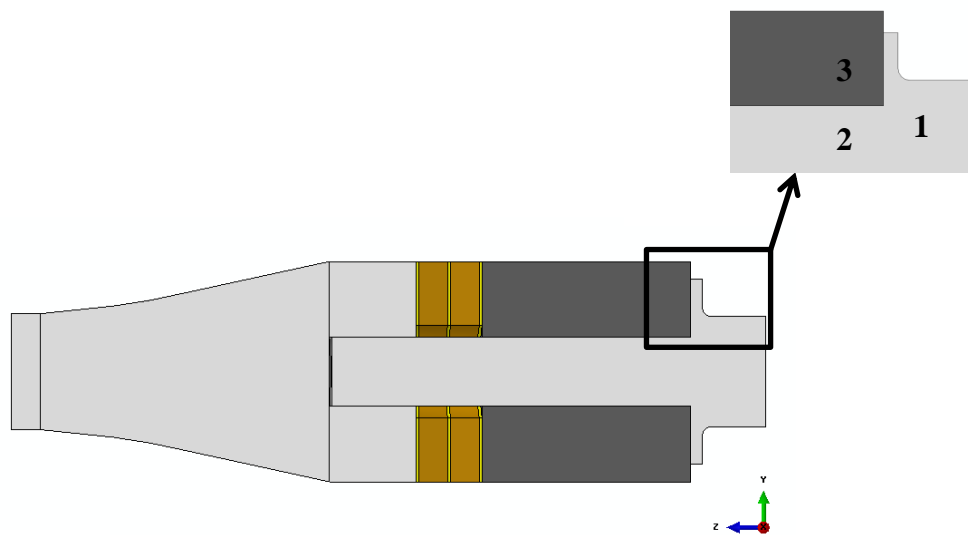


Figure 3-10 Multi contact nodes.

Within these algorithms, three attributes are required to be defined. These are: contact properties, surface properties and contact formulation. The contact properties define the normal and shearing contact parameters, whilst the surface properties are used to change the contact thickness. This can be different from the original parent element thickness. Finally, the contact formulation is used to specify contact discretisation, tracking approach and assignment of master and slave roles to the contact surfaces.

In the current analysis, the pair contact algorithm is used to define the frictionless sliding between the bolt body and the hollow cylinder of the back mass and is also used to define the tie contact between the bolt shank and the front mass. All other contacted surfaces are modelled with the general contact algorithm. A surface to surface formulation is used in these algorithms as opposed to a node to surface formulation. This may lead to

discontinuity problems, so some surfaces may not appear as opposed to a surface as they should when contact occurs. The contact properties of normal behaviour are used for all of the contacted surfaces in both algorithms. An additional frictionless tangential behaviour is used between the bolt and the back mass, whilst friction penalty behaviour is chosen for all other surfaces to prevent unrealistic vibration patterns.

3.5.7. Imposing boundary conditions

Boundary conditions (BC) specify the values of all the basic variables at nodes. These may include the displacement and electrical potentials. In the current model, they are used to constrain the electrical potential dof of the piezoceramic components so as to remove the numerical singularities arising from the dielectric part of the element operator [78].

It should be noted that applying the BC on both sides of each piezoceramic component will produce a series electrical connection that gives the resonance frequency of the transducer. However, it is also possible to apply an electrical BC on one side of each component to produce a parallel electrical connection which, in turn, gives the anti-resonance frequency [83].

3.5.8. Preloading the transducer

Langevin transducers employ a central bolt to apply a static bias compressive load on the piezoceramic stack components. This is important to ensure that the stack remains in compression during operation because the piezoceramic is inherently weak in tension. The preload bias causes a frequency shift of the resonance and anti-resonance values. Therefore, for accurate analysis, it is recommended to include this influence. In the static state, the tension force on the pre-stressed bolt is equal to the compression force on the piezoceramic components. Therefore the following relationship can be used:

$$\frac{\sigma_c}{\sigma_b} = \frac{S_b}{S_c} \quad 3.25$$

where σ_c and σ_b are the axial stress in the piezoceramic and the bolt, respectively. S_b and S_c are the cross-sectional area of the bolt and the piezoceramic rings, respectively. The recommended value for the pre-stress of piezoceramic materials is 20-30MPa. Therefore the stress and required tensile force for the bolt is calculated by inserting the dimensions of the piezoceramic ring and the bolt in Equation 3.25. A general step is created prior to the

frequency step in order to apply the prestress. The bolt load module is used to apply the calculated force as shown in Figure 3-11.

The prestress affects the elasticity, piezoelectricity and the permittivity of the piezoceramic material. Abaqus, however, only simulates the effect on the elasticity. The load stiffness is considered in the frequency step analysis. The frequency shift due to the application of different loads is shown in Figure 3-12. However, this small change in resonance frequency does not represent the overall actual frequency shift because it does not consider the change in the piezoelectric material properties (such as the charge constant d_{33}) which results in a larger frequency shift.

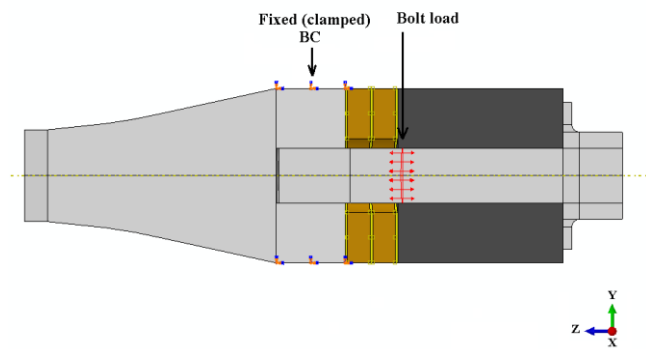


Figure 3-11 Preloading the bolt.

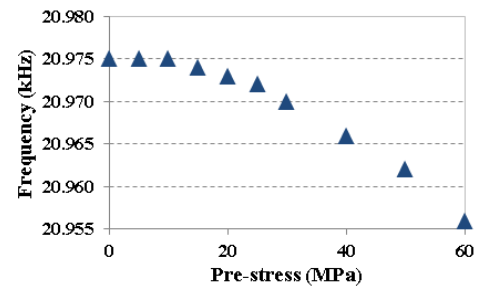


Figure 3-12 Resonance frequency reduction for different pre-stress bias.

3.5.9. Solving the system’s equations

A system of matrix equations is obtained to solve for the unknown nodal values of the domain. The system equations for modal and dynamic analysis are generally given in the following form:

$$[M]_{n \times n} \{ \ddot{u} \}_{n \times 1} + [K]_{n \times n} \{ u \}_{n \times 1} = \{ P \}_{n \times 1} \tag{3.26}$$

where $[M]$ and $[K]$ are the inertia and stiffness matrices, $\{ \ddot{u} \}$ and $\{ u \}$ are the acceleration and displacement vectors of unknown field variables and $\{ P \}$ is the load vector. The system of these matrices can be linear or non-linear. In the case of a non-linear system, a linearization procedure is applied to transform the system into a series of linear equations to apply ordinary solution techniques.

3.5.10. Post processing the solution

The post-processing module is used to extract the solution data and to obtain additional variables, such as stress and strain in mechanical problems, from the solution calculations.

3.6. Frequency extraction procedure

The frequency extraction procedure is used to optimise the performance of the LT transducer design for three different cross-sectional slot profiles which are: a rectangular cut, a trapezoidal cut and a quarter circle cut. These cuts are created and lofted along the exponential section of the front mass as shown in Figure 3-13. The optimisation procedure included a study of the effects of cross-sectional area and twisting angle on the transducer performance parameters. These parameters are the resonance frequencies of the LT mode, the torsionality, the frequency spacing between the LT and the surrounding modes of vibration, the location of the nodal plane along the transducer, and the ratio of the longitudinal response of the output surface to the back mass surface. For particular dimensions of the initial design, four slots are chosen as a profile on a plane at the large end of the exponential section of the front mass. Each profile is then extruded with twist along the exponential section length l_e through the use of a pitch feature. The pitch is defined as the extrusion distance in which a 360° of twist occurs. The following expression is used to calculate the pitch value for different twist angles [78]:

$$pitch = l \frac{360}{\theta} \quad 3.27$$

where θ is the angle of twist. Six different twist angles are chosen for the optimisation study. These are: 60° , 120° , 180° , 240° , 300° and 360° , which represents $\frac{1}{6}$, $\frac{1}{3}$, $\frac{1}{2}$, $\frac{2}{3}$, $\frac{5}{6}$ and one whole twist rotation along the given length of the section, respectively. The depth of the cut of each slot is chosen as 4, 8 and 12mm and is measured from the outside of the large end section. For each depth category, the cross-sectional areas of slot profiles are equal for these cuts. Therefore the profile width can be calculated as demonstrated in Table 3-8. The large width of the trapezoidal section is assumed to be twice the small width: $a = 2b$.

Three steps of analysis are used in the current procedure. The default initial step is used to define the interaction properties between parts and the BC of the electrical potential for the

piezoceramic rings. A general static step is used to apply the prestress on the piezoceramic stack through the use of the bolt load module. Finally a linear permutation frequency step is created to calculate the eigenvalues of the transducer.

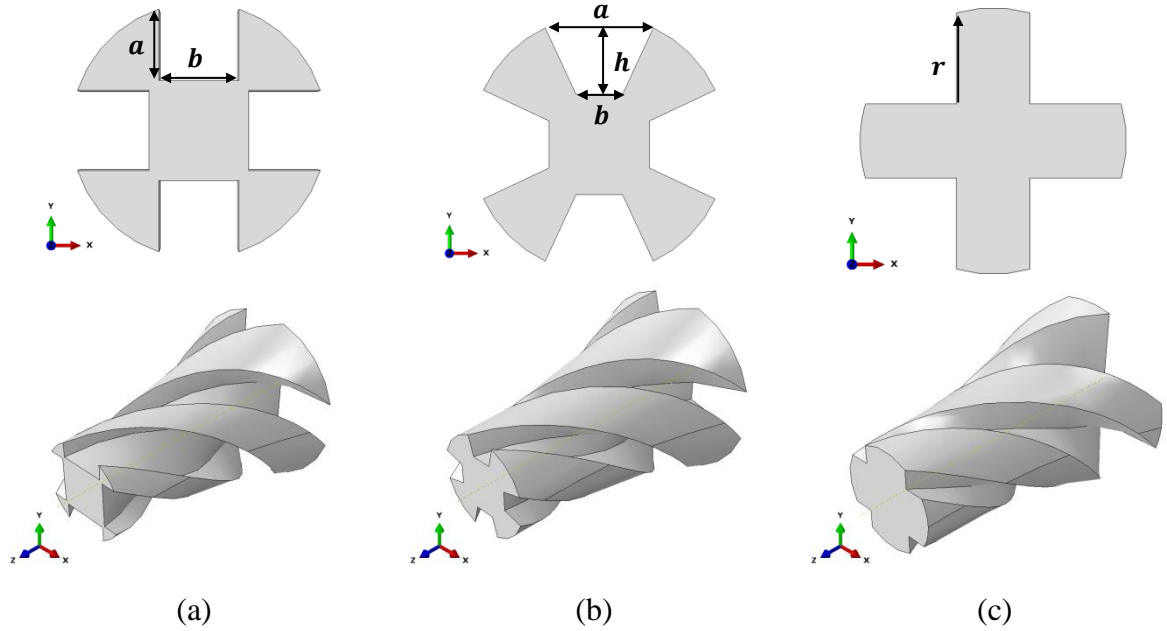


Figure 3-13 Different slotted cross-sections from (a) rectangular, (b) trapezoidal and (c) quarter circle cuts.

Table 3-8 Dimensions for the profiles of the cuts.

Rectangular cut		Trapezoidal cut			Quarter circle cut
$area\ of\ cut = a\ b$		$area\ of\ cut = \frac{a + b}{2} h$			$area\ of\ cut = \frac{\pi r^2}{4}$
$a\ (mm)$	$b\ (mm)$	$h\ (mm)$	$a\ (mm)$	$b\ (mm)$	$r\ (mm)$
4	3.125	4	4.2	2.1	4
8	6.25	8	8.4	4.2	8
12	9.2	12	12.2	6.1	12

To investigate the accuracy of the modelling results, and the computing time required prior to the optimisation procedure, a frequency convergence study is conducted for the unslitted transducer model. This is shown in Figure 3-14. The desired L mode and the surrounding F and T modes are calculated for a different numbers of elements and the results are plotted in Figures 3-14(a), (b) and (c). The computing time is evaluated by the size of output file, as shown in Figure 3-14(d).

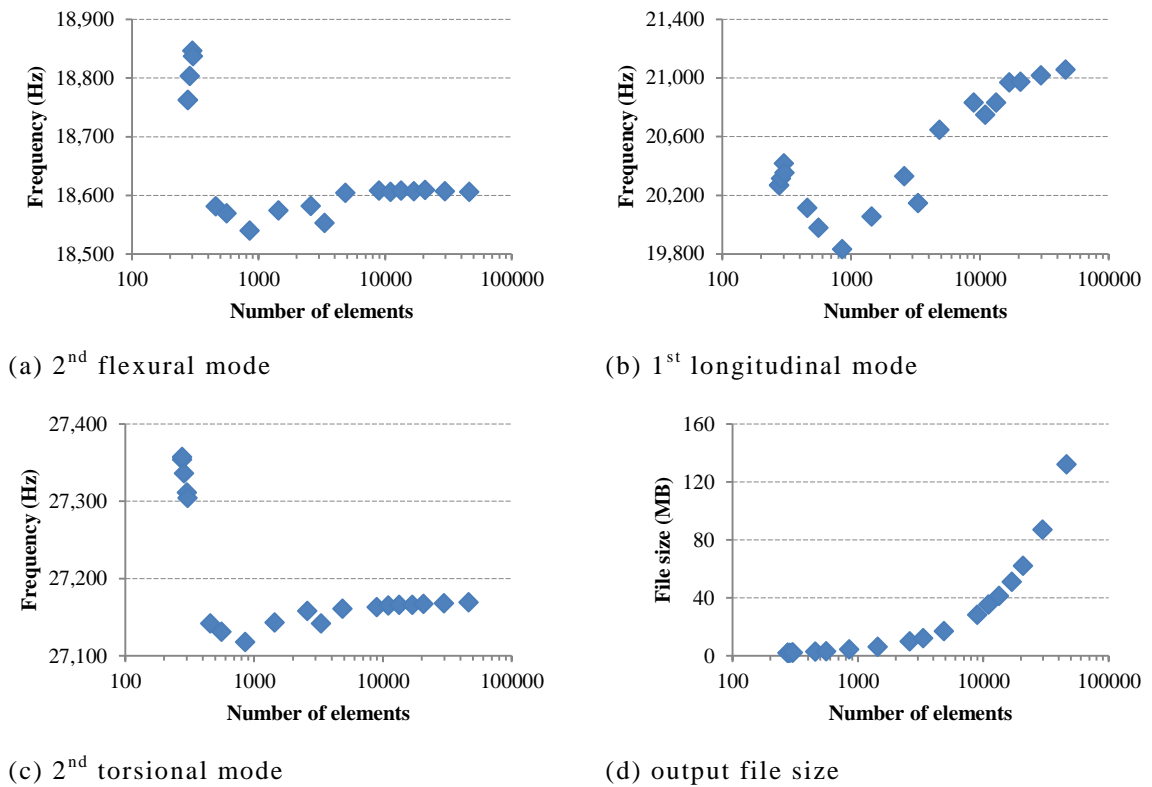


Figure 3-14 Convergence of resonance frequencies and the size of the output file for a different number of elements.

It can be observed that the F and T modes converge when the number of elements reaches 9,000. However, the L mode requires a finer mesh for convergence, where the change in frequency settles at 17,000 elements. For a course mesh, the outer elements of the front mass are misshapen due to the curvature of the exponential decay. Therefore the results show divergence at a low number of elements. The volume of the transducer changes due to the slotting process. Therefore the size of element (also known as seeds in Abaqus), which gives the L mode convergence, is chosen for the optimal mesh and subsequent models. In the current study, the number of elements is chosen over 17,000.

The 1st L mode occurs at a frequency higher than the initial design value of 20kHz. This is due to the introduction of the pre-stressed bolt, which is not considered in the initial calculation. The pre-stressed bolt increases the stiffness of the back mass and piezoceramic sections. Therefore the overall stiffness of the model is increased.

The optimisation results for rectangular, trapezoidal and quarter circle cuts are shown in Figures 3-15, 3-16 and 3-17, respectively. For all types of cuts, the 4mm depth, which produces slots that have a length of 1/3 the total length of the exponential section, does not provide any torsionality. This suggests that the converted wave at these slots may vanish

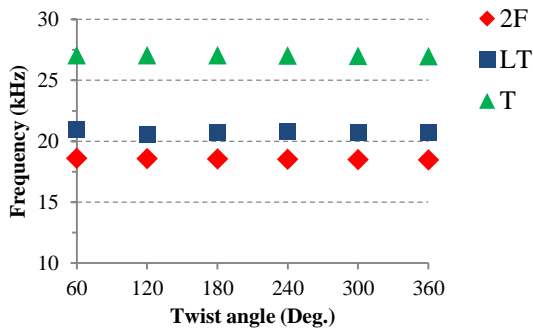
before reaching the output surface of the transducer. Also the ratio of cut section to solid section is small and therefore less L wave can be converted into T wave.

For the rectangular section, the torsionality can reach up to 0.22 for 8mm depth in cut. Whereas the maximum torsionality for a 12mm is 1.33 at a twisting angle of 300°. At these specifications, the nodal plane is located at the intersection between the piezoceramic stack and the front mass. The ratio of L response between the output surface and the back mass surface is 5.4. However the frequency spacing between the LT and the second flexural mode (2F) is only 2.8% which is not enough to prevent coupling between these modes.

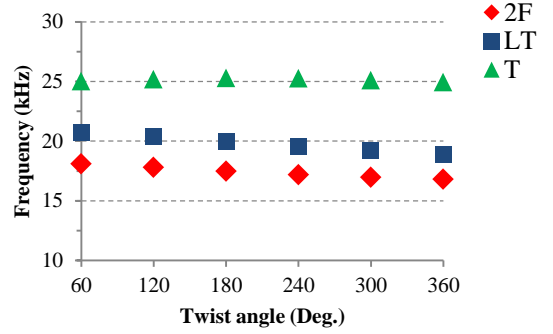
The trapezoidal cut produces torsionality up to 0.27 for 8mm depth. This is considered to be a low ratio, However it can reach up to 0.94 for a 12mm depth at 240°. At these dimensions, the nodal plane is located at the piezoceramic stack (0.5mm backwards from the intersection plane) and the ratio of L response is 4.7. Furthermore, the frequency spacing is only 3%, which gives a high possibility of coupling between LT and 2F modes.

The best results were obtained with the quarter circle cut where, for a 12mm depth of cut, the torsionality can reach up to 0.74 at a twist angle of 240°. A good frequency spacing of 15% is obtained at this angle and this spacing is enough to prevent any possibility of coupling between LT and 2F modes. Also the nodal plane is located on the front mass (1mm in front of the intersection plane) and the ratio of L response between the output surface and the back mass is 4.55.

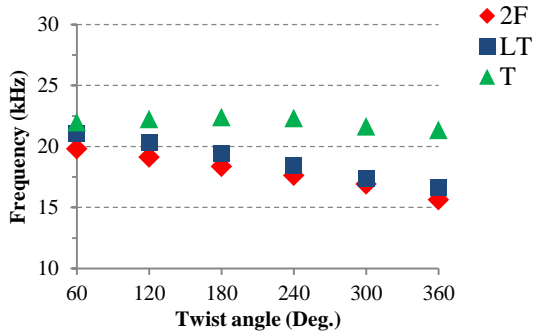
The resonance frequency of the LT response for all 12mm depth cuts is reduced with increasing twist angle. This suggests that the reduction in front mass stiffness is higher than the reduction of inertia. The resonance frequency for the quarter circle cuts, at maximum torsionality, is 18,288Hz. This is below the threshold value. Therefore, for this particular size of transducer, a twist angle of 180° is chosen for fabrication giving a resonance frequency of 19,500Hz and a torsionality of 0.64.



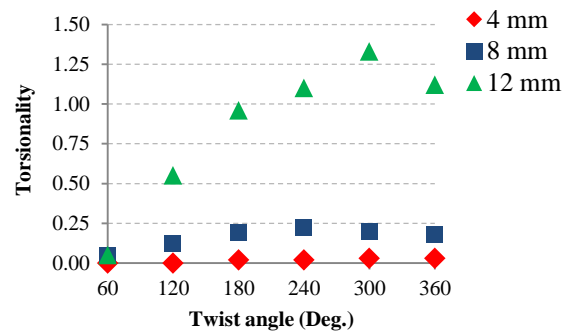
(a) 4mm depth of cut.



(b) 8mm depth of cut.

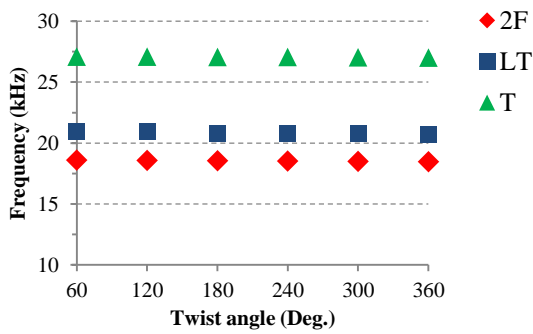


(c) 12mm depth of cut.

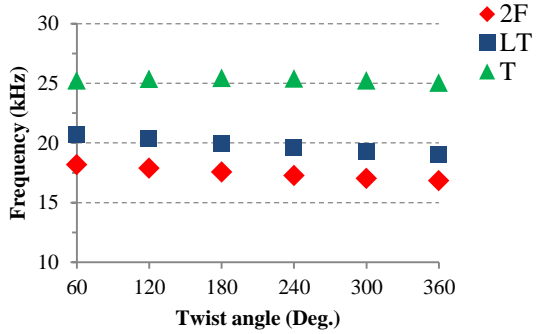


(d) Torsionality.

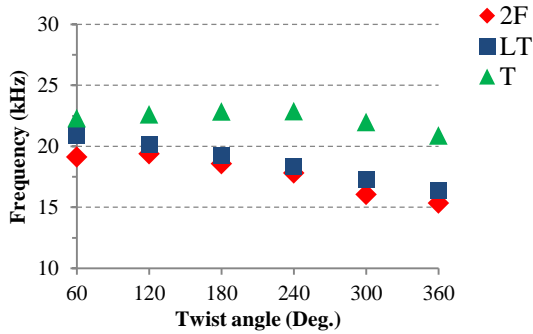
Figure 3-15 Frequency spacing and torsionality of a rectangular cut for different depths of cut.



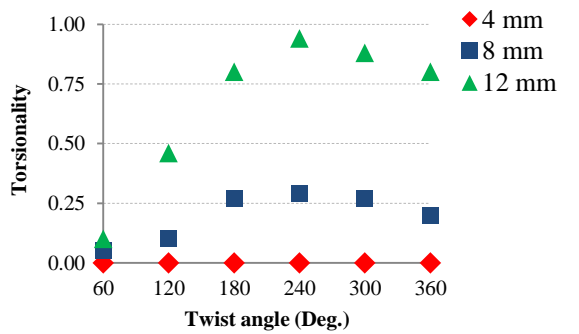
(a) 4mm depth of cut.



(b) 8mm depth of cut.

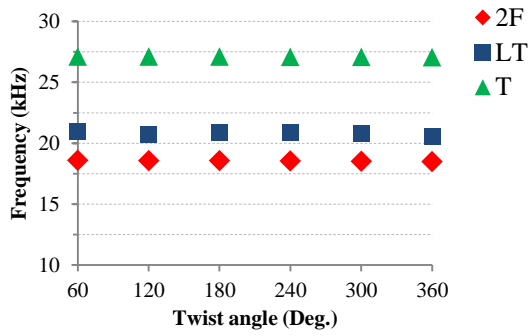


(c) 12mm depth of cut.

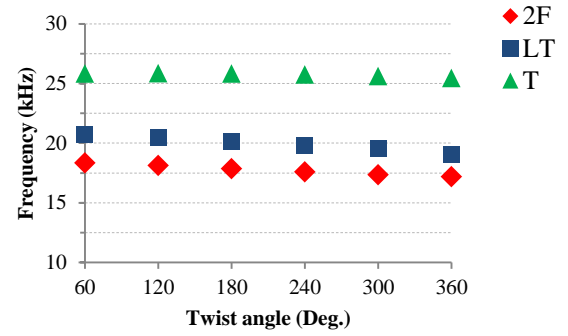


(d) Torsionality.

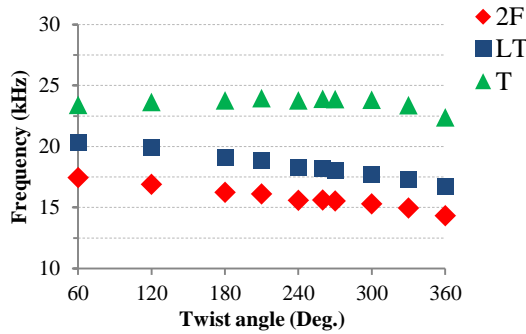
Figure 3-16 Frequency spacing and torsionality of a trapezoidal cut for different depths of cut.



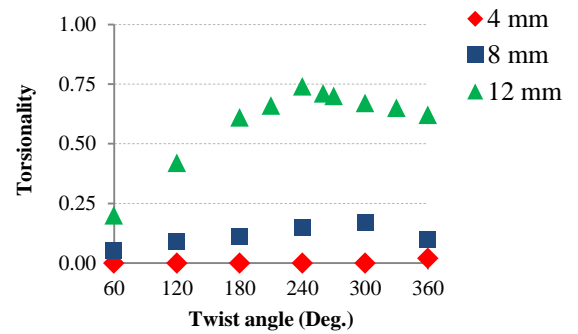
(a) 4mm depth of cut.



(b) 8mm depth of cut.



(c) 12mm depth of cut.



(d) Torsionality.

Figure 3-17 Frequency spacing and torsionality of a quarter circle cut for different depths of cut.

3.7. Dynamic analysis procedure

The optimised transducer model is developed for harmonic analysis to study the transducer performance under a harmonic excitation loads. The initial and general analysis steps, which are used in the frequency extraction procedure, are used again and are followed by a steady-state dynamic linear perturbation step. This step provides the steady-state amplitude and phase of the response of a system due to harmonic excitation. The excitation load is applied as a voltage function at a series of different frequencies (frequency sweep) where the response of the system is recorded. The excitation is applied during this step through the BC of the piezoceramic rings. Different excitation levels are selected and the response of a point on the circumference of the output surface is calculated[78].

In general, there are three types of damping which occur in piezoelectric transducers, these are viscous damping that is due to energy dissipation, structural damping that is due to material properties and friction damping that is due to mechanical sliding between surfaces. Normally, the viscous damping occurs at a low frequency range (few kHz). Therefore, it is considered to be in this work and applied through the use of the Rayleigh formula; where the mass proportional damping coefficient, α , is assumed to be zero and

the stiffness proportional damping coefficient, β , is defined by the following expression [84]:

$$\beta = \frac{1}{\omega_r Q_m} \quad 3.28$$

In this expression ω_r is the modal frequency and Q_m is the overall mechanical quality factor, which represents the structural mechanical damping. Further information about this formula is provided in section 5.8. The quality factor is estimated at the beginning of the analysis and is then corrected after completing an electrical impedance analysis of the fabricated transducer. The values of the resonance and anti-resonance frequencies for the mode shape r can be used to find Q_m of the transducer [85].

3.8. Electrical analysis procedure

Abaqus provides the capability to estimate the generated electrical current I in the piezoceramic materials due to electrical excitation in the harmonic analysis step. A reactive electrical nodal parameter (*RCHG*) is requested at the output module where the total electrical charge q_e on the positive sides of the piezoceramic rings is calculated as the sum of *RCHG* of nodes on the surface. The following equation is then used to calculate the generated current:

$$I = i\omega \sum q_e \quad 3.29$$

where i and ω are the imaginary unit and the angular frequency of the excitation. The electrical impedance Z_e can then be calculated by:

$$Z_e = \frac{V}{I} \quad 3.30$$

where V is the excitation voltage. The complex form of electrical impedance can be used to calculate the impedance magnitude and the phase difference between current and voltage [86].

3.9. Generalisation of transducer design

It is important to consider the scalability in the dimensions of any mechanical design. In the case of ultrasonic transducer design, the piezoelectric components (rings, discs, plates, etc.) are fabricated to specific dimensions. Therefore, resizing the transducer model to

meet these dimensions can simplify the design, reduce the cost and, most importantly, allow sizing for different applications.

The optimised model is used to generalise the LT transducer ranges, where the dimensions of all parts are considered relative to the thickness of piezoceramic component, as is shown in Figure 3-18. Different component thicknesses are chosen (between 1-10mm) and new FE models are created, where the total length of the transducer is varied between 26-260mm. These models are evaluated through a comparison of the torsionality at the output surface, as well as the frequency spacing between the desired LT mode and the surrounding F and T modes, as shown in Figures 3-19 and 3-20 respectively. It can be observed that torsionality is almost constant. This suggests that the main design parameters for the LT transducer, which are the ratio of slotted to solid area and the twist angle of the slots, are not influenced by the size of the model. Also the frequency spacing between modes remains to prevent coupling at these different range of sizes.

Two transducers with 1.5mm and 5mm ring thicknesses and 180° twist angle were fabricated in order to validate the optimisation and the predicted results through the generalised model. Also, the smaller sized transducer will have a higher resonant frequency (higher than the ultrasonic threshold value). It is also possible to fabricate another transducer of 1.5mm with a 240° twist angle to validate the maximum torsionality prediction.

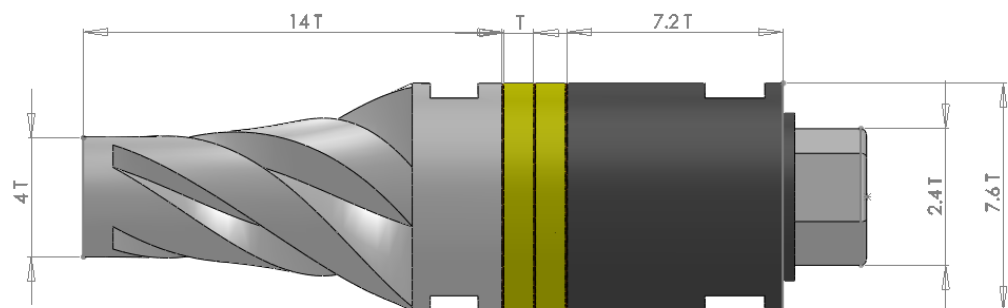


Figure 3-18 Dimensions of the optimum transducer model relative to the piezoceramic thickness.

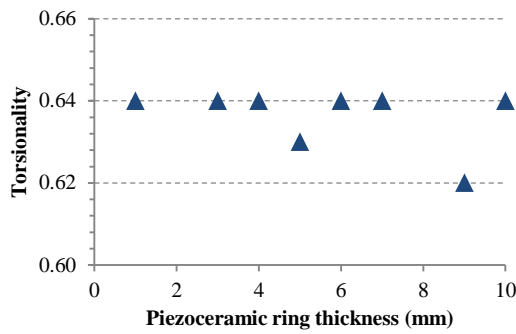


Figure 3-19 Torsionality for different sizes of transducers.

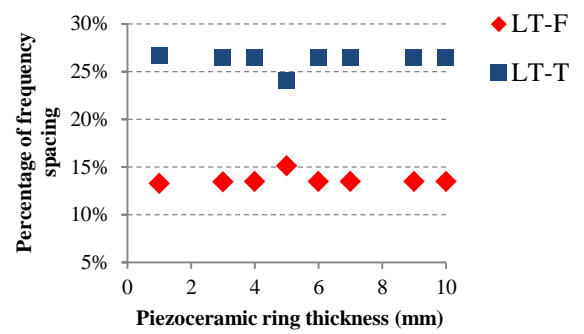


Figure 3-20 Frequency spacing ratio of LT-F and LT-T modes for different sizes of transducer.

3.10. Summary

The principles of ultrasonic transducer design was used to calculate the initial design parameters of a Langevin longitudinal transducer with an exponential front mass. Different cross-sectional cuts of slots were introduced to the front mass in order to degenerate the longitudinal vibration into a combination of longitudinal and torsional vibration at the output surface of the transducer. A set of criteria was presented to evaluate the performance of these different cuts and to optimise the transducer design. Finite element modelling code, Abaqus, was employed to perform three analysis procedures which were the frequency modal extraction, the dynamic response and the electrical analysis. The frequency extraction procedure was used to optimise the design whilst the dynamic response and electrical analysis procedures were used to study the optimised model under different boundary conditions. The optimised model was also generalised by a dimensional scaling procedure so that different sizing of the transducer could be created.

Chapter 4 Analytical modelling of LT transducer

4.1 Introduction

Improvements to the ultrasonic transducer's performance require a detailed investigation of its mechanical and electrical aspects under different operating conditions. It is also important to simulate the effects of the mechanical, dielectric and piezoelectric losses that are associated with the transducer prior to fabrication. For instance, the numerical models based upon the finite element (FE) method, as shown in chapter 3, allows for an accurate description of the mechanical behaviour; where the stresses and strains can be calculated precisely. However it does not generally provide an adequate insight into the electrical characteristics. Numerical models also require intensive computational power and sometimes, due to the numerical characterisation, the physical meaning of the model may be lost [87]. Therefore, integrating purely upon the optimised numerical model at the fabrication stage may lead to a mismatch between the actual and the expected performance. Analytical modelling of wave motion in acoustic media is employed as an alternative method to design ultrasonic transducers. The dimensions of the transducer parts are normally calculated through analytical analysis at the initial design stage. It is widely used in one-dimensional (1D) vibration theory when the longitudinal dimension of the transducer is greater than its lateral dimension. The method considers the longitudinal modes of vibration and it assumes that a plane stress wave propagates in the axial direction of the transducer parts [88]. Analytical modelling is also used in two-dimensional (2D) and three-dimensional (3D) models to consider both flexural (or radial) and thickness modes of vibration [89], but these models are usually expensive in terms of computation time and they also require advanced mathematics for their solution, they are often unrealistic for the purpose of modelling dynamic behaviour [62]. In the current work, a 1D model is used to represent the proposed design. The analytical solution is used first, as presented in section 3.4, to calculate the longitudinal dimensions of the half wavelength transducer parts; this includes the solid exponential horn as the front mass. Then the model is optimised by FE code where slits are introduced into the front mass and their geometry

effects on the transducer performance are studied. In this chapter, the dimensions and properties of the optimised FE model are used to create a complete analytical model, this can be used to study the electrical aspects of the transducer. The analytical model is created through a different approach than the FE model. Therefore it can also be used to validate some of the FE calculations. The proposed transducer is excited longitudinally and it can produce a combination of longitudinal and torsional responses. Thus, the 1D model must be modified so that the region of combined motion is described by two separate 1D models.

The analytical model is simple, and requires low computing resources, however it can be used to achieve the following goals:

- 1- Investigation of the electrical aspects of the transducer through the extraction of the electrical impedance, the phase diagram and the coupling coefficient between the electrical and mechanical energy.
- 2- Consideration of a linear form of the elastic, piezoelectric, and dielectric losses, this gives a more realistic model than the more frequently used lossless models.
- 3- Calculation of the input electrical power and the output mechanical response for different excitation levels.
- 4- Extraction of the mode shape of the transducer, which represents the response distribution along the transducer and which can be used to locate the nodal plane. These calculations can also be used to validate the similar findings of the FE model.

4.2 Theory of wave motion in an elastic solid

In physics, a wave is a disturbance (or oscillation) that travels through space and time, transporting or transforming energy [90]. Generally, waves can be classified into two categories according to their motion: electromagnetic waves, which can travel in a vacuum, and mechanical waves, which require a medium. The propagation of mechanical waves in solids can be generally divided into four categories: elastic, viscoelastic, plastic, and shock [91]. In this work, mechanical elastic waves in a bounded isotropic solid medium are considered. These waves can be divided further based on the motion of the particles in the medium relative to the direction of energy propagation: longitudinal waves, which cause the medium's particles to oscillate parallel to the direction of wave propagation, transverse waves, which cause a perpendicular movement of the medium with respect to the wave direction and surface waves which are both transverse waves and longitudinal waves. Also,

there are torsional waves which are defined as a two-dimensional transverse wave. This type of wave twists along the direction of wave motion.

Mechanical waves are described by a wave equation which sets out how the disturbance proceeds over time. The mathematical form of this equation varies depending on the type of waves [92].

4.2.1 Theory of one-dimensional wave propagation

A straight, homogenous rod is subjected to a dynamically varying stress field (x, t) , simply referred to as σ , so that the adjusted sections are subjected to varying stresses where x refers to the point location along the section of the rod while t refers to time. It is assumed that the planes that are parallel to the cross-sections remain parallel. Therefore a uniform distribution of stress along the section exists. The stress can be expressed as:

$$\sigma = \frac{P}{S} \quad 4.1$$

where P , and S are the applied load and the cross-sectional area of the rod normal to the x -direction, respectively.

The longitudinal displacement of the cross-section is given by $u(x, t)$, or simply referred to as u . The equation of motion in the x -direction can be then given by applying Newton's second law to a differential element as shown in Figure 4-1:

$$-\sigma S + \left(\sigma + \frac{\partial \sigma}{\partial x} dx \right) S + qS dx = \rho S dx \frac{\partial^2 u}{\partial t^2} \quad 4.2$$

where q and ρ are the body force per unit volume and the mass density respectively. Simplifying Equation 4.2 by neglecting the body forces gives:

$$\frac{\partial \sigma}{\partial x} = \rho \frac{\partial^2 u}{\partial t^2} \quad 4.3$$

If the material is assumed to behave elastically, which is an adequate assumption when analysing wave propagation [92], then the linear relationship between stress and strain (Hooke's law) can be applied:

$$E = \frac{\sigma}{\varepsilon} \quad 4.4$$

where E is the Young's modulus of elasticity and ε is the axial strain, which can be defined as:

$$\varepsilon = \frac{\partial u}{\partial x} \quad 4.5$$

Substituting Equation 4.5 into Equation 4.4:

$$\sigma = \frac{\partial u}{\partial x} E \quad 4.6$$

Differentiating Equation 4.6 with respect to x :

$$\frac{\partial \sigma}{\partial x} = E \frac{\partial^2 u}{\partial x^2} \quad 4.7$$

Then substituting Equation 4.7 into Equation 4.3 yields:

$$E \frac{\partial^2 u}{\partial x^2} = \rho \frac{\partial^2 u}{\partial t^2} \quad 4.8$$

or:

$$\frac{\partial^2 u}{\partial x^2} - \frac{1}{c^2} \frac{\partial^2 u}{\partial t^2} = 0 \quad 4.9$$

where

$$c = \sqrt{\frac{E}{\rho}} \quad 4.10$$

c is the velocity of propagation of a longitudinal wave in the rod. Equation 4.9 is the wave equation which is a second order partial differential equation that can be used to analyse 1D wave motion in an elastic medium. It is important to mention that in this analysis, it is assumed that a uniaxial stress state exists. However due to the Poisson's effect, there are lateral expansions and contractions arising from the axial stress that can be determined through the use of a generalised Hooke's law. However, to simplify the solution, these effects are neglected [92].

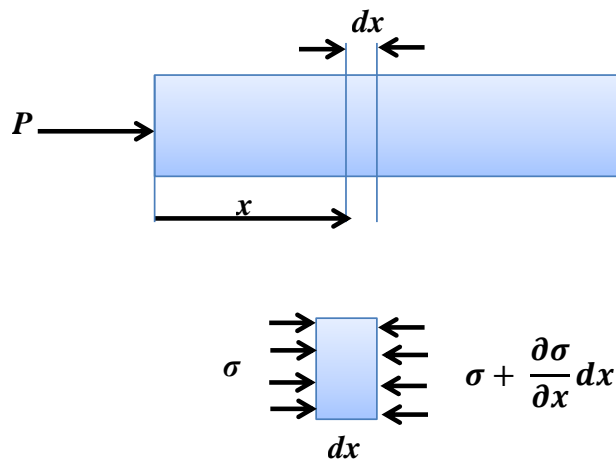


Figure 4-1 Normal stresses acting on a differential element of a uniform rod.

4.2.2 Higher order wave equation

The literature review discussed how 2D and 3D analytical models have been used to analyse one element of piezoceramic [33, 93-97] or a complete ultrasonic transducer model that has a short length of metal parts [89, 98]. These models are used to predict both the thickness and the radial (or flexural) modes of vibrations in structures when the longitudinal dimension is less than or equal to the lateral dimensions [34, 98]. However, these models are expensive in terms of computation time and often unrealistic for modelling purposes [62]. They also require advanced mathematics (matrix form) for solution due to the high number of variables, but in many cases simplified 1D models are sufficient for a physical interpretation of the problem [55, 57, 99-101]. This simplification matches the real-world operation better in the case where the transducer under study has longitudinal dimensions that are larger than its lateral dimensions, so that it can be regarded as laterally free of external force [88]. Also, for the 1D model, high accuracy results can be obtained if the operating longitudinal vibration mode is the fundamental mode. It is well known that when the radial dimensions are less than a quarter of the longitudinal wavelength, one dimensional theory can be used and the error between the measured and theoretical resonance frequencies is negligible [87].

One final advantage of the 1D assumption is that it allows the use of an equivalent electrical circuit approach, which provides a systematic and easy interpretation of the physical concept.

4.2.3 Solution of the one-dimensional wave equation

The general solution of Equation 4.9 can be written in the form of two independent variables ξ and η as follows [92]:

$$\xi = c t + x \quad 4.11a$$

$$\eta = c t - x \quad 4.11b$$

These variables indicate that the displacement u of the material is not only a function of time t and position x , but also wave velocity c . Using a solution that is developed by D'Alembert [102], the one-dimensional wave equation can be expressed by:

$$u(x, t) = J(x - c t) + K(x + c t) \quad 4.12$$

where J and K are functions of the boundary conditions of the problem. The function $J(x - c t)$ represents the wave front that propagates in the positive x direction, whilst the function $K(x + c t)$ represents the wave that travels in the negative x direction.

In linear continuous systems, based on the Fourier transform, a general travelling waveform can be constructed from harmonic traveling wave components. Therefore it is sufficient to study the propagation of only harmonic waves [102]. The harmonic forms of J and K functions are:

$$J(x - c t) = Ae^{i(kx - \omega t)} \quad 4.13a$$

$$K(x + c t) = Ae^{i(kx + \omega t)} \quad 4.13b$$

where A is the wave amplitude and k is called the wavenumber and is defined as the ratio of the angular frequency of the wave ω to the wave velocity:

$$k = \frac{\omega}{c} \quad 4.14$$

Then Equation 4.12 can be written as:

$$u(x, t) = Ae^{i(kx - \omega t)} + Be^{i(kx + \omega t)} \quad 4.15$$

In this equation, the first term represents a traveling wave in the positive direction of x , whilst the second term represents the wave traveling in the negative direction of x . If a wave travels in a medium in the positive direction, while initially no wave travels in the negative direction, then the second part of Equation 4.15 can be ignored and the displacement equation will be:

$$u(x, t) = Ae^{i(kx - \omega t)} \quad 4.16$$

The medium's particle velocity $v(x, t)$ is obtained by differentiation of Equation 4.16 with respect to time, so that:

$$v(x, t) = -i\omega Ae^{i(kx - \omega t)} \quad 4.17$$

Also, by combining Equations 4.6 and 4.17, the stress can be expressed as:

$$\sigma(x, t) = ikEAe^{i(kx - \omega t)} \quad 4.18$$

From Equation 4.1, the force acting is obtained by multiplying Equation 4.18 by the cross-sectional area S so that:

$$P(x, t) = ikES Ae^{i(kx - \omega t)} \quad 4.19$$

The acoustical (mechanical) impedance Z of a point on a structure is the ratio of the force applied at a point $P(x, t)$ to the resulting velocity at the same point $v(x, t)$. This can be obtained by dividing Equation 4.19 by Equation 4.17 so that:

$$Z = \frac{P(x, t)}{v(x, t)} = \frac{kES}{\omega} \quad 4.20$$

Then, by applying Equations 4.10 and 4.14 into Equation 4.20, the acoustical impedance can be obtained by:

$$Z = \rho c S \quad 4.21$$

The product of the mass density ρ , the velocity c and the cross-sectional area S of a given medium is the acoustical impedance Z , which can be defined as a measure of the medium's resistance to the motion when subjected to a given force. It relates the forces with the velocities acting in a mechanical system.

Wave propagation may encounter a discontinuity at the boundary between two different media. This can produce reflected waves that will affect the transmission of energy. This is shown in Figure 4-2 where two different media are separated by a discontinuity at $x = 0$. In medium 1, a wave u_i travels in the positive direction of x whilst initially no wave travels in the negative direction. This is considered to be an incident wave that can be expressed as:

$$u_i = A_i e^{i(k_1 x - \omega t)} \quad 4.22$$

where A_i is the amplitude of the incident wave. When the incident wave encounters the interface between mediums 1 and 2, reflected and transmitted waves are generated.

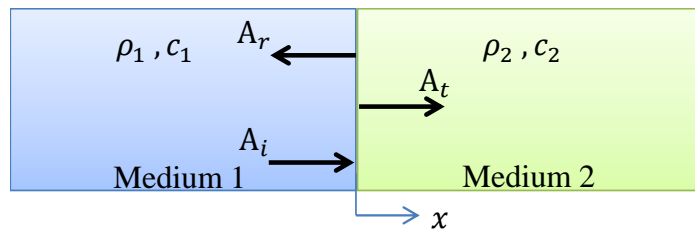


Figure 4-2 Reflection and transmission at an interface between different mediums.

The reflected wave $u_r(x, t)$ can be expressed in terms of travelling waves in the negative direction of x , whilst the transmitted wave $u_t(x, t)$ is assumed to be travelling waves in the positive direction of x as follows:

$$u_r(x, t) = A_r e^{i(k_1 x + \omega t)} \quad 4.23$$

$$u_t(x, t) = A_t e^{i(k_2 x - \omega t)} \quad 4.24$$

where A_r and A_t are the amplitudes of the reflected and transmitted waves respectively.

The boundary conditions at the interface require that the velocity is continuous and the forces across the interface are balanced [92], so that:

$$v_i(x, t) + v_r(x, t) = v_t(x, t) \quad 4.25$$

$$P_i(x, t) + P_r(x, t) = P_t(x, t) \quad 4.26$$

Submitting Equation 4.17 into Equation 4.25, and Equation 4.19 into Equation 4.26, by assuming the incident wave is known, the solution of these two equations derived in reference [92] produced the following expressions:

$$\sigma_t(x, t) = \frac{2S_1\rho_2c_2}{S_1\rho_1c_1 + S_2\rho_2c_2} \sigma_i(x, t) \quad 4.27$$

$$\sigma_r(x, t) = \frac{S_2\rho_2c_2 - S_1\rho_1c_1}{S_1\rho_1c_1 + S_2\rho_2c_2} \sigma_i(x, t) \quad 4.28$$

Often, to describe the transmission and the reflection of waves in terms of acoustical impedances, through the use of Equation 4.21, the stresses of the transmission and reflection waves are expressed as:

$$\sigma_t(x, t) = \frac{2 \left(\frac{Z_2}{Z_1}\right) \left(\frac{S_1}{S_2}\right)}{1 + \left(\frac{Z_2}{Z_1}\right)} \sigma_i(x, t) \quad 4.29$$

$$\sigma_r(x, t) = \frac{\left(\frac{Z_2}{Z_1}\right) - 1}{1 + \left(\frac{Z_2}{Z_1}\right)} \sigma_i(x, t) \quad 4.30$$

From Equation 4.30, in order to minimise the reflected wave, it is necessary to match the impedances of the media that the waves travel through. Similar principles are applied in the selection of materials for ultrasonic transducers, where in general, the wave travels between three different media: the back mass, the piezoelectric section, and the front mass. For optimum transmission of acoustical energy from the piezoelectric section, the following equation must be satisfied [62, 72, 103]:

$$Z_c = \sqrt{Z_f Z_b} \quad 4.31$$

where Z_c , Z_f , and Z_b are the acoustical impedances of the piezoelectric material, the front mass and the back mass, respectively.

4.3 General wave equation and equivalent circuit approach

The general wave form in Equation 4.9 can be applied for uniform cross-sectional media, but, for a non-uniform cross-sectional medium, the one-dimensional wave equation can be written in terms of a linear differential equation of the second order as follows [53, 104] :

$$\frac{\partial^2 u}{\partial x^2} + \frac{1}{S(x)} \frac{\partial S(x)}{\partial x} \frac{\partial u}{\partial x} - \frac{1}{c^2} \frac{\partial^2 u}{\partial t^2} = 0 \quad 4.32$$

where $S(x)$ is the cross-sectional area at distance x .

Equation 4.32 requires a solution approach that is capable of representing the material behaviour, the interaction between parts and the loss parameters accurately [100]. In ultrasonics, the system behaviour at resonance is the main goal for solving the wave equation. There is a similarity in the resonance behaviour between mechanical systems and electrical systems. This behaviour makes it possible to compare and borrow electrical concepts (inductance, capacitance and resistance) to represent mechanical concepts (inertia, stiffness, and damping). The analogy between these systems can be defined as follows: in terms of an electrical system, based on Kirchoff's current law, the algebraic summation of the currents meeting at a junction (node) is equal to zero, analogously, the summation of the forces at a point of a system in equilibrium is equal to zero. Also, based on Kirchoff's voltage law, the voltage drop around a closed loop is equal to zero. In the mechanical system, the velocity drop around a closed loop is equal to zero. These similarities can be used to make the following analogies between the variables in these two systems:

Electrical system	\longleftrightarrow	Mechanical system
Current	\longleftrightarrow	Velocity
Voltage	\longleftrightarrow	Force

As described in section 4.2.3, the mechanical impedance represents the ratio of the force acting on a point to the velocity produced at that same point. The electrical impedance is defined as the voltage across an element divided by the current through the element. By noticing the similarity of the definitions, it is possible to represent the impedance of the acoustical system by the impedance of the electrical system. The acoustical structure can be given by an equivalent electrical T-network [105] as shown in Figure 4-3.

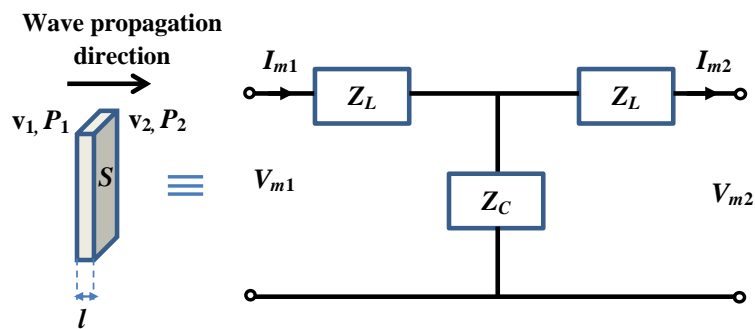


Figure 4-3 Analogue of uniform cross-section of acoustical structure to equivalent T-circuit of one-dimensional acoustic wave.

In this figure, the equivalent T-network of the acoustical structure has two acoustical ports with two terminal acoustical impedances Z_L and one cross-acoustical impedance Z_c . The terminal impedances correspond to the front S_1 and back S_2 surfaces. Therefore, for a uniform cross-sectional structure, the impedances are identical. The velocities v_1, v_2 and the forces P_1, P_2 on the acoustical structure are represented by the voltages V_{m1}, V_{m2} and the currents I_{m1}, I_{m2} on the equivalent circuit, respectively. The impedances of the equivalent T-network are defined in terms of density, wave velocity, cross-sectional area, wave number and the wave path length as follows [104, 106]:

$$Z_L = j \rho c S \tan\left(\frac{k l}{2}\right) \quad 4.33$$

$$Z_c = \frac{-j \rho c S}{\sin(kl)} \quad 4.34$$

where ρ, c, S, k, l are the material mass density, the wave velocity, the cross-sectional area, the wave number, and the length of the wave path in the direction of wave propagation, respectively.

For non-uniform sections, such as the exponential decay horn considered in this work, the equations of the equivalent T-network impedances can be derived. As shown in Figure 4-4, the cross-sectional area $S(z)$ varies with the location along the axial direction (z -axis) according to the following relationship:

$$S(z) = S_0 e^{-2\gamma z} \quad 4.35$$

S_0 is the cross-section area at $z = 0$ (the large end of the section) and γ is the area decay coefficient, which can be found from:

$$\gamma = \frac{\ln(n)}{l} \quad 4.36$$

where ($n = r_o/r_i$) is the ratio of radii at the large end to the small end of the exponential section and l is the length of the section. Since the sound particle velocity is ($v = \partial u / \partial t$), then by applying Equation 4.35 into the general form of the wave equation (Equation 4.32), the following relationship is obtained [53, 107]:

$$\frac{\partial^2 v}{\partial x^2} - 2\beta \frac{\partial v}{\partial x} + k^2 v = 0 \quad 4.37$$

The solution of Equation 4.37 yields:

$$v = e^{\gamma z} (A_1 \cos(k' z) + A_2 \sin(k' z)) \quad 4.38$$

where:

$$k' = \sqrt{k^2 - \gamma^2} \tag{4.39}$$

k is the wave number which is defined in Equation 4.14. These equations are used to derive the equations for the equivalent impedances and the resulting relationships for the assumption that $k > \gamma$ are [104]:

$$Z_{L1} = j \rho c S_0 \frac{k'}{k} \left(\frac{1 - n \cos(k'l)}{n \sin(k'l)} \right) + \frac{\gamma}{k'} \tag{4.40}$$

$$Z_{L2} = j \rho c S_0 \frac{k'}{k n^2} \left(\frac{n - \cos(k'l)}{\sin(k'l)} \right) - \frac{\gamma}{k'} \tag{4.41}$$

$$Z_C = -j \rho c S_0 \frac{k'}{k n \sin(k'l)} \tag{4.42}$$

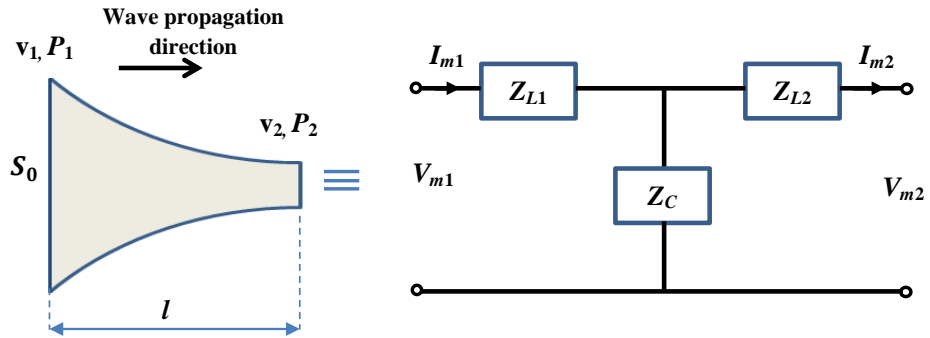


Figure 4-4 Analogue of exponential cross-section of acoustical structure to equivalent T-circuit of one-dimensional acoustic wave.

For piezoelectric materials, where the mechanical and electrical properties are coupled, if the above analogue is applied directly, then the impedances produced will consist of elements that exhibit complicated mixtures of electrical and mechanical parameters. Therefore, another approach based on the Mason model [100] is used. This model was developed in 1948 to represent piezoelectric materials through an equivalent circuit with three ports: an electrical port and two acoustical ports. These ports are separated by an ideal electromechanical transformer [55]. Based on the similarity between the electrical and acoustical systems, the voltage V_e and the current I_e on the electrical port can be transferred to force P_m and velocity v_m on the acoustical port as follows:

$$P_m = N V_e \tag{4.43a}$$

$$v_m = \frac{I_e}{N} \tag{4.43b}$$

where N is a transformation coefficient. By using Ohm’s law for the relationship between voltage, current and impedance, the transformation of impedances between the electrical Z_e and acoustical Z_m ports can be given as:

$$Z_m = N^2 Z_e \tag{4.44}$$

As shown in Figure 4-5, the electrical port has two electrical capacitances, C_o , which are equal in value but opposite in sign. These represent the capacity of the piezoceramic discs under zero strain. The capacitance is calculated from the piezoelectric properties and the geometry of the piezoelectric parts as follows [108]:

$$C_o = \frac{n_o \varepsilon_{33}^T S_3}{t} (1 - k_t^2) \tag{4.45}$$

where n_o and t are the number of piezoelectric discs and the thickness of each disc. ε_{33}^T , S_3 and k_t are the clamped permittivity of the piezoelectric material in the thickness mode, the cross-sectional area normal to the thickness direction and the electromechanical coupling coefficient of the piezoelectric material in the thickness mode, respectively.

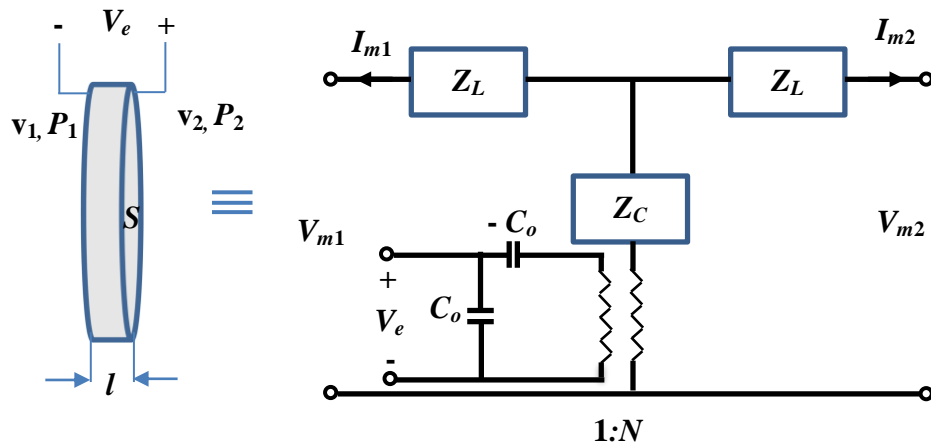


Figure 4-5 Mason equivalent circuit of a piezoelectric disc operation in the thickness mode.

These two analogies can be combined to describe the wave propagation in piezoelectric transducers. This approach is called the equivalent electrical circuit approach. It was first introduced by Mason [109], and then used widely to characterise and optimise piezoelectric transducers [33, 59, 108, 110]. In this approach each mechanical piece of the transducer can be represented by the equivalent T-network while the piezoelectric section can be represented by Mason’s equivalent circuit. A complete transducer network is then modelled as a combination of these circuits. This network is analysed using the basic laws of circuit theory in order to obtain the electromechanical parameters such as the impedance spectrum, phase diagram, input current, power and output response.

The equivalent circuit approach can be used to represent the wave propagation in the longitudinal [108], torsional [111], and flexural [112, 113] modes of ultrasonic transducers and it is also used to study the combination of these modes in vibration [34, 96]. This approach has many advantages:

- 1- It is simple, direct, and concise in its physical meaning.
- 2- It has the ability to model different losses where the mechanical, piezoelectric, and dielectric losses can be taken into account.
- 3- It can recognise the effect of external loads and surrounding boundaries.
- 4- It also permits for efficient modelling of the interaction between the electrical and non-electrical components of an electromechanical system.
- 5- Finally, it is possible to apply in reverse, i.e. the electrical system can be easily converted into a mechanical system.

4.4 Alternative equivalent models

Within the equivalent circuit approach, many models have been created to represent different mechanical systems. The most common models in the case of piezoelectric transducers are: the Mason's equivalent circuit model [100], Redwood's model [56], and the Krimholtz, Leedom, and Mattaei, (KLM) model [58]. Each of these models has its own advantages and limitations, its best application area, and its own importance. The model to be applied is selected according to the specific application when these models are applied, it is of course important to consider the system's excitation method [114, 115].

Mason's model provides a powerful tool for the analysis and simulation of piezoelectric transducer elements. It can simulate both the coupling between the mechanical and electrical systems and the coupling between the mechanical and acoustical systems. The drawback of this model is that it can produce a negative capacitance, which cannot be represented by a physical circuit element. However it has proved useful in many ultrasonic applications.

4.5 Equivalent circuit of longitudinal-torsional (LT) Transducer circuit

In general, a piezoelectric transducer experiences coupling between the electrical energy inputs and the mechanical motion outputs. To simplify this analysis, it can be divided into an electrical (static) branch and a mechanical (motional) branch. The electrical branch consists of the electrical description of the piezoelectric material whilst the mechanical

branch represents the other parts as well as the mechanical aspects of the piezoelectric material.

For the transducer under study, shown in Figure 4-6, construction of the equivalent circuit is done by dividing the model into six regions between which there is a change in the material, a change in the cross-section, or a change in both. After defining the material properties and the geometrical dimensions of each region, Equations 4.33 and 4.34 can be used to calculate the inductance and capacitance impedances of each region as functions of frequency.

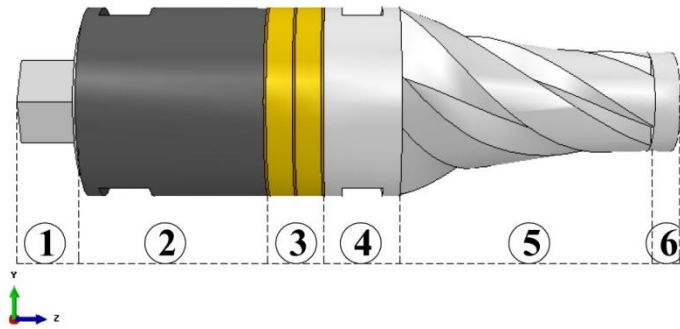


Figure 4-6 Schematic representation of the piezoelectric transducer and the different regions.

Region 1 represents the head of the pre-stressed bolt which has a uniform hexagonal cross-sectional area. The acoustical impedances and wave velocity are calculated based on the following expressions:

$$Z_{L1} = j \rho_1 c_1 S_1 \tan\left(\frac{2\pi l_1 f}{2}\right) \quad 4.46a$$

$$Z_{C1} = \frac{-j \rho_1 c_1 S_1}{\sin(2\pi l_1 f)} \quad 4.46b$$

$$c_1 = \sqrt{\frac{E_1}{\rho_1}} \quad 4.46c$$

Region 2 is a composite structure with two different parts: the hollow back mass and the bolt running through the back mass. The additional stiffness and mass of the pre-stressed bolt are usually much less than for the other parts [59]. Therefore, some studies have shown that neglecting the effect of the bolt section is an acceptable approximation because the added stiffness is usually much less than that of the back mass [34, 87]. However, for a more accurate model, it is possible to extend the equivalent circuit to include the bolts effect [59, 108]. Considering the bolt's effect on the section as a whole, there are three

different approaches. The first assumption considers that at small excitations, the same deformation will occur in both parts. It has been shown previously that the acoustical-electrical analogue matches the velocity (or deformation) in the acoustical system to the current in the electrical system. Therefore, it is possible to represent the two parts of region 2 as two electrical impedances in series [59, 108]. The second assumption considers that the same force will act on both parts. Since the acoustical-electrical analogue matches the forces to voltages, it is possible to represent these parts as two electrical impedances in parallel. Finally, the third assumption considers the average values of material properties of these parts as a ratio to the cross-sectional area of each [116], so that:

$$\rho_{2\text{ avg}} = \frac{\rho_{\text{bolt}} S_{\text{bolt}} + \rho_{\text{back mass}} S_{\text{back mass}}}{S_{\text{bolt}} + S_{\text{back mass}}} \quad 4.47a$$

$$c_{2\text{ avg}} = \frac{c_{\text{bolt}} S_{\text{bolt}} + c_{\text{back mass}} S_{\text{back mass}}}{S_{\text{bolt}} + S_{\text{back mass}}} \quad 4.47b$$

These average values are used in Equations 4.33 and 4.34 to calculate the impedances of the combined region.

The three assumptions are evaluated by applying the optimised dimensions and material specifications of the back mass and the pre-stressed bolt in the FE model. Using Equations 4.33 and 4.34 but ignoring the mechanical losses, the acoustical impedance of each part of region 2 can be obtained as a function of frequency, as shown in Table 4-1.

By using the definition of each assumption, and Equations 4.47a and 4.47b to calculate the average values of the material properties, the equivalent acoustical impedances can be calculated as shown in Table 4-2.

Table 4-1 Acoustical impedance of back mass and bolt section of region 2.

No.	Section	Area S $\times 10^{-6} \text{ m}^2$	Length l (m)	Density ρ (kg/m ³)	Speed of sound c (m/s)	Z_L	Z_C
1	Back mass	1021	0.036	8000	4743	$j 38741 \tan(0.113f)$	$-j 38741 / \sin(0.226f)$
2	Bolt section	113	0.036	4430	5068	$j 2537 \tan(0.113f)$	$-j 2537 / \sin(0.226f)$

Table 4-2 Equivalent acoustical impedances of different assumptions for region 2.

No.	Assumption	Z_L	Z_C
1	Assumption 1: in series	$j 41,278 \tan(0.113f)$	$-j 41,278 / \sin(0.226f)$
2	Assumption 2: in parallel	$j 2,381 \tan(0.113f)$	$-j 2,381 / \sin(0.226f)$
3	Assumption 3: average properties	$j 41,391 \tan(0.113f)$	$-j 41,391 / \sin(0.226f)$

Assumptions 1 and 3 produce close results, while assumption 2 gives significantly different results. The possible explanation for this result is that the assumption of the similar force on both parts is incorrect as the low impedance of the bolt section, Table 4-1, is not expected to significantly affect the overall impedance of the combined parts. Also the similar applied force will produce a larger deformation in the bolt section than the back mass and this tends to remove the pre-stress on the piezoceramic stack. This situation is not noticed in reality, therefore it is reasonable to ignore the second assumption and select either assumption 1 or 3 to calculate the equivalent values. Assumption 3 is simpler and more applicable for calculations. Therefore it will be considered in this analysis.

The equivalent acoustical impedances of region 2 are then calculated by:

$$Z_{L2} = j \rho_{2 \text{ avg}} c_{2 \text{ avg}} (S_{\text{bolt}} + S_{\text{back mass}}) \tan\left(\frac{2\pi l_2 f}{2}\right) \quad 4.48a$$

$$Z_{C2} = \frac{-j \rho_{2 \text{ avg}} c_{2 \text{ avg}} (S_{\text{bolt}} + S_{\text{back mass}})}{\sin(2\pi l_2 f)} \quad 4.48b$$

Region (3) is another combined structure which has the piezoelectric rings, the electrodes and another part of the pre-stressed bolt. The electrodes are usually made from thin plates and therefore their mechanical impedances can be neglected. As shown previously, the piezoelectric rings have two aspects, electrical and mechanical, which are calculated separately. The electrical side is given by a separate electrical circuit, in which the electrical capacitance is calculated directly from the piezoelectric properties of the material as shown in Equation 4.45 [55]. The electrical impedance of the static capacitance can be calculated as:

$$Z_{e-co} = \frac{1}{j 2\pi f C_o} \quad 4.49$$

The mechanical section of the piezoceramic region is given by the acoustical impedances which are calculated from the average values of material properties as follows:

$$\rho_{3 \text{ avg}} = \frac{\rho_{\text{bolt}} S_{\text{bolt}} + \rho_{\text{piezo}} S_{\text{piezo}}}{S_{\text{bolt}} + S_{\text{piezo}}} \quad 4.50a$$

$$c_{3 \text{ avg}} = \frac{c_{\text{bolt}} S_{\text{bolt}} + c_{\text{piezo}} S_{\text{piezo}}}{S_{\text{bolt}} + S_{\text{piezo}}} \quad 4.50b$$

$$Z_{L3} = j \rho_{3 \text{ avg}} c_{3 \text{ avg}} (S_{\text{bolt}} + S_{\text{piezo}}) \tan\left(\frac{(2\pi l_3 f)}{2}\right) \quad 4.51a$$

$$Z_{C3} = \frac{-j \rho_{3 \text{ avg}} c_{3 \text{ avg}} (S_{\text{bolt}} + S_{\text{piezo}})}{\sin(2\pi l_3 f)} \quad 4.51b$$

The relationship between the electrical and acoustical sections is defined by the ideal electromechanical conversion coefficient N , which is calculated by [108]:

$$N = \frac{S_3 d_{33}}{t s_{33}^E} \quad 4.52$$

where d_{33} and s_{33}^E are the piezoelectric constant and the elastic compliance constant for the piezoelectric material in a constant electrical field.

Region (4) represents the uniform cross-sectional part of the front mass where the acoustical impedances can be calculated by:

$$Z_{L4} = j \rho_4 c_4 S_4 \tan\left(\frac{2\pi l_4 f}{2}\right) \quad 4.53a$$

$$Z_{C4} = \frac{-j \rho_4 c_4 S_4}{\sin(2\pi l_4 f)} \quad 4.53b$$

4.5.1 Exponential slotted section

Region (5) represents the slotted helical geometry of quarter circle cut for the front mass. This complex structure has an inner uniform solid core and an outer exponential slotted section as shown in Figure 4-7a. The generated force P at the piezoelectric section acts along the uniform section (region 4) axially and is then converted at the slotted section into two components: longitudinal force P_L and shear force P_T , these are expressed as [32]:

$$P_L = P \cos(\theta) \quad 4.54a$$

$$P_T = P \sin(\theta) \quad 4.54b$$

where θ is the helix angle of the slots.

Based on the theory of longitudinal and flexural vibration, the longitudinal force component will create longitudinal vibration, while the shearing force component will create torsional vibration [20]. The shearing component produces a torsional moment M along the axis of the horn, which can be expressed as:

$$M = \int_S r p dS \quad 4.55$$

Where p is the shearing force acting on a unit area dS at radius r .

The cross-sectional area of this region is a combination of the slotted area and the solid core area (shown in Figure 4-7b) which can be found as:

$$S_1 = \pi r_1^2 \quad \text{for} \quad 0 < r_1 \leq r_c \quad 4.56a$$

$$S_2 = \pi r_2^2 - \pi(r_2 - r_c)^2 \quad \text{for} \quad r_c < r_2 \leq r_z \quad 4.56b$$

simplify S_2 to get:

$$S_2 = 2\pi r_c r_2 - \pi r_c^2 \tag{4.57}$$

then differentiate these equations so that:

$$dS_1 = 2\pi r_1 dr_1 \tag{4.58a}$$

$$dS_2 = 2\pi r_c dr_2 \tag{4.58b}$$

By applying Equations 4.54a, 4.54b, 4.58a and 4.58b into Equation 4.55:

$$M = \int_0^{r_c} r_1 \frac{P \sin(\theta)}{\pi r_1^2} 2\pi r_1 dr_1 + \int_{r_c}^{r_z} r_2 \frac{P \sin(\theta)}{2\pi r_c r_2 - \pi r_c^2} 2\pi r_c dr_2 \tag{4.59}$$

the simplified equation is:

$$M = 2P \sin(\theta) \left(\int_0^{r_c} dr_1 + \int_{r_c}^{r_z} \frac{r_2 dr_2}{2r_2 - r_c} \right) \tag{4.60}$$

The following solution can be used to solve this integration [117]:

$$\int \frac{x dx}{ax + b} = \frac{x}{a} - \frac{b}{a^2} \ln |ax + b| \tag{4.61}$$

By comparing Equations 4.60 and 4.61, it can be found that $a = 2$ and $b = -r_c$, therefore the integral solution can be applied to the shear moment equation as follows:

$$M = 2P \sin(\theta) \left(\frac{r_c}{2} - \frac{r_c}{4} \ln|r_c| + \frac{r_z}{2} + \frac{r_c}{4} \ln|2r_z - r_c| \right) \tag{4.62}$$

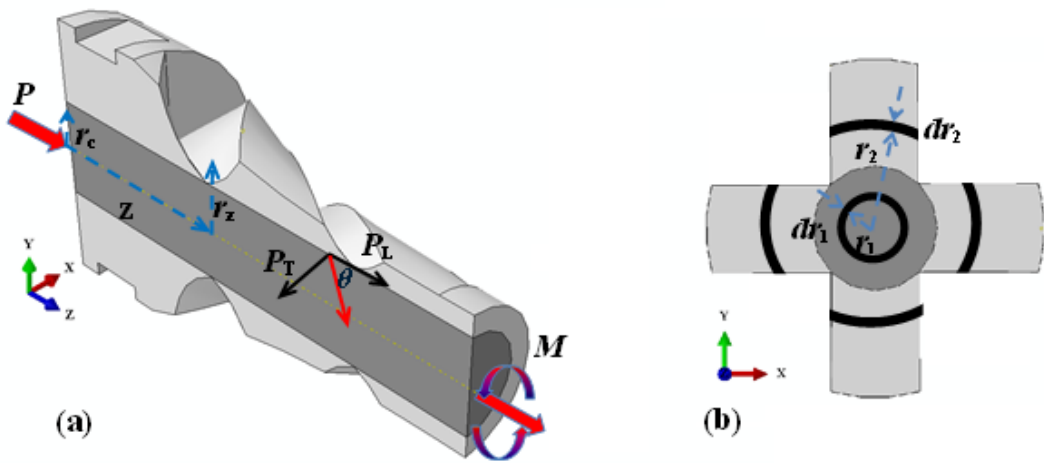


Figure 4-7 Representation of forces and torsional moment directions (a) and a cross-sectional area (b) of the slotted section (region 5).

The equivalent circuit of region 5 can be obtained by two separate circuits of the 1D model. The first circuit represents the longitudinal vibration component and the other circuit represents the torsional vibration component. Each circuit interacts with region 4 through a conversion coefficient that is the ratio of degenerated vibration to the generated vibration at the dividing surface (the output surface of region 4). The conversion coefficient of longitudinal vibration N_L is given by:

$$N_L = \frac{P_L}{P} \quad 4.63$$

whereas the conversion coefficient of torsional vibration N_T can be expressed as:

$$N_T = \frac{M}{P} \quad 4.64$$

By substituting Equations 4.54a and 4.62 into Equations 4.63 and 4.64 respectively, the following expressions can be obtained:

$$N_L = \cos(\theta) \quad 4.65$$

$$N_T = 2 \sin(\theta) \left(\frac{r_c}{2} - \frac{r_c}{4} \ln|r_c| + \frac{r_z}{2} + \frac{r_c}{4} \ln|2r_z - r_c| \right) \quad 4.66$$

The conversion coefficients can predict the ratio of the division of generated L waves into degenerated L and T waves with respect to the helix angle. When the helix angle is equal to zero, the longitudinal conversion coefficient N_L will be unity whilst the torsional conversion coefficient N_T is equal to zero. This is the situation when the cutting slots are parallel to the axial direction of the exponential horn. This does not produce any torsionality, as shown in the numerical analysis, section 3.6. For other values of the helix angle, the torsional vibrations vary along the axial direction of the horn (z-direction). The relationship between the position z and the radius of the exponential section r_z is given by:

$$r_z = r_0 e^{-\gamma z} \quad 4.67$$

where r_0 is the radius at the large end of the exponential section $z=0$ and γ is the decay coefficient which is defined in Equation 4.36.

For a particular case of the optimised FE model: where $r_0=19\text{mm}$, $r_l=10\text{mm}$, $l=50\text{mm}$, $r_c=7\text{mm}$ and $\gamma = 0.0128$; the variation of N_T along the centre line of the horn is shown in Figure 4-8, at which N_T has its highest value near to the largest cross-section and reduces linearly toward the smallest cross-section.

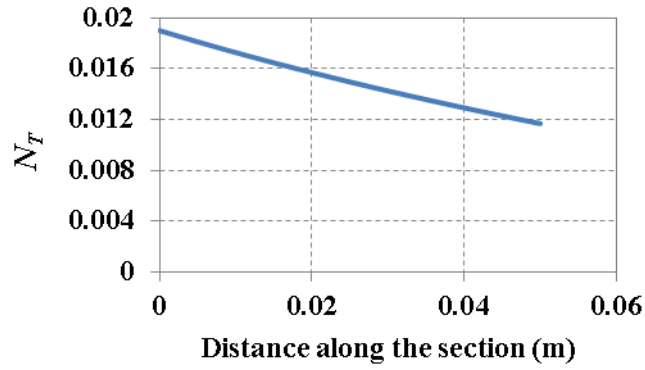


Figure 4-8 Variation of the torsional conversion coefficient along the axial direction of the horn.

In order to find the value of N_T , to be used as a conversion coefficient, the value at the geometric centroid of the horn is calculated and compared with the average value obtained from the curve of Figure 4-8. The location of the geometrical centroid of a solid exponential horn can be found by dividing the area weighted integral $\langle z \rangle$ by the volume of the solid [118]. As shown in Figure 4-7 and by using Equation 4.57 for the cross-sectional area, the volume V_o of the slotted exponential horn is given by:

$$V_o = \int_0^l S dz = \int_0^l (2\pi r_z r_c - \pi r_c^2) dz \quad 4.68$$

Applying Equation 4.67 into Equation 4.68 will produce:

$$V_o = 2\pi r_c r_o \int_0^l e^{-\gamma z} dz + \pi r_c^2 \int_0^l dz \quad 4.69$$

Then by carrying out these integrations, and applying their limits, the volume of the slotted horn can be calculated by:

$$V_o = \frac{2\pi r_c r_o - 2\pi r_c r_o e^{-\gamma l} - \pi r_c^2 l \gamma}{\gamma} \quad 4.70$$

The area weighted integral $\langle z \rangle$ can be found from:

$$\langle z \rangle = \int_0^l Sz dz = 2\pi r_c r_o \int_0^l z e^{-\gamma z} dz - \pi r_c^2 \int_0^l z dz \quad 4.71$$

The following integration solution can be used in Equation 4.71 [117]:

$$\int x e^{cx} dx = \frac{e^{cx}}{c^2} (cx - 1) \quad 4.72$$

A comparison of the first integration term of Equation 4.71 to Equation 4.72 shows that $c = -\gamma$, therefore the solution of Equation 4.70, after applying the integration limit, will be:

$$\langle z \rangle = \frac{4\pi r_c r_o [1 - l\gamma e^{-\gamma l} - e^{-\gamma l}] - \pi r_c^2 l^2 \gamma^2}{2\gamma^2} \tag{4.73}$$

The centroid \bar{z} is found by dividing Equation 4.72 by Equation 4.69 so that:

$$\bar{z} = \frac{\langle z \rangle}{V_o} = \frac{4[1 - l\gamma e^{-\gamma l} - e^{-\gamma l}] - \frac{\gamma^2}{r_o} r_c l^2}{4\gamma - 4\gamma e^{-\gamma l} - \frac{2\gamma^3}{r_o} r_c l^2} \tag{4.74}$$

For the above particular values, the centroid is found to be at $\bar{z} = 19\text{mm}$. Then from Equation 4.65, the torsional conversion coefficient N_T at the centroid is equal to 0.0158. This value is very close to the average value of N_T along the axial direction which is equal to 0.0151. Therefore the value of N_T at the geometrical centroid will be considered for the analysis.

A further investigation of the variation of N_T with the helix angle θ and the position z is shown in Figure 4-9. At a helix angle of zero, the value of the torsional coefficient is zero along the axial direction. This increases with helix angle and reaches its maximum value at a helix angle of 90° . Increasing N_T leads to improved degeneration to torsional vibration in the front mass of the transducer, however this is not the only parameter that controls the conversion. There are other parameters which can affect the torsionality, such as the geometric stiffness of the slotted section, the method of securing the transducer, and the effect of the external applied load at the output surface.

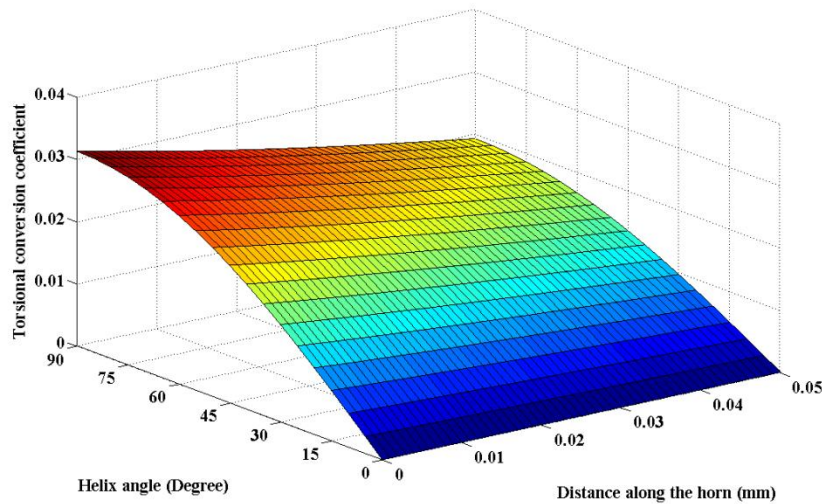


Figure 4-9 Variation of torsional conversion coefficient with helix angle and position.

In the case of the equivalent L circuit, the acoustical impedances can be calculated through the use of Equations 4.40 to 4.42. Here the cross-sectional area is the summation of S_1 and S_2 of Equations 4.56a and 4.56b. The resulting impedance equations are [34, 53, 104]:

$$Z_{L51-L} = j \rho_5 c_{5-L} S_{5-0} \frac{k'_{5-L}}{k_{5-L}} \left(\frac{1 - n \cos(k'_{5-L} l_5)}{n \sin(k'_{5-L} l_5)} \right) + \frac{\gamma}{k'_{5-L}} \quad 4.75a$$

$$Z_{L52-L} = j \rho_5 c_{5-L} S_{5-0} \frac{k'_{5-L}}{k_{5-L} n^2} \left(\frac{n - \cos(k'_{5-L} l_5)}{\sin(k'_{5-L} l_5)} \right) - \frac{\gamma}{k'_{5-L}} \quad 4.75b$$

$$Z_{C5-L} = -j \rho_5 c_{5-L} S_{5-0} \frac{k'_{5-L}}{k_{5-L} n \sin(k'_{5-L} l_5)} \quad 4.75c$$

$$k'_{5-L} = \sqrt{\left(\frac{2\pi f}{c_{5-L}} \right)^2 - \gamma^2} \quad 4.75d$$

A procedure which is similar to that used to derive Equations 4.75 to 4.75d can be used to derive the acoustical impedances of the equivalent torsional circuit. To do this the force P_i and the velocity v_i are replaced by a moment M_i and an angular velocity ϕ_i respectively. The following equations can be obtained for the assumption of $k_{2T} > 2\gamma$ [34]:

$$Z_{L51-T} = j \rho_5 c_{5-T} I_{05-T} \frac{k'_{5-T}}{k_{5-T}} \left(\frac{1 - n^2 \cos(k'_{5-T} l_5)}{n^2 \sin(k'_{5-T} l_5)} \right) + \frac{2\gamma}{k'_{5-T}} \quad 4.76a$$

$$Z_{L52-T} = j \rho_5 c_{5-T} I_{05-T} \frac{k'_{5-T}}{k_{5-T} n^4} \left(\frac{n^2 - \cos(k'_{5-T} l_5)}{\sin(k'_{5-T} l_5)} \right) - \frac{2\gamma}{k'_{5-T}} \quad 4.76b$$

$$Z_{C5-T} = -j \rho_5 c_{5-T} I_{05-T} \frac{k'_{5-T}}{k_{5-T} n^2 \sin(k'_{5-T} l_5)} \quad 4.76c$$

$$k'_{5-T} = \sqrt{\left(\frac{2\pi f}{c_{5-T}} \right)^2 - \gamma^2} \quad 4.76d$$

where c_{5-T} , I_{05-T} and k_{5-T} are the speed of sound of the torsional wave, the area moment of inertia, and the torsional wave number respectively. The speed of sound of the torsional wave can be calculated by:

$$c_{5-T} = \sqrt{\frac{G}{\rho}} \quad 4.77a$$

$$G = \frac{E}{2(1 + \nu)} \quad 4.77b$$

where G is the shear modulus of elasticity and ν is the Poisson's ratio.

Finally, region (6) represents the front part of the transducer front mass where L and T waves will progress together. Therefore, it can be considered to be continuous so that the longitudinal and torsional circuits, and their impedances, can be expressed as:

$$Z_{L6-L} = j \rho_6 c_{6-L} S_{6-L} \tan\left(\frac{2\pi l_6 f}{2}\right) \tag{4.78a}$$

$$Z_{C6-L} = \frac{-j \rho_6 c_{6-L} S_{6-L}}{\sin(2\pi l_6 f)} \tag{4.78b}$$

$$Z_{L6-T} = j \rho_6 c_{6-T} S_{6-T} \tan\left(\frac{2\pi l_6 f}{2}\right) \tag{4.78c}$$

$$Z_{C6-T} = \frac{-j \rho_T c_{6-T} S_{6-T}}{\sin(2\pi l_6 f)} \tag{4.78d}$$

The complete equivalent network of the transducer is shown in Figure 4-10. Two additional acoustical impedances are added at each end of the network to represent the front Z_{front} and back Z_{back} external loads. These impedances are neglected when the transducer is tested in unloaded conditions because they represent the surrounding space impedances which have a negligible value [116]. Their values should be considered when the transducer is modelled under the influence of an operating load.

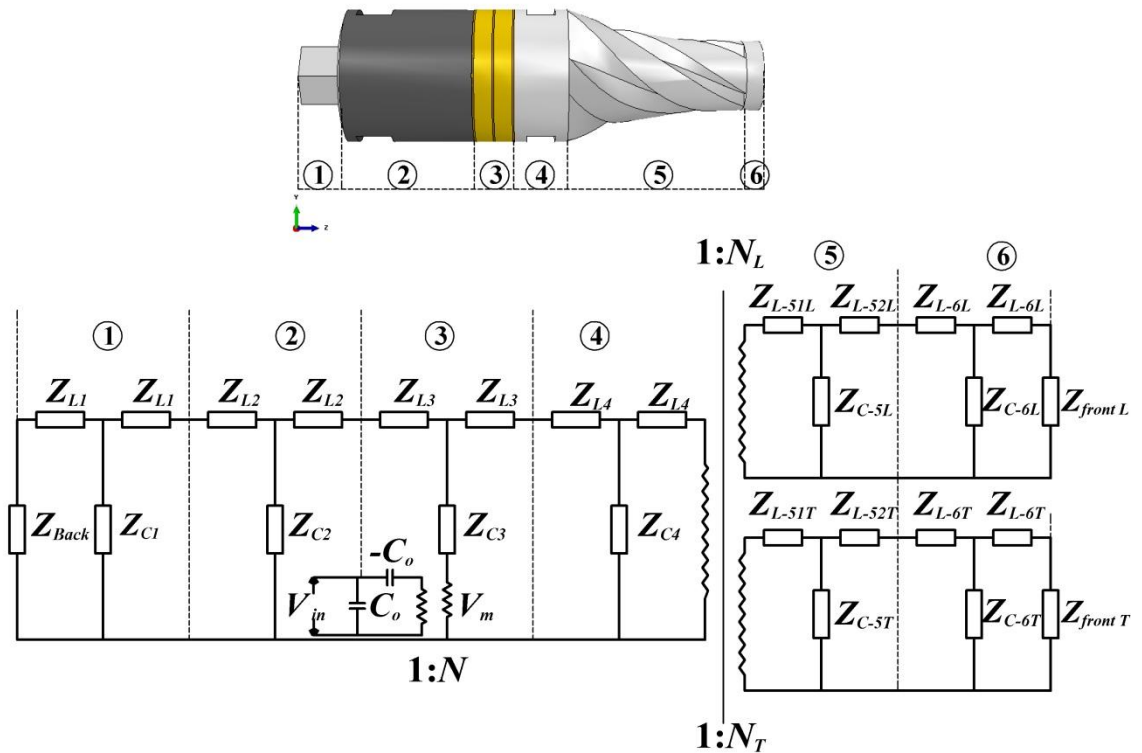


Figure 4-10 The complete equivalent network of the transducer based on Mason's model.

The input parameter for this network is the excitation voltage V_{in} and the possible outputs are the electrical impedance spectrum and the phase diagram. The outputs can be used to extract the following: the resonance and anti-resonance frequencies of the thickness modes, the total input current and electrical power of the transducer, the effective coupling coefficient between the electrical and mechanical energy, the mechanical velocities (and hence displacements) at the boundaries between the regions, and finally the vibration amplitude at the output surface of the transducer for different excitation levels.

The equivalent network is solved through the principles of Kirchhoff's current and voltages laws, where new impedance expressions are introduced to simplify the connecting impedances (parallel or series) of the mechanical parts. The overall acoustical impedance Z_m is then calculated and transferred through the transmission line to the electrical branch, where the same principles are used to extract the overall electrical impedance of the transducer Z_T . The total input current I_T is calculated from the applied excitation voltage V_{in} and then the voltage across the transferred acoustical impedance is calculated and transferred back to the mechanical branch to represent the generated force F_m at the piezoelectric section. Kirchhoff's principles are used again within the mechanical branch to calculate the forces and velocities of each region.

Current loops are used to calculate the branch currents I_i which are equivalent to the velocities v_i (and therefore representative of the displacements u_i) at the boundaries of each region as mentioned previously. These simplification steps are carried out as follows: From the left side of the network in Figure 4-10, the back load impedance Z_{back} is in series with Z_{L1} and both are in parallel with Z_{C1} . This can be simplified as:

$$Z_7 = \frac{(Z_{back} + Z_{L1}) Z_{C1}}{(Z_{back} + Z_{L1} + Z_{C1})} \quad 4.79$$

Z_7 is now in series with Z_{L1} and Z_{L2} , and they are all in parallel to Z_{C2} , hence:

$$Z_8 = \frac{(Z_7 + Z_{L1} + Z_{L2}) Z_{C2}}{(Z_7 + Z_{L1} + Z_{L2} + Z_{C2})} \quad 4.80$$

Finally, Z_8 is in series with Z_{L2} and Z_{L3} , therefore:

$$Z_9 = Z_8 + Z_{L2} + Z_{L3} \quad 4.81$$

These simplification steps of the left side are shown in Figure 4-11.

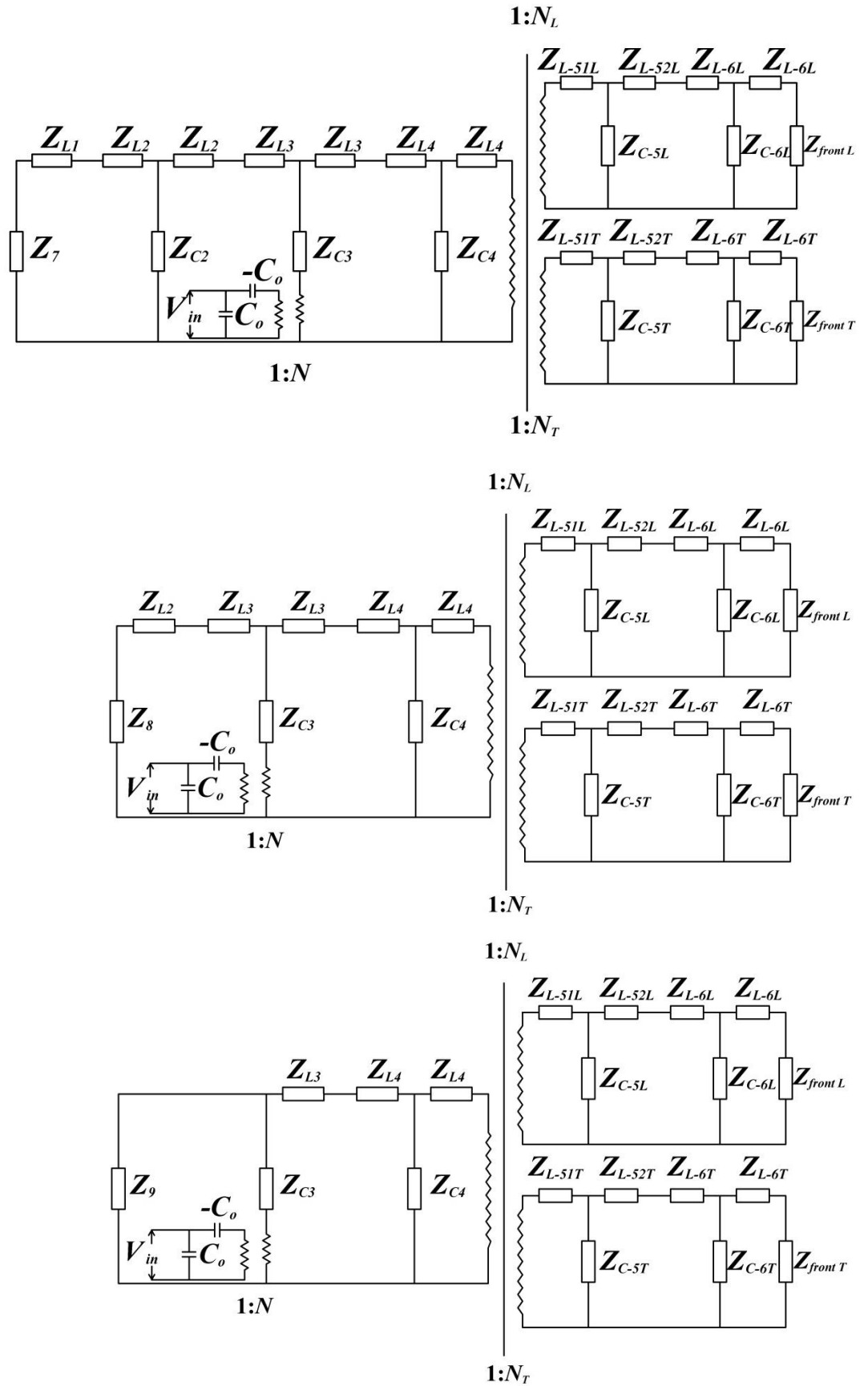


Figure 4-11 Simplifying the left side of the equivalent network.

From the right side of the network of Figure 4-10, for the longitudinal equivalent circuit, the front load impedance Z_{front} is in series with Z_{L6-L} and both are in parallel with Z_{C6-L} .

Therefore it can be simplified to:

$$Z_{10} = \frac{(Z_{front} + Z_{L6-L}) Z_{C6-L}}{(Z_{front} + Z_{L6-L} + Z_{C6-L})} \quad 4.82$$

This impedance Z_{10} is now in series with Z_{L6-L} and Z_{L5-L} , and as all are in parallel with Z_{C5-L} :

$$Z_{11} = \frac{(Z_{10} + Z_{L6-L} + Z_{L5-L}) Z_{C5-L}}{(Z_{10} + Z_{L6-L} + Z_{C5-L} + Z_{C5-L})} \quad 4.83$$

Z_{11} is in series with Z_{C5-L} , then:

$$Z_{12} = Z_{11} + Z_{C5-L} \quad 4.84$$

The above simplification steps are shown in Figure 4-12, and a similar procedure is applied to the equivalent torsional circuit in Figure 4-11 to get:

$$Z_{13} = \frac{(Z_{front} + Z_{L6-T}) Z_{C6-T}}{(Z_{front} + Z_{L6-T} + Z_{C6-T})} \quad 4.85$$

$$Z_{14} = \frac{(Z_{13} + Z_{L6-T} + Z_{L5-T}) Z_{C5-T}}{(Z_{13} + Z_{L6-T} + Z_{C5-T} + Z_{C5-T})} \quad 4.86$$

$$Z_{15} = Z_{14} + Z_{C5-T} \quad 4.87$$

The equivalent impedances of the longitudinal and torsional circuits, Z_{11} and Z_{15} respectively, are then transferred to the left side of the conversion line, through the use of the conversion coefficients in Equations 4.64 and 4.65.

This network can be further simplified by:

$$Z_{16} = \frac{\left(\frac{Z_{11}}{N_L}\right) \left(\frac{Z_{15}}{N_T}\right)}{\left(\frac{Z_{11}}{N_L}\right) + \left(\frac{Z_{15}}{N_T}\right)} + Z_{L4} \quad 4.88$$

$$Z_{17} = \frac{Z_{16} Z_{C4}}{Z_{16} + Z_{C4}} + Z_{L4} + Z_{L3} \quad 4.89$$

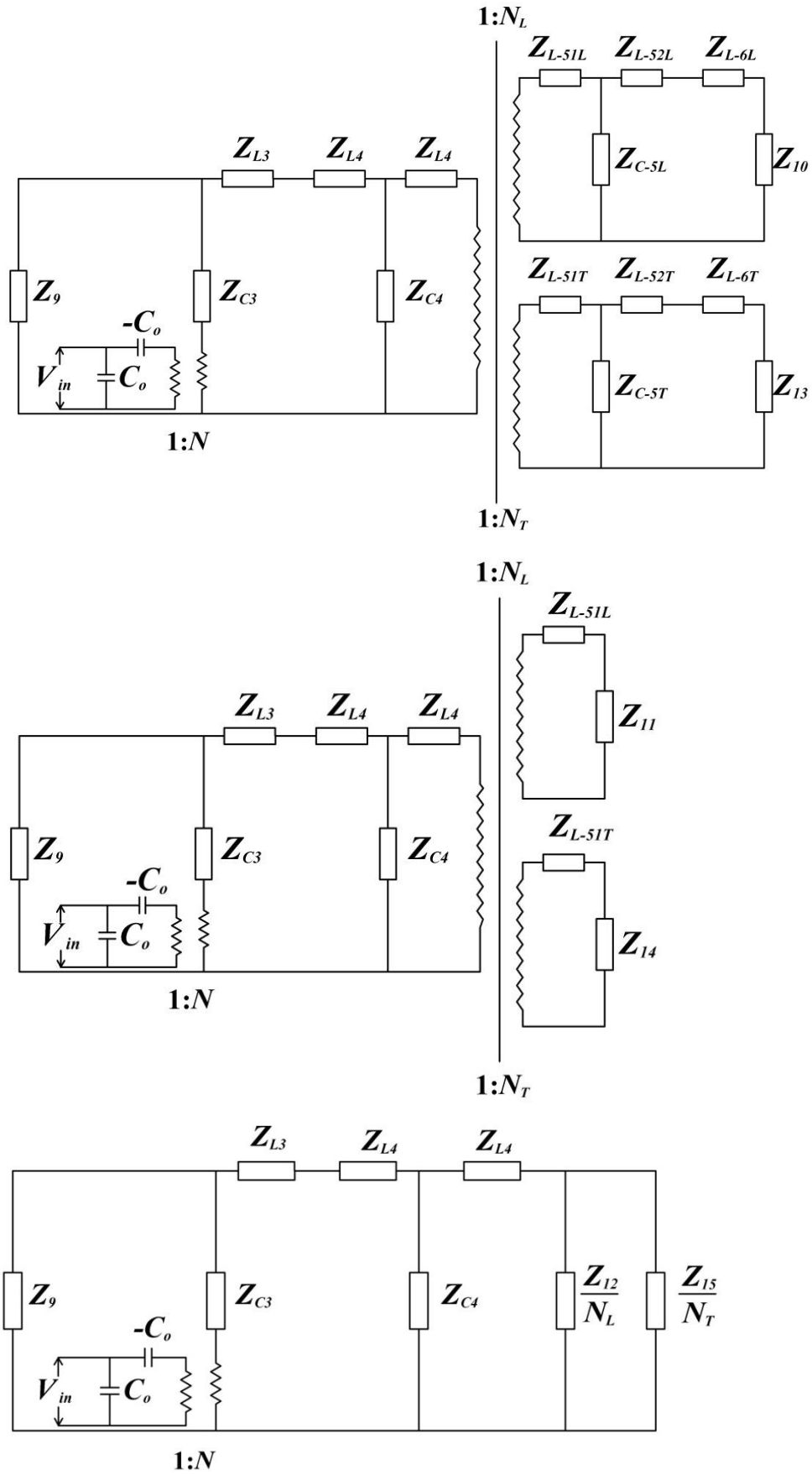


Figure 4-12 Simplifying the right side of the equivalent network.

The simple form of the equivalent network is shown in Figure 4-13, where the left and right sides of the mechanical branches are given by Z_9 and Z_{17} respectively.

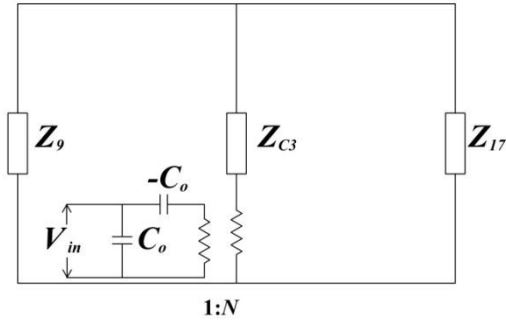


Figure 4-13 The equivalent network after simplification.

The total acoustical impedance of the mechanical section Z_m of the transducer can then be calculated by:

$$Z_m = \frac{(Z_{C3} Z_{17} + Z_9 Z_{17} + Z_9 Z_{C3})}{(Z_9 + Z_{C3} + Z_{17})} \quad 4.90$$

This impedance is transferred across the electromechanical conversion line to the electrical section, through the use of the conversion coefficient in Equation 4.52. The produced circuit is shown in Figure 4-14. The total impedance of the transducer, Z_T , is calculated as follows:

$$Z_T = \frac{\left[\left(\frac{Z_m}{N^2}\right) - Z_{Co}\right] Z_{Co}}{\left(\frac{Z_m}{N^2}\right)} \quad 4.91$$

The total impedance has real and imaginary parts, which are represented by a complex form, $a \pm jb$. The phase angle, θ , is calculated as follows:

$$\tan(\theta) = \frac{b}{a} \quad 4.92$$

The effective electromechanical coupling coefficient, k_{eff} , between the input electrical energy and the output mechanical energy can also be calculated from the impedance spectrum. By assuming that losses have a limited effect on the transducer frequencies and that the transducer has a high mechanical quality factor, the resonance, f_r , and anti-resonance, f_a , frequencies can be used to calculate k_{eff} . These frequency values can be obtained from the impedance spectrum, Z_T , where the minimum value of the impedance spectrum occurs at f_r whilst the maximum value occurs at f_a of the specific mode of vibration. Therefore, k_{eff} can be calculated as follows [119, 120]:

$$k_{eff}^2 = 1 - \frac{f_r^2}{f_a^2} \tag{4.93}$$

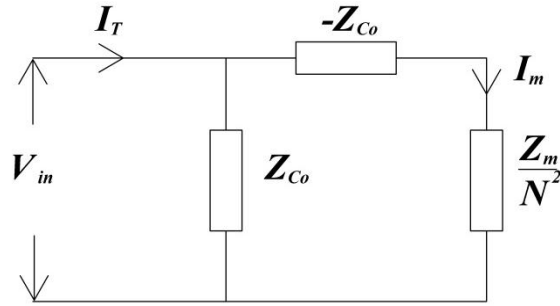


Figure 4-14 Transfer the total acoustical impedance to the electrical branch.

The total input current and the average input power can found from:

$$I_T = \frac{V_{in}}{Z_T} \tag{4.94}$$

$$\hat{P}_e = V_{in} I_T \cos \theta \tag{4.95}$$

The current divider is then used to calculate the current I_m across the transferred acoustical impedance $\frac{Z_m}{N^2}$, which is used to calculate the voltage V_m across this impedance as shown in the circuit of Figure 4-14. The following equations are used in these calculations:

$$I_m = \left(\frac{Z_{Co}}{\frac{Z_m}{N^2}} \right) I_T \tag{4.96}$$

$$V_m = \frac{Z_m}{N^2} I_m \tag{4.97}$$

This voltage V_m is then transferred back to the mechanical branch, across the electromechanical transformer, by multiplying by the transformation coefficient N to represent the applied force of the piezoelectric region F_m . The mechanical network is shown in Figure 4-15, where the velocities between the regions (v_2, v_3, v_4, v_5, v_6) are given by current loops ($I_{m2}, I_{m3}, I_{m4}, I_{m5}, I_{m6}$), which can be calculated by applying Kirchhoff's current and voltage laws. The solution of the current loops is given in a matrix form as follows:

$$[z] \begin{bmatrix} I_{m1} \\ I_{m2} \\ I_{m3} \\ I_{m4} \\ I_{m5} \\ I_{m6} \end{bmatrix} = \begin{bmatrix} 0 \\ 0 \\ V_m \\ -V_m \\ 0 \\ 0 \end{bmatrix} \tag{4.98}$$

where $[z]$ is:

$$\begin{pmatrix} (Z_{back} + Z_{L1} + Z_{C1}) & -Z_{C1} & 0 & 0 & 0 & 0 \\ -Z_{C1} & (Z_{C1} + Z_{L1} + Z_{L2} + Z_{C2}) & -Z_{C2} & 0 & 0 & 0 \\ 0 & -Z_{C2} & (Z_{C2} + Z_{L2} + Z_{L3} + Z_{C3}) & -Z_{C3} & 0 & 0 \\ 0 & 0 & -Z_{C3} & (Z_{C3} + Z_{L3} + Z_{L4} + Z_{C4}) & -Z_{C4} & 0 \\ 0 & 0 & 0 & -Z_{C4} & (Z_{C4} + Z_{L4} + \frac{Z_{12}}{N_L}) & -\frac{Z_{12}}{N_L} \\ 0 & 0 & 0 & 0 & -\frac{Z_{12}}{N_L} & (\frac{Z_{12}}{N_L} + \frac{Z_{15}}{N_T}) \end{pmatrix}$$

For the longitudinal output response, the current ($I_{m5} - I_{m6}$) is transferred across the longitudinal conversion line to the L circuit. More current loops are created as shown in Figure 4-16. Kirchhoff's laws are applied to calculate the current I_{m9-L} , which represents the longitudinal response velocity at the output surface of the transducer. A similar procedure is used with the T circuit. The current I_{m6} is transferred through the torsional conversion line and the current loops are created as shown in Figure 4-17. Kirchhoff's laws are used once again to calculate the current I_{m9-T} , which represents the torsional velocity response at the output surface of the transducer. Currents are functions of frequency and input voltage; therefore they can be used to calculate the output response for different levels of excitation.

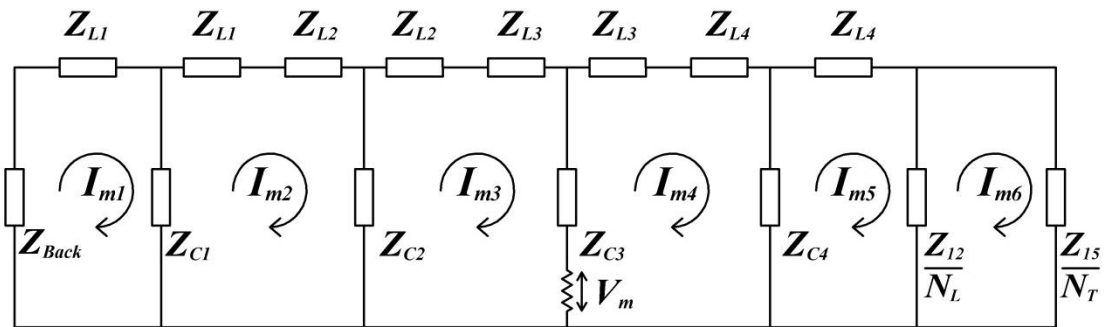


Figure 4-15 The current loops of the equivalent network.

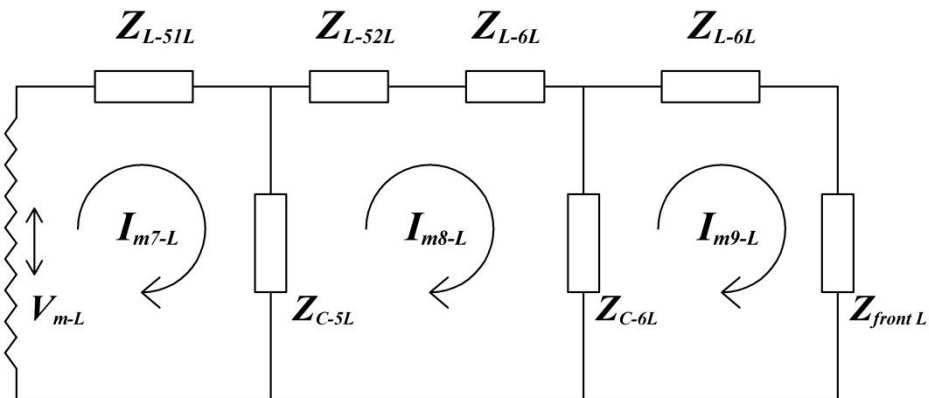


Figure 4-16 Current loops analysis of the L-circuit.

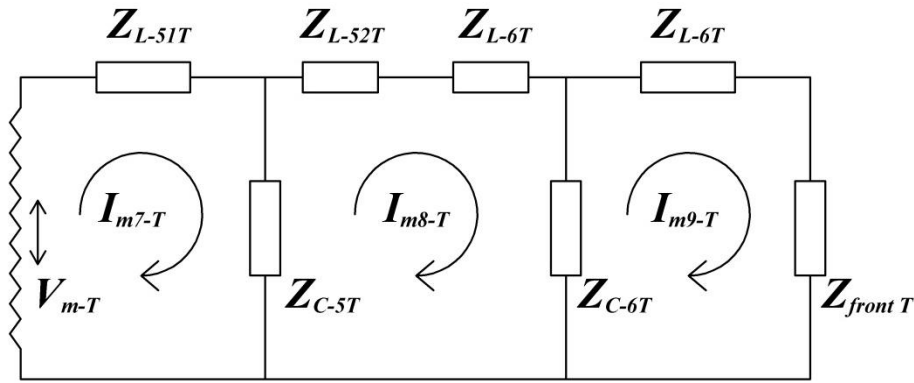


Figure 4-17 Current loops analysis of the T-circuit.

4.6 Piezoceramic transducer losses

Early analytical models of ultrasonic transducers considered the transducer as an ideal device where all types of losses are neglected [57, 121]. Later, when continuously generating power systems appeared, the study of these losses began [114]. The first introductions of losses were given through a resistance and a reactance at the electrical branch of the transducer. These losses are valid only at a specific frequency and at low levels of excitation.

In general, there are three types of losses which are associated with ultrasonic transducers: dielectric (electrical) losses, piezoelectric (electromechanical) losses, and mechanical losses [122]. The dielectric and piezoelectric losses are associated only with the piezoelectric material, whereas the mechanical losses are associated with both the piezoelectric and the acoustical materials. The dielectric losses depend on the type of piezoelectric material and the level of driving voltage that is applied to the transducer. The piezoelectric losses are related to both stress and electrical field and are proportional to the piezoelectric loss tangent [122].

Finally, the mechanical losses include contact losses at the interfaces between the parts, frictional damping in the screw-threads and internal damping of the metal parts [123]. The effects of the contact losses can be represented by lumped resistance parameters between the regions in the equivalent network. In the case that the piezoelectric section is located near to the amplitude nodal plane, which is considered in the current design, the contact losses have negligible effect on the resonance frequency. This is reasonable with the assumption of flatness and smoothness of the part surfaces [123]. Moreover, the frictional damping effect of the screw-threads, which are located near to the nodal plane, is also assumed to be limited, and so, only the internal damping is considered in this analysis.

At high power, the effect of these losses becomes complex and depends on other factors. For example, the dielectric losses become nonlinear at large input power and the mechanical losses increase rapidly as the excitation level is increased. These losses become increasingly complex at high frequency excitation [124, 125]. However, there are methods available to formulate these losses at low excitation levels [88]. The losses considered can be introduced into the analytical model through the use of complex definitions of the material properties, here the imaginary components represent the losses or out of phase components in a linear form. This yields a better agreement with the experimentally measured results than would have been possible using only the real values of the constants. The complex form of material properties are defined as follows [59, 122, 126, 127]:

$$c_{33}^{E*} = c_{33}^E (1 + j \tan \delta_m) \quad 4.99a$$

$$s_{33}^{E*} = s_{33}^E (1 - j \tan \delta_m) \quad 4.99b$$

$$\varepsilon_{33}^{T*} = \varepsilon_{33}^S (1 - j \tan \delta_e) \quad 4.99c$$

$$d_{33}^* = d_{33} (1 - j \tan \delta_k) \quad 4.99d$$

$$k_{33}^* = k_{33} (1 + j \tan \delta_k) \quad 4.99c$$

where c_{33}^E is the elastic stiffness of the non-piezoelectric materials, s_{33}^E is the elastic compliance of the piezoelectric material at a constant electrical field and ε_{33}^T , d_{33} and k_{33} are the clamped dielectric permittivity, the piezoelectric constant in the thickness mode, and the electromechanical coupling constant for the thickness mode of a disc respectively. δ_m , δ_e , δ_k are the elastic, dielectric, and electromechanical coupling factor loss tangents, these can be found in the manufacturer data sheets for the piezoelectric material or can be calculated from the quality factors as follows [63]:

$$\tan \delta_m = \frac{1}{Q_m} \quad 4.100a$$

$$\tan \delta_e = \frac{1}{Q_e} \quad 4.100b$$

$$\tan \delta_k = \frac{1}{Q_k} \quad 4.100c$$

where Q_m , Q_e and Q_k are the Q-factors for the elastic stiffness constant, piezoelectric constant and dielectric constant respectively. The piezoelectric constant can also be calculated as follows [10, 128]:

$$d_{33} = \varepsilon_{33}^T g_{33} \quad 4.101$$

where g_{33} is the voltage constant of the piezoelectric material.

4.7 Modelling of pre-stress effect

The acoustical properties of the pre-stressed bolt are added stiffness and mass to the transducer. These effects are considered in the previously derived analysis. However, these are not the only effects of the pre-stressed load because the applied static pre-compression also results in a shift of the resonance and anti-resonance frequencies of the transducer. There are two possible explanations for this shift: the physical characteristics of the piezoelectric material are changed under compression and the contact conditions between the transducer parts are changed under pre-loading [129-131]. For effective analytical model, it is required that the modified constants of the piezoelectric material are considered. This is more practical than considering the contact conditions between the transducer parts [59].

4.8 Modelling of external loads

In high power ultrasonics, the ultrasonic transducer is composed of piezoelectric elements sandwich between a metal front and back mass. The front mass is normally in contact with the external load while the back mass is usually free. Therefore for the operation of transducers, the load on the front mass should be considered, while the load on the back radiation face of the transducer can be ignored. As shown in Figure 4-10 in the complete equivalent network of the transducer, the load impedance Z_{front} represents the reaction of the load on the output surface of the front mass. This changes for different ultrasonic applications and is particularly hard to determine in high power ultrasonics. However, an approximate expression can be used to calculate the load impedance value and is given by [132]:

$$Z_{front} = j\rho_L c_L S_L \tan(k_L l) \quad 4.102$$

where ρ_L , c_L , S_L , k_L , and l are the density, the wave speed, the cross-sectional area of the load medium, the wave number and the length of the load medium, respectively. The length of the load medium depends on the application and is considered as the length of the tool used for ultrasonic drilling or machining applications.

4.9 Mathematica script

The symbolic environment software, Mathematica, is used to solve the impedance equations of the transducer regions and to solve the equivalent electrical network. The program has the power and the flexibility to describe the variables in complex form. A script is written according to the flow chart which is shown in Figure 4-18.

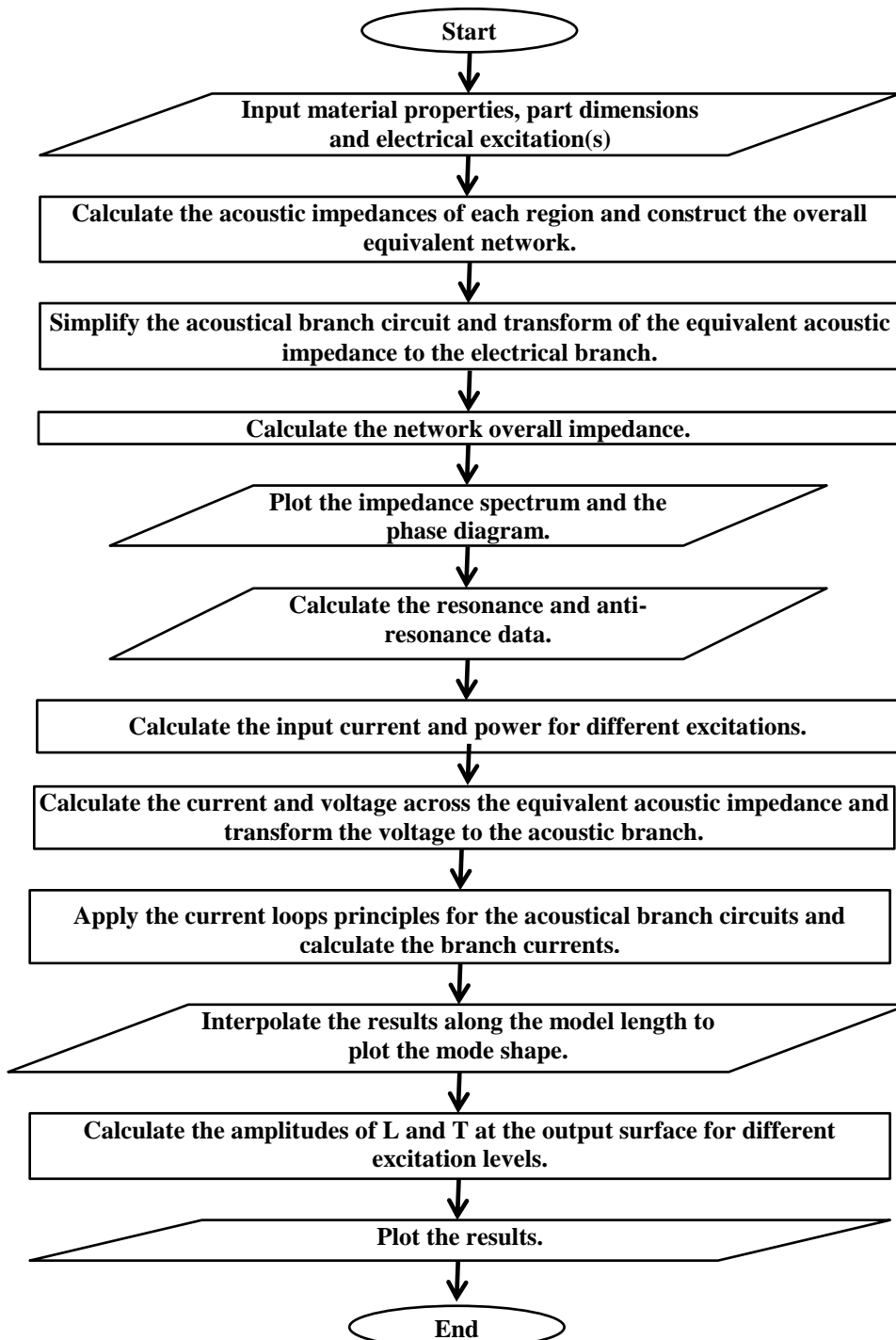


Figure 4-18 Flowchart for computing the equivalent network of the transducer.

4.10 Summary

In this chapter, the theory of one-dimensional wave motion in an elastic solid is used to create an analytical model for LT transducers which is used to calculate the electromechanical parameters. The equivalent circuit approach is employed to solve the wave equation through the principles set out by the one dimensional Mason's model. This is applied to create the equivalent electrical network of the transducer. The coupling between L and T vibrational motions of the transducer's front mass is analysed and represented by two separate equivalent circuits. The L and T response can be calculated using a Mathematica script that simplifies the network based on Kirchhoff's laws. The model can predict the electrical impedance spectrum, the phase difference between the input voltage and current, the resonance and anti-resonance frequencies of the desired mode, the effective coupling coefficient of electrical and mechanical energy, the responses at the boundaries between the transducer parts, as well as, the input current, power, and output response for different excitation levels. The responses at the part boundaries are interpolated along the transducer model and the data is employed to plot the mode shape of the LT mode. This is used to locate the nodal plane and validate the numerical calculation that will be presented in chapter 5.

Chapter 5 Experimental analysis and results

5.1 Introduction

Computer modelling such as numerical and analytical models, have become more powerful for many aspects of analysis, design and product refinements. The current FE codes can provide accurate and precise results which can reduce the required time and cost of prototype testing, however they cannot totally replace the prototyping technique. It is difficult and even impossible to consider all parameters that may affect the accuracy of FE results such as uncertainty of material properties and manufacturing tolerances. The approximation methods of analytical modelling can also provide high uncertainty in calculations. Furthermore, there are difficulties in modelling certain aspects such as the dynamics of joints, damping, and boundary conditions. Therefore, it is important to validate the model through experimental analysis.

In addition to validation purposes, experimental analysis is used to update computer models. It is also employed in troubleshooting to build an experimental model or to compute structural modifications and it can be used as a benchmark with which to understand the dynamic behaviour of a structure without the need to create complicated models.

In the design of ultrasonic transducers, experimental tests such as experimental modal analysis (EMA), harmonic response analysis and electrical impedance analysis are used to extract the vibrational and electrical characteristics of the transducers. The results of such tests are employed to validate and update computer models as shown in the block diagram in Figure 5-1.

In this chapter, two differently sized prototypes of the optimised LT transducer are fabricated in order to validate the size scaling feature and therefore the possibility of applying this design for different ultrasonic applications. An electrical impedance analysis is used to accurately measure the pre-stress on the piezoceramic components during the assembly process. Then it is utilised to extract the electrical impedance spectra which is used to calculate the resonance, anti-resonance frequencies, and the effective coupling

coefficient between electrical and mechanical energy. The impedance spectrum is also essential for electrically matching the prototypes to the power supply which is important in minimising the losses due to mismatching between devices. Additionally, the extracted data is used to validate the findings of analytical and FE models of electrical impedance spectra and the frequencies of the desired LT and the surrounding modes of vibration.

The second experimental test is the EMA which is performed to extract the modal parameters (resonance frequencies and mode shapes) of all modes of vibration over a broad-band of excitation. The measurements are used to extract the resonance frequencies and the frequency spacing between the LT and surrounding modes as well as the mode shapes and the location of nodal planes along the structure of the prototypes. The extracted data is also used to validate the findings of the mathematical modelling. It is also possible to extract the damping coefficients of vibrational modes which can be used to update the FE models. However, the difficulty in specifying the excitation force prevents accurate estimation of these coefficients. Instead, harmonic excitation analysis based on a frequency sweep technique is used for this purpose. Harmonic analysis is employed to characterise the prototypes, where the measurements of frequency response are used to extract the magnitude of the responses at the output surface at different excitation levels. These data is used to validate the predictions of the mathematical models and to update the FE models for damping coefficients of the LT mode.

The effectiveness of the design is assessed by the magnitude of the L response to a given input and the torsionality, previously defined as the ratio of torsional to longitudinal response at the output surface. The tangential component of the vibration at the tip edge is adopted as an approximation for T response amplitude; care should be taken to ascribe it only to T modes so as to avoid misinterpretation of F modes. The torsionality value gives the degree of degeneration of L vibration in the prototypes, where a value above unity indicates a transducer operating with dominant T behaviour and values below indicate a prevailing L motion. When the torsionality is one, the excursion at the edge of the horn tip describes a partial spiral with a helix angle of 45° indicating balanced LT interaction [16].

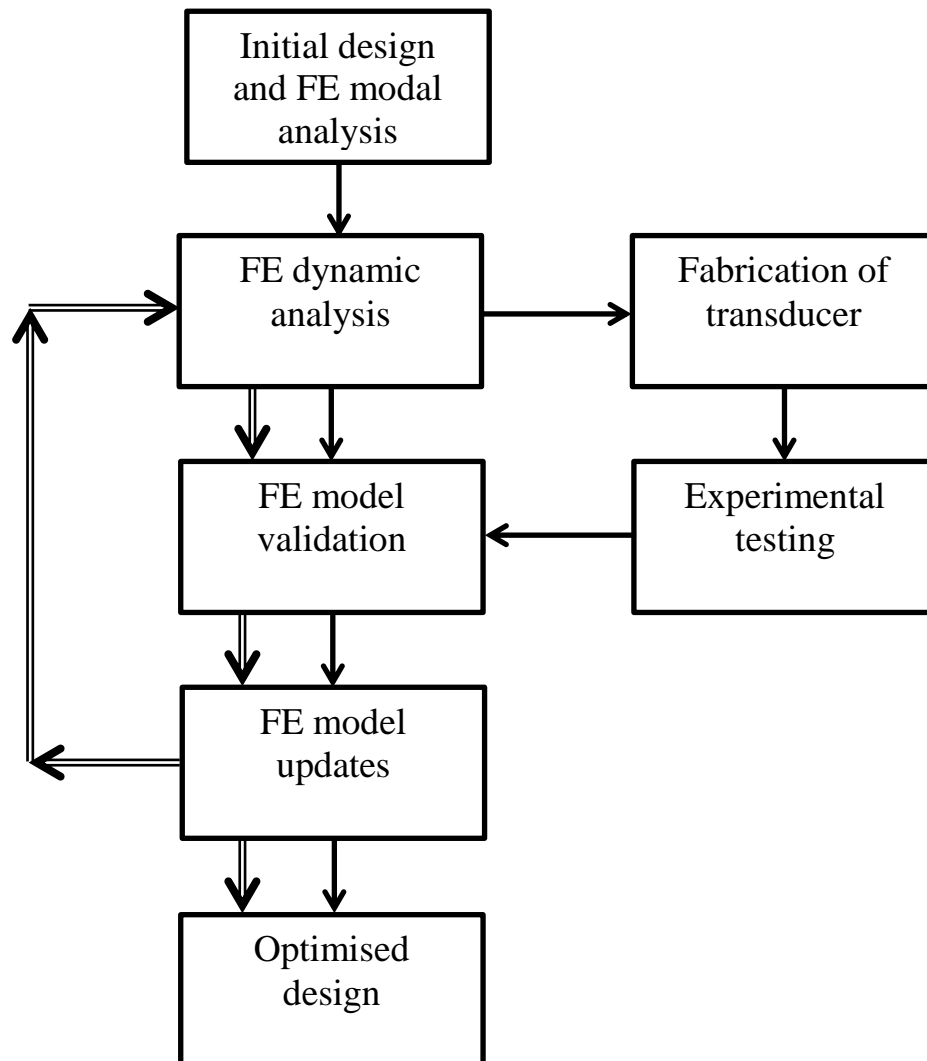


Figure 5-1 Validation and updating of finite element model.

5.2 Fabrication of LT transducer

Piezoceramic rings are available in certain dimensions. Therefore the principles of size scaling, presented in section 3.9 are used to calculate the dimensions of two different sizes of the optimum FE transducer model. The fabricated prototypes are examined to characterise the performance and to validate and update the mathematical modelling of LT transducers. They are also used to validate the prediction of the size scaling study where the performance of the two prototypes, which are fabricated for 180° twisting angle of slots, is compared to the FE calculations. The key dimensions of these transducers are

shown in Table 5-1, in which the selected piezoceramic rings are supplied by CeramTec GmbH and PI Ceramic for transducers 1 and 2, respectively.

Table 5-1 Dimensions of fabricated transducers.

No.	Transducers	Piezoceramic rings type	Outer diameter of rings (mm)	Thickness of rings (mm)	Transducer total length (mm)	Diameter of output surface (mm)
1	Transducer 1	Sonox [®] P8	38	5	130.5	20
2	Transducer 2	PIC 181	12.7	1.5	43	4

In addition to the effect of materials and design factors, the performance of the fabricated prototypes largely relies on the fabrication processes which can be divided into two general steps, preparation and assembly.

5.2.1 Preparation of transducer parts

In the preparatory stage, the transducer parts (front mass, back mass, electrode rings and pre-stressed bolt) are fabricated, where the material properties are presented in Chapter 3. For both prototypes, the front masses are made from titanium alloy Ti-6-4 due to its low specific acoustic impedance which only produces a low loss of acoustic energy when acoustic waves pass through them. The back masses are made from low carbon steel which is heavier than the titanium alloy, so that as the acoustic impedance will be higher, more acoustic energy is guided toward the front mass.

The pre-stressed bolt of size M12 for transducer 1 is fabricated according to international standard (ISO 262) from the titanium alloy due to its high tensile strength. A stainless steel (grade A) bolt of size M5 is chosen for transducer 2 because of the difficulty in fabricating a small size bolt. Both bolts are attached by washers to ensure a symmetrical distribution of the axial stress on the cross-sectional area of the piezoceramic rings. Finally, surface grinding treatments are applied to all contact surfaces of the transducer parts to ensure high surface quality which can enhance the mechanical coupling between the parts. The components of prototypes 1 and 2 are shown in Figures 5-2 and 5-3, respectively. An additional flange is added to the front mass of transducer 2 in order to simplify the mounting configuration during operation.



Figure 5-2 Components of transducer 1.



Figure 5-3 Components of transducer 2.

5.2.2 Assembly of transducer parts

Assembly plays an influential role in transducer performance because a transducer is a multi-component system that resonates as a single object. Therefore it requires good electrical and mechanical contact between the components in order to reduce any energy losses due to improper assembly. In the assembly process, parts are first cleaned by acetone to remove any grease or oil from the surfaces and then assembled together carefully. Additional fabricated clamps are used to hold the assembled structure properly and to prevent unexpected movements during the pre-loading process. As the pre-stressed bolt is inserted inside the inner ring of the piezoceramic stack, insulation is required to avoid an electrical short circuit. Insulation tape of 0.1mm thickness is used to cover the pre-stressed bolt section where it is exposed to the inner piezoceramic rings. The piezoceramic rings are sandwiched by copper electrodes which are arranged so as to be mechanically in parallel but electrically in series. This is achieved by pointing the negative side of the first ring towards the front mass while its positive side is pointed towards the positive side of the second ring, after which its negative side is pointed to the back mass. The positive sides of both rings are, therefore, in contact with the middle copper electrode. An exploded schematic of the assembly of the transducer is shown in Figure 5-4.

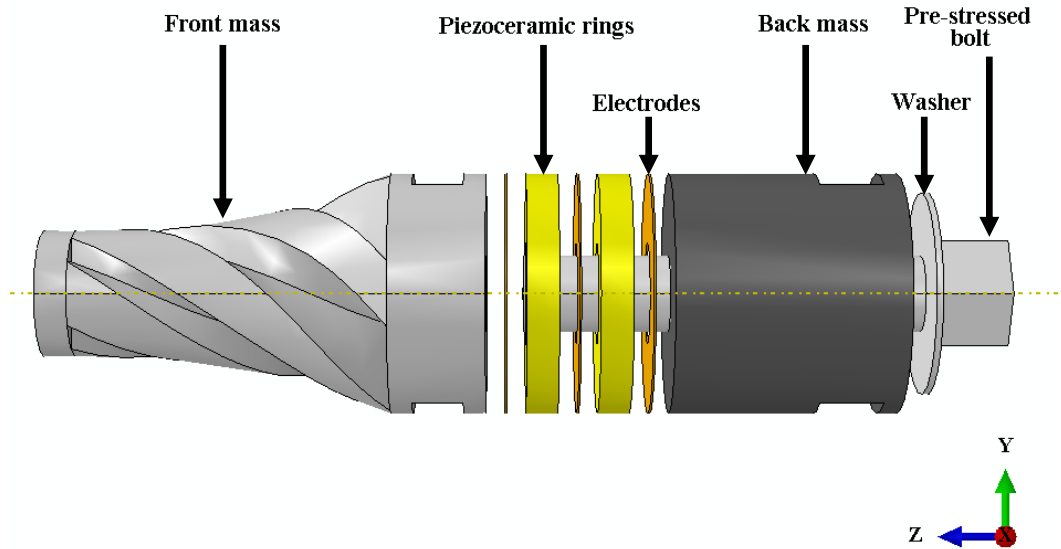


Figure 5-4 Exploded schematic of transducer assembling.

5.3 Pre-loading of LT transducers

Preloading is important for multi-component transducers to ensure that the components, particularly the piezoceramic rings, remain in compression during operation since they are inherently weak in tension. Controlling the preload is necessary because inadequate compression results in dynamic gapping at the interfaces of each joint, thus producing higher impedance and heating of the piezoceramic stack. On the other hand, excessive preload can depolarise the piezoelectric material and produce unstable impedance and ageing during operation. Piezoceramic materials can withstand pressures up to a few hundred MPa before breaking mechanically. However this limit should not be approached in practical applications. This is because depolarisation occurs at a pressure of about 20-30% of the mechanical strength limit. It is therefore recommended that the stress applied to hard piezoceramic components is in the region of 15-30MPa [11, 133-135].

For Langevin transducers with a central pre-stressed bolt, the required preload on the piezoceramic ring stack is calculated by multiplying the value of recommended stress by the cross-sectional area of the rings. This load is, statically, equal to the tension load in the central pre-stressed bolt F_t [59]. The required torque T_o to be applied to the pre-stressed bolt is then calculated by considering the bolt geometry and the friction coefficients, using the following equation:

$$T_o = F_t \left(\frac{d_2}{2} \left(\frac{\mu}{\cos \vartheta_1} + \tan \vartheta_2 \right) + \mu_n \frac{d_n}{2} \right) \quad 5.1$$

where d_2 and d_n are the mean diameters of the bolt threads and the bolt head, μ and μ_n are the coefficients of friction in the threaded section and at the contact between the bolt head and back mass, ϑ_1 and ϑ_2 are the half angle of the screw thread and the lead angle, respectively [136-138].

Different stress values, ranging between 5-25MPa for transducer 1 and 5-30MPa for transducer 2, were tested and the calculated torques, calculated by Equation 5.1, were applied to the pre-stressed bolt of each prototype through sequenced steps as indicated in tables 5-2 and 5-3. The calculated torques was applied by using a gauged torque wrench. Two torque wrenches of various scales were used to accurately apply the torques for transducer 1, the first torque wrench (Norbar SL1, 8-54Nm) was used for steps 1 and 2 whilst the second wrench (TRI FXL 200, 40-200Nm) was used for the other steps. For transducer 2, a torque driver (Britool TD50, 1-6Nm) was used for all steps [139-141].

The actual stresses on the piezoceramic components were calculated by measuring the generated charge in the piezoceramic stack during the preloading steps by using a short electrical circuit arrangement. In this circuit, a non-electrolytic capacitor of $1\mu\text{F}$ was connected to the electrical terminals of the piezoceramic stack and to a DC voltmeter with high internal resistance. A multi-meter (FLUKE 115) was used for this purpose, with internal resistance of $10\text{M}\Omega$. The generated charge was stored in the capacitor, allowing sufficient time to accurately measure the charge by measuring the generated voltage across the capacitor. At each step, the pre-stressed bolts were tightened quickly to prevent charge drop, which must otherwise be prevented by higher internal resistance of the voltmeter [11, 136, 142]. The generated charge q_e in the piezoceramic stack was calculated by:

$$q_e = CV \quad 5.2$$

where C and V are the capacitance (in Farads) and the voltage across the capacitor (in Volts), respectively. The preload on the piezoceramic stack F for each step was calculated by using the charge constant of the piezoceramic rings in the thickness mode d_{33} as follows:

$$F = \frac{q_e}{n_o d_{33}} \quad 5.3$$

where n_o is the number of piezoceramic rings. The actual stress was then calculated by dividing the preload by the cross-sectional area of the piezoceramic ring. The test steps and the measured and calculated parameters for transducer 1 and transducer 2 are listed respectively in Tables 5-2 and 5-3. For both transducers, the difference between applied stress and the derived stress from the charge increased slightly with increased pre-stress

values. This may be partially related to the possible measurement tolerances in the multi-meter and the torque wrenches. The reduction in measured stress can also be related to the increase in the piezoelectric charge constant d_{33} with pre-stress, which led to a reduction in the calculated preload, as indicated in Equation 5.3, and therefore in the derived stress [143]. However these differences are still within acceptable levels, which is a good indicator of success in using this circuit to measure the actual pre-stress on piezoceramic components. The test setup for transducer 1 is shown in Figure 5-5.

Table 5-2 Pre-stressing calculations of transducer 1.

Step	Applied stress (MPa)	Calculated torque (Nm)	Measured voltage (V)	Measured charge $\times 10^{-6}$ (C)	Force (N)	Derived stress (MPa)	% diff.
1	5	26.76	2.3	2.30	4,792	5.14	2.7%
2	10	53.52	4.573	4.57	9,527	10.21	2.1%
3	15	80.29	6.53	6.53	13,604	14.58	2.8%
4	20	107.05	8.53	8.53	17,771	19.05	4.7%
5	25	133.81	10.59	10.6	22,063	23.65	5.4%

Table 5-3 Pre-stressing calculation of transducer 2.

Step	Applied stress (MPa)	Calculated torque (Nm)	Measured voltage (V)	Measured charge $\times 10^{-6}$ (C)	Force (N)	Derived stress (MPa)	% diff.
1	5	0.65	0.25	0.25	472	5.05	0.9%
2	10	1.30	0.5	0.50	943	10.09	0.9%
3	15	1.96	0.76	0.76	1,434	15.34	2.2%
4	20	2.61	0.96	0.96	1,811	19.38	3.1%
5	25	3.26	1.203	1.20	2,270	24.29	2.8%
6	30	3.91	1.53	1.53	2,887	30.89	2.9%

5.4 Experimental analysis of fabricated transducers

The fabricated prototypes were experimentally analysed after assembly by three types of tests. The first type was the electrical impedance analysis which was used to evaluate the electrical properties of the transducers, the second type was the experimental modal analysis to extract the modal parameters, and the third type was the harmonic excitation analysis to characterise the performance at different levels of excitation. The measured data was used to validate and update the findings of the computer models.

5.4.1 Electrical impedance analysis

The electrical impedance magnitudes of the broad-band frequency were experimentally measured using an Agilent 4294A impedance analyser. The analyser was calibrated prior to performing the test and its impedance probe (PROPE 42941A) was connected to the terminals of the transducers which were unrestrained by being freely placed on a foam layer as shown in Figure 5-6 for transducer 1. A swept signal of 500mV over a selected bandwidth of frequency was applied and the impedance spectra with a phase change between voltage and current was measured. This analysis was used to further optimise the pre-stressing process whereby, after each preloading step, the transducers were connected to the analyser through which the magnitude of electrical impedance $|Z_e|$ and the series and parallel resonance frequencies, f_s and f_p , were measured for the desired LT mode. The applied electrical signal in this test was small enough to permit the assumption that f_s and f_p were equal to resonance and anti-resonance, f_r and f_a , frequencies, respectively. This assumption was discussed in section 3.3.3 of Chapter 3 and Equation 4.94 was used to calculate the effective electromechanical coupling coefficient k_{eff} . This coefficient was used to evaluate the effectiveness of electrical to mechanical energy conversion by the fabricated transducers [12, 120].

The impedance analysis measurements were implemented for each preload step of transducers 1 and 2 and the results are presented in Figures 5-7 and 5-8, respectively. For the first few preload steps, where the applied torques were less than the recommended range, the electrical resonance and anti-resonance frequencies of the LT mode increased with the applied torques. The rate of increase slowed as the applied torque reached the recommended range, indicating that electrical stability of the transducer had been reached. The stable values for the resonance frequencies for transducers 1 and 2 were reached for

torque values above 80Nm and 3.2Nm, respectively. As seen in Table 5-2 and Table 5-3, these torque values are equivalent to respective pre-stresses of 15MPa and 25MPa. Therefore they are considered the minimum values for producing the required compressive stress for the piezoceramic stacks. The change in electrical resonance and anti-resonance frequencies and the effective coupling coefficient corresponding to different applied torques for transducers 1 and 2 are presented in Figure 5-9 and Figure 5-10, respectively. The desirable stable resonance frequency and highest coupling coefficient can be achieved at torque values of 133.8Nm for transducer 1 and 3.26Nm for transducer 2, where the pre-stress on the piezoceramic stacks of both prototypes is approximately 25MPa. Therefore, these values were used as the optimum torques for the fabricated transducers.

In order to check that the pre-stressed bolts can withstand the applied torques, the generated tensile and shear stresses are calculated, with the elastic properties of each bolt, and are used to find its design safety factor. The safety factor is defined as the ratio of the tensile-shear stress combination (Von Mises stress) generated by pre-loading to the yield strength of the bolt material. For optimum values of torques, safety factors of 3.2 and 4 were calculated for the pre-stressed bolts of transducers 1 and 2, respectively. These values are high enough to prevent any failure in the bolts during transducers operation [11, 144, 145].



Figure 5-5 Preload setup of transducer 1.

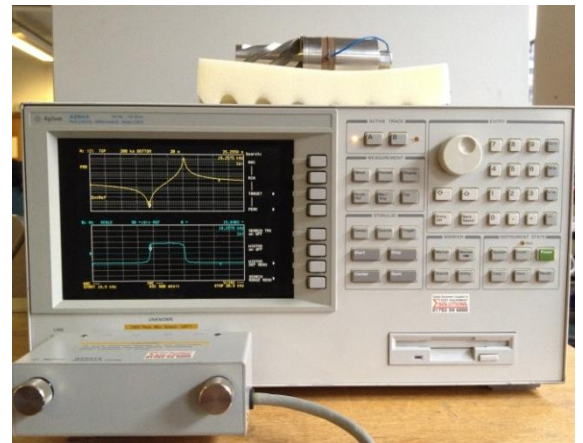


Figure 5-6 Agilent 4294A Impedance analyser.

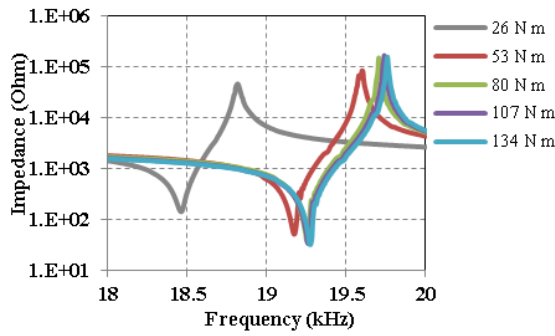


Figure 5-7 Experimental electrical impedance magnitude of transducer 1 for different applied torque.

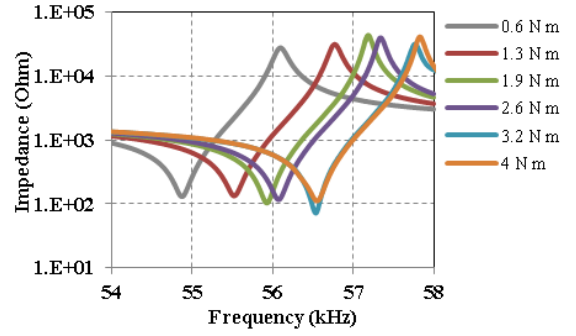


Figure 5-8 Experimental electrical impedance magnitude of transducer 2 for different applied torque.

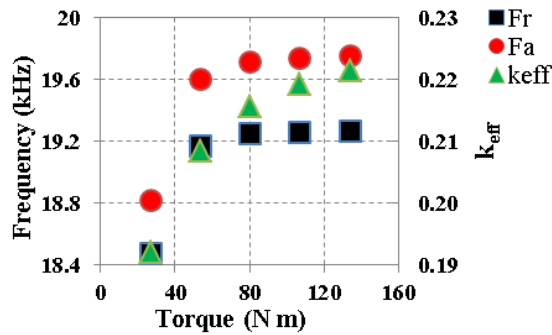


Figure 5-9 F_r , F_a and k_{eff} of transducer 1 for different applied torques.

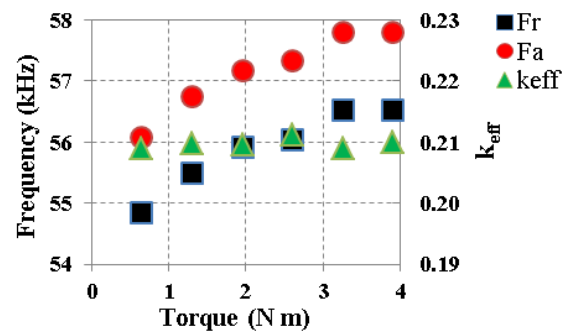


Figure 5-10 F_r , F_a and k_{eff} of transducer 2 for different applied torques.

5.4.1.1 Evaluation of FE model

Further investigation of transducer 1 was conducted by using the impedance analyser to validate the FE model. A comparison between FE estimations and experimental findings of the electrical impedance spectra and the phase change for LT and T modes of vibrations is presented in Figure 5-11. The FE prediction was calculated by simulating an excitation across the piezoceramic rings in a steady state dynamic analysis step. The calculated reactive electrical nodal charges on the positive electrodes of piezoceramic rings were used in Equations 3.29 and 3.30 of Chapter 3 to calculate the magnitude of the electrical impedance and the electrical phase difference. The resonance frequencies for the LT mode from the FE and experimental results are in good agreement which indicates that, at low excitation levels, the FE assumptions of materials properties, interaction between parts and boundary conditions are accurate. This correlation also suggests that the preparation, assembly and preloading steps of fabricated transducer 1 are sufficient to ensure good contact between parts. However, there was a difference in impedance magnitude which is

significant at the anti-resonance frequency. Also the frequency difference for the anti-resonance frequency suggests that the FE model is unable to predict all electromechanical parameters. The other limitation of the FE model was the need for powerful computing to calculate the electrical impedance spectra.

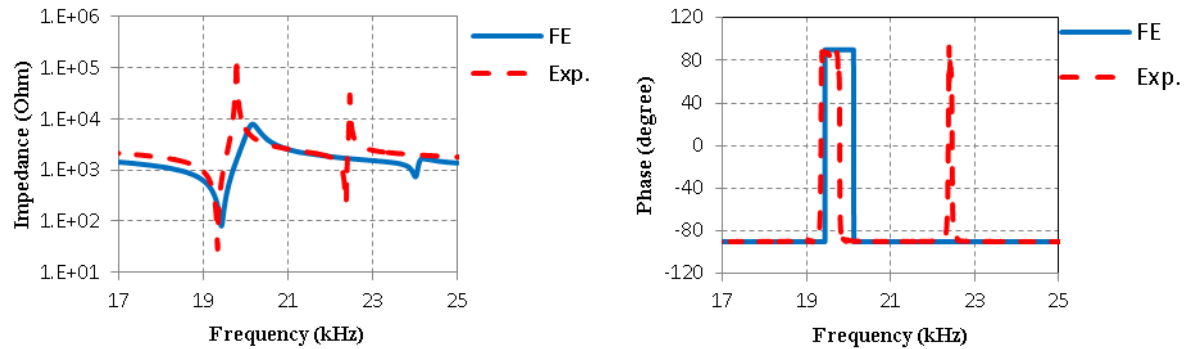


Figure 5-11 Experimental and FE impedance spectra magnitude (left) and the phase diagram (right) for transducer 1.

5.4.1.2 Evaluation of the analytical model

The principles of the equivalent circuit approach, which was presented in Chapter 4, were used to predict the electrical impedance and phase diagrams for the analytical model of the fabricated transducers. For transducer 1, the calculated impedance magnitude and phase diagram were compared to the experimental findings shown in Figure 5-12, where the results indicate a considerable frequency difference between these results. The experimental data is at a lower resonance and anti-resonance frequency. This can be related to the reduction in stiffness of the front mass due to the creation of slots. This effect was not considered in the calculation in the analytical model. Similar results can be noted in connection with the calculation of transducer 2, for which the frequency difference is shown in Figure 5-13. From these results, a linear relationship between the reduction of stiffness due to slitting and the size of front mass was defined, with the relationship constants calculated from the measured impedance data. The linear relationship was then applied to the stiffness definition in the analytical model of transducers 1 and 2. The corrected data are re-plotted as shown in Figures 5-14 and 5-15.

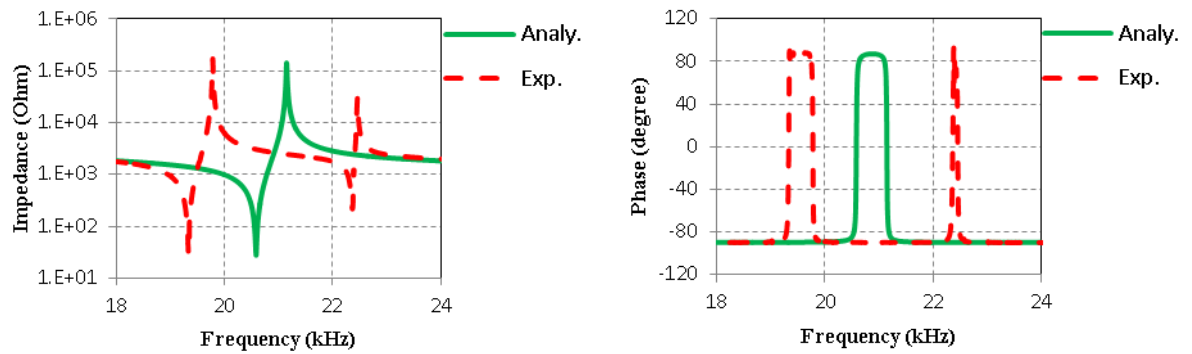


Figure 5-12 Experimental and analytical impedance spectra magnitude (left) and the phase diagram (right) for transducer 1.

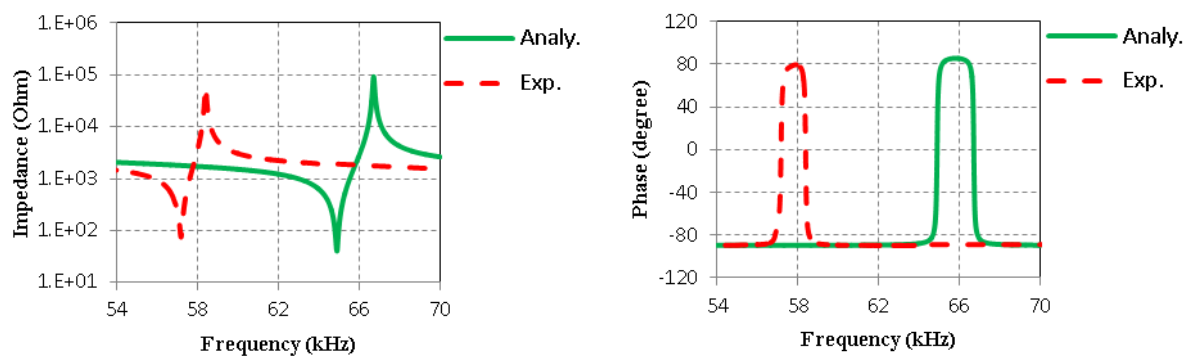


Figure 5-13 Experimental and analytical impedance spectra magnitude (left) and the phase diagram (right) for transducer 2.

This linear assumption shifted the analytical calculation of impedance to match the measured results for both transducers. However this assumption would need to be checked for other, differently sized, transducers. As this relationship is only connected to the frequency shifting of the vibrational mode and not of the impedance magnitude, it is possible to carry out a check by comparing it with the FE findings for other differently sized transducers. This is shown in Figure 5-16. An excellent correlation between the analytical and FE results was noted, illustrating another advantage of the use of analytical model as an initial design tool rather than as a validation tool. The analytical code was developed to make it possible to check the electrical parameters as well as the resonance frequencies for LT transducer models, by providing the material properties and the thickness and number of piezoceramic rings required. The code calculates the recommended dimensions of other parts of the LT transducer and the piezoceramic rings inner and outer diameters. It is also possible to adjust the available dimensions of piezoceramic rings so as to match the general size criteria of the transducer design.

The corrected analytical calculations and the experimental data of the electromechanical parameters are listed in Table 5-4. Excellent correlation in terms of resonance and anti-

resonance frequencies can be noted. The impedance magnitudes at resonance are also well predicted in analytical models. However, there was poor correlation between predicted and measured values of impedance magnitude at the anti-resonance frequency, particularly for transducer 2. Nevertheless, these values do not affect the proposed modelling approach as the designed LT transducers are set to operate at resonance conditions. The difference between predicted and measured effective coupling coefficients is related to the application of the manufacturer data for piezoceramic properties in the analytical model. These represent the maximum values of the properties and can change for several different reasons.

Finally, it should be noted that the analytical model is based on the one-dimensional wave equation. Therefore it can only calculate the impedance for L and, in this study, the degenerated LT mode. Although the FE model can predict all modes of vibration which may be considered an advantage when compared to the analytical model, this factor must be balanced against the inaccuracies in impedance values for the LT mode estimated from the FE model, as shown in Figure 5-11.

Table 5-4 Analytical and experimental data of transducers 1 and 2.

	Transducer 1					Transducer 2				
	$ Z _{min}$ (Ohm)	f_s (Hz)	$ Z _{max}$ (Ohm)	f_p (Hz)	k_{eff}	$ Z _{min}$ (Ohm)	f_s (Hz)	$ Z _{max}$ (Ohm)	f_p (Hz)	k_{eff}
Analytical	29.98	19,283	150,825	19,803	0.23	45.5	57,157	108,735	58,890	0.24
Experimental	28.49	19,337	170,829	19,785	0.21	75	57,177	58,143	58,392	0.2
% diff.	5.2%	0.3%	11.7%	0.1%	9.5%	39.3%	0.0%	87.0%	0.9%	20.0%

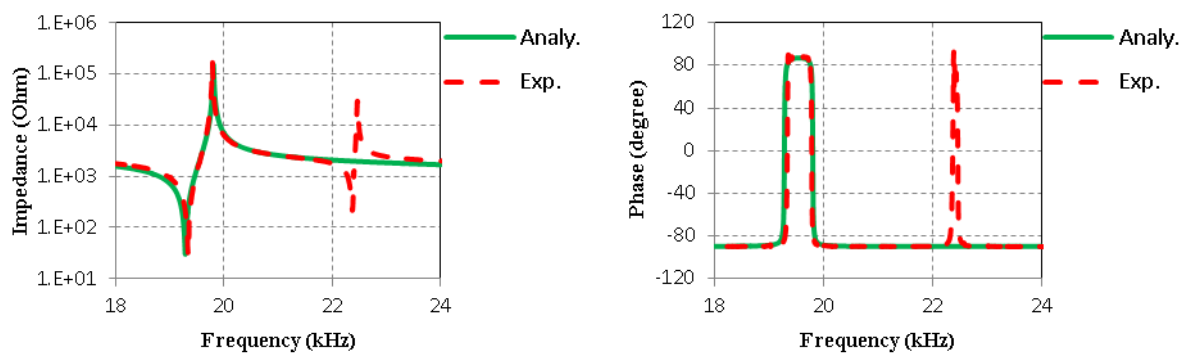


Figure 5-14 Experimental and corrected analytical impedance spectra magnitude (left) and the phase diagram (right) for transducer 1.

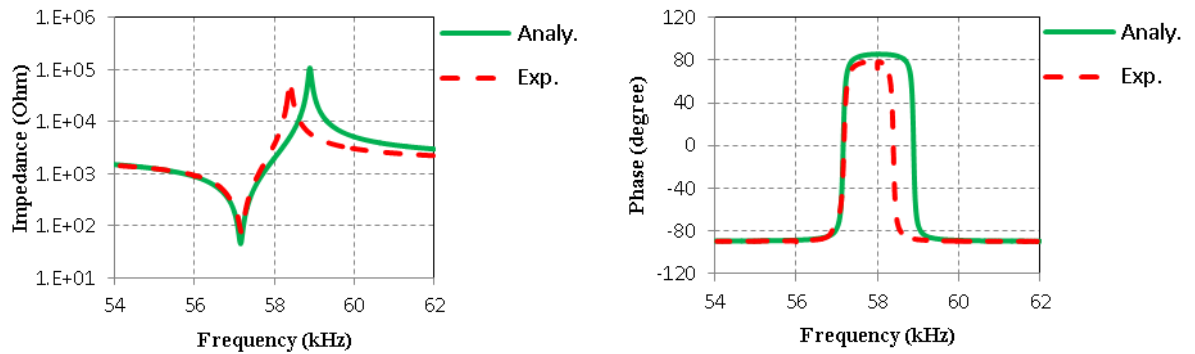


Figure 5-15 Experimental and corrected analytical impedance spectra magnitude (left) and the phase diagram (right) for transducer 2.

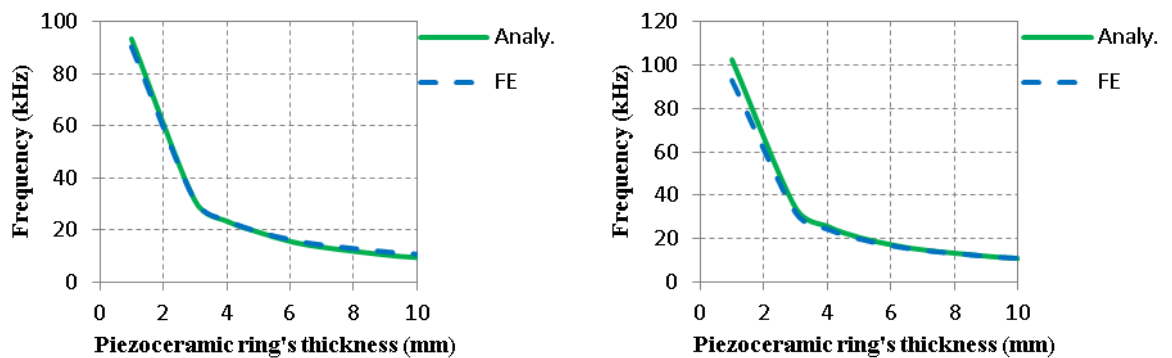


Figure 5-16 Corrected analytical and FE prediction of LT frequencies for different sizes of transducer, resonance frequency (left) and anti-resonance frequency (right).

5.4.2 Experimental modal analysis

Experimental modal analysis (EMA) is a testing process to accurately estimate the modal parameters of a structure. In general, this process is carried out through two different measurement techniques that depend on the excitation methods; namely, free and forced vibration techniques. The free vibration technique is used to measure the natural vibrational response of a structure; it is normally used in studying large structures such as bridges to yield the natural frequencies and the modal damping factors of the structure.

The forced vibration technique is used to measure the structural response for a given excitation force which can be applied by a number of different mechanisms such as a hammer or an electromagnetic shaker. The collected data of input excitation and output response are converted from the time domain to the frequency domain in order to create a frequency response function (FRF). A FRF expresses the response amplitude to an applied force as a function of frequency, thus representing a practical tool to extract modal

damping, natural frequencies and mode shapes of the structure. FRF can also be presented as the ratio of velocity response or acceleration response to an input force.

In the ultrasonic transducer, the input electrical signal is regarded as the applied excitation which converts into mechanical motion at the piezoelectric component(s). The experimental setup of EMA for ultrasonic transducers comprises of the signal generator, power amplifier, laser vibrometer, data acquisition and PC. The signal generator feeds the excitation signal into the power amplifier which then amplifies and inputs to the transducer and causes the vibration. The transducer response is measured by the laser vibrometer, which collects and analyses the acquired signals through data acquisition hardware interfaced to the PC. The visualisation of the mode shapes of the whole transducer requires the recording of multiple measurements from a grid of points covering the transducer surface. Therefore, the density of the grid points should be sufficient to enable all mode shapes within the test frequency range to be identified. In the present work, the measured results were used to extract the modal parameters and to validate the equivalent predicted parameters by FE and the analytical models for the LT and surrounding, F and T, modes. The test steps were performed as described below:

5.4.2.1 Excitation signals

The excitation signal for the EMA can be generated by three different methods, depending on the requirements of the test; these are the periodic, transient and random methods. However, EMA for ultrasonic devices uses the periodic or the random method to generate a swept sine signal or a true random signal, respectively. Although the response of an ultrasonic device under periodic excitation can be identically related to the excitation signal, random excitation is more common because it excites all frequencies at the same time and can be easily implemented.

5.4.2.2 Boundary conditions

The boundary conditions, which could be either free or grounded conditions of the vibrating structure, significantly affect the experimental results. Free conditions require no fixture to the ground at any point on the structure, which is an ideal state, whilst, in grounded conditions, the structure is rigidly fastened to a non-vibrating base. The grounded

conditions are normally used for large scale structures which cannot be suspended or for structures governed by operating conditions closer to grounded conditions.

For relatively small structures, such as ultrasonic transducers, it is possible to imitate free conditions by using unrestrained supports. This condition can be achieved by supporting or suspending the structure by soft elastic materials, such as soft spring, sponge or elastic string, as long as the structure's stiffness is not affected. It is also possible to minimise any possible stiffness effects of these materials by holding the supports in normal relation to the direction of motion excitation or, in the suspending case, by clamping the structure at the nodal points.

5.4.2.3 Measurement instruments

A wide variety of instruments can be used to measure the response of vibrating structures. They can be categorised into two general groups, contact and non-contact instruments. Traditional contact instruments, which include force transducers, accelerometers and impedance heads, need to be attached to the structures. However this attachment will introduce a mass loading which can lead to damping and stiffness errors particularly for small structures. Other disadvantages of contact instruments are related to the time consumed by the positioning, attaching and calibration processes and also to the limitations of testing bandwidth and work environments [146].

Non-contact instruments are non-invasive devices which do not change the properties of the vibration structures. Therefore they are widely employed in vibrational measurements of ultrasonic devices. This group includes laser Doppler vibrometers (LDV), ultra-high speed cameras and speckle interferometry instruments. In the current work, a 3D LDV was used, which is capable of measuring three vibrational response components, two in plane and the third out of plane of the structural surface.

5.4.2.4 Data processing

In general, a spectrum analyser is used to extract and display the frequency response function by collecting, digitising and transforming the measurement time domain signals to frequency domain which can then be displayed on a monitor. Spectrum analysers can vary depending on the sampling rate and the resolution of the frequency spectrum.

The data collected from the measuring instruments are in analogue signal forms; these signals are first filtered to ensure that there was no aliasing of high frequency signals into the analysis frequency range. The next step is to digitise the data in a digital representation form; this is achieved by using an analogue to digital converter (AD) which controls the resolution of the digitised signals to resemble the sampling rate parameter. The signals are then transformed from time domain to frequency domain by using Fast Fourier Transforms (FFT), a process which requires the data to be recorded as a set of discrete values spaced over a period of time, i.e. as periodic repetition data. For random excitation, the collected data takes the form of non-periodic signals, which, when used directly in the FFT process, leads to a data leakage problem causing serious distortion of the results in the frequency domain. The leakage result can be effectively minimised by the imposition of weighting functions (windows) prior to the FFT process. These functions cause the sampled data to appear in a form more satisfactory to the periodicity requirements of the FFT. Different windows functions are available for time domain signals such as rectangular, hanning and exponential, with each function having its area of application. For continuous signals such as steady state periodic or random, the hanning function is commonly used.

When the measured data is discretised into samples by the weight functions technique, part of each sample, generally at the boundary between two samples, will be ignored because of it contains low values. This circumstance creates the possibility of important analysis data being omitted. To overcome this problem, it is possible to use overlapping correlation, whereby the sampling can start before the previous record has finished. This mechanism will prevent loss or discontinuity of data and reduce the total time needed to acquire data. The application of the correlation technique can change the statistical properties of the collected data as it is possible for data points from one record to appear in the following record. Therefore, a data averaging process is used to ensure reliability of obtained results, in cases where a number of individual records are compared and averaged by a specific technique such as peak hold, exponential or linear averaging. This process can also improve results by removing random noise from the signals.

In the present work, the sample frequency of the spectrum analyser was 204.8kHz and the number of spectral lines used was 51200, giving a resolution of 1.56Hz over a frequency range of 0-80kHz.

5.4.2.5 FRF curve fitting

The EMA of grid points over the transducer structure produces a set of FRFs which need to be fitted when a curve fitting technique is employed to calculate the modal parameters from the measurement data. ME'ScopeVES ver.5.2., which stands for Mechanical Engineering Oscilloscope - Visual Engineering Series, was used as a post-testing analysis tool for curve fitting and displaying the modes of vibration in a 3D computer model.

5.4.3 Evaluation of FE model for transducer 1

The EMA setup for transducer 1 is shown in Figure 5-17. The test was carried out by exciting the transducer, using a random excitation signal generated by a signal generator/analyser, Data Physics Quattro DP240. The excitation signal was then amplified by a power amplifier, ETS Solutions HFVA-62, before exciting the transducer. The vibration velocity response from a grid of measurement points over the transducer was measured by using a 3D LDV, Polytec CLV 3000. The measurement grid consisted of four equally spaced axial lines around the transducer circumference, each with 23 grid points on the transducer surface, which were located as shown in Figure 5-17. Data acquisition software, SignalCalc 240 from Data Physics Corp., was specialised to produce the FFTs, which were then exported to the specialised modal extraction software, ME'ScopeVES, Vibrant Technology Inc, for curve fitting and mode shapes extraction steps.

The normalised modal peaks functions of EMA of transducer 1 are shown in Figure 5-18 where it can be noted that the frequency spacing between modes is sufficient to prevent any unwanted modal coupling. The LT mode resonance frequency is 19,344Hz whilst the resonance frequency of the nearest F and T modes are 16,300Hz and 22,387Hz, respectively. This gave frequency separation of 16% between the LT and these modes. The EMA mode shapes of these three modes are used to validate the FE prediction as shown in Figure 5.19. There is a high correlation in the mode shape and resonance frequencies between the experimental and FE findings. This suggests that the FE model assumption as to material properties, interactions and boundaries were accurate. There is a difference of 9% in estimating the resonance frequency of the torsional mode, which suggests in turn that the model is slightly stiffer in torsion than the fabricated transducer. However, this is related to the ties of the boundary in the model which provide higher constraint than the real mechanical interfaces. This shortcoming is not extended to the frequencies of the F or

LT modes, in which the assumption of a perfect tie at boundaries was more realistic. The mismatches between predicted and extracted frequencies of these modes are being only 2% and 0.4%, respectively.

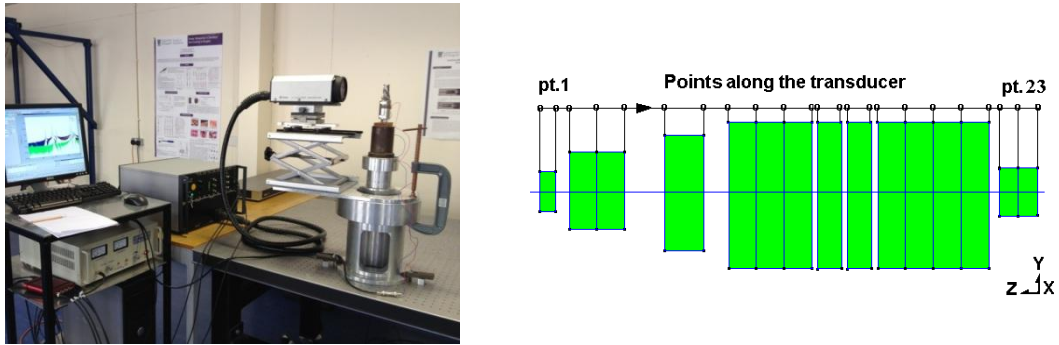


Figure 5-17 EMA setup for transducer 1 (left) and grid points along the transducer (right).

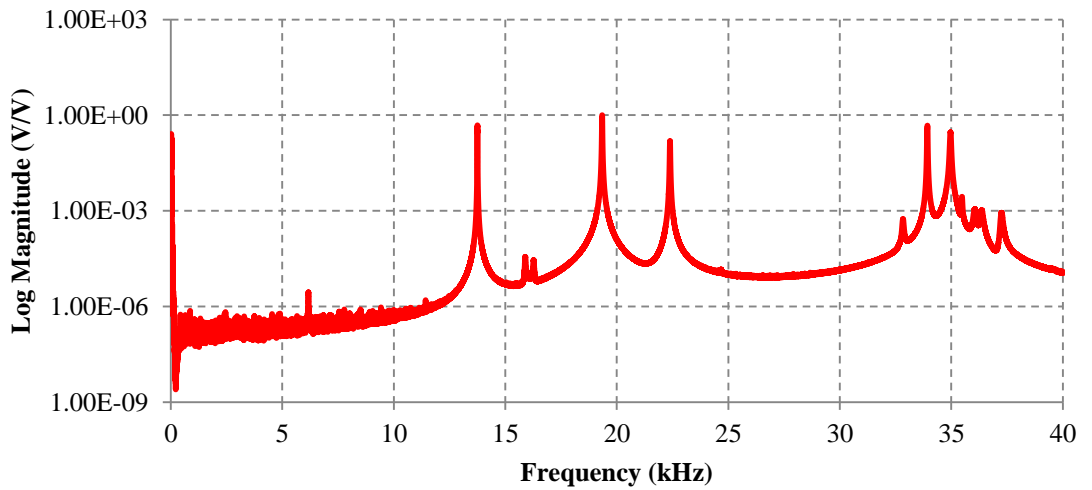


Figure 5-18 Normalised modal peaks functions of EMA for transducer 1.

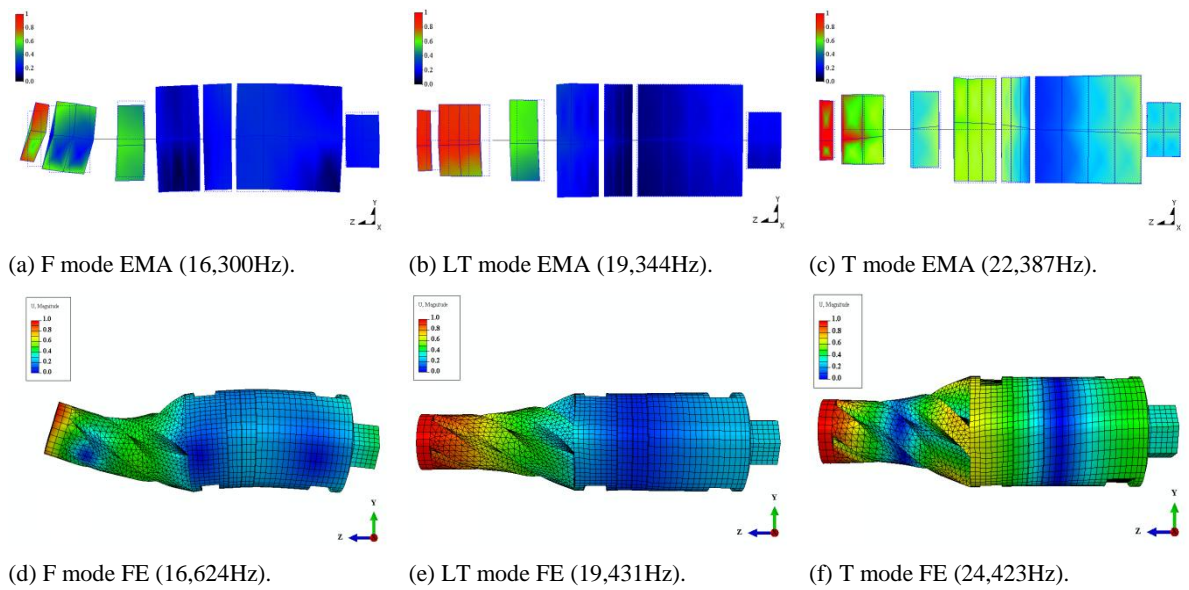


Figure 5.19: Normalised mode shapes of EMA and FE of transducer 1.

5.4.4 Evaluation of the FE model for transducer 2

Similar measurement steps for transducer 1 were used for transducer 2 and the normalised modal peaks functions of EMA are shown in Figure 5-20. The resonance frequency of LT, F and T modes are 57,964Hz, 48,959Hz and 64,079Hz, respectively. These results gave frequency separations of 16% between T and LT mode and 12% between LT and F modes, which are also sufficient to prevent any unwanted modal coupling. The mode shapes are also used to validate the FE findings, in which excellent correlation in mode shapes can be noted, as shown by Figure 5-21. The resonance frequencies of the FE model are comparable to the experimental results and the differences for F, LT and T mode are 0.5%, 0.8% and 1.7%, respectively. It should be noted that the predicated frequency of the T mode for transducer 2 is much closer to the measured value than that of transducer 1. This may be related to the fact that, as the cross-sectional area of transducer 2 is small, the effect of ties assumption at boundaries between parts is minimised.

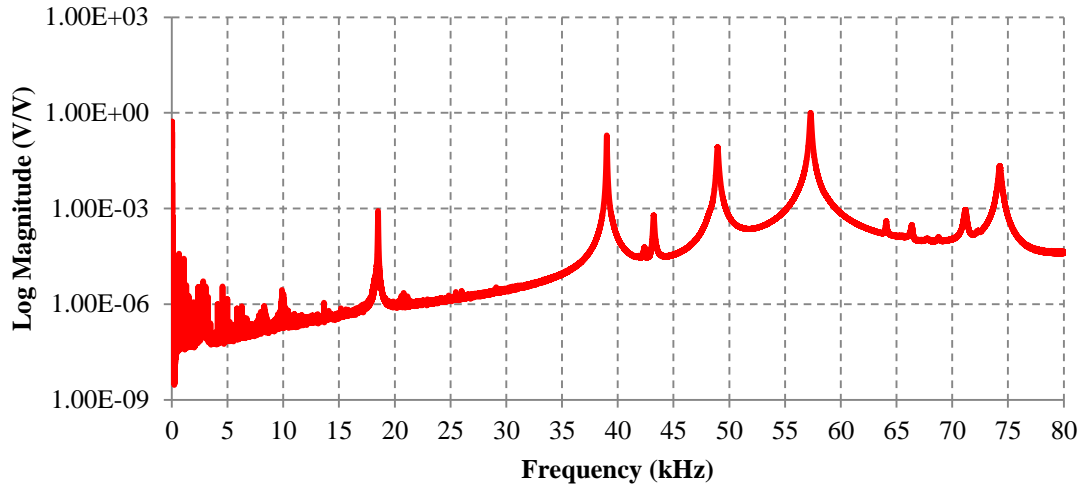


Figure 5-20 Normalised modal peaks functions of EMA for transducer 2.

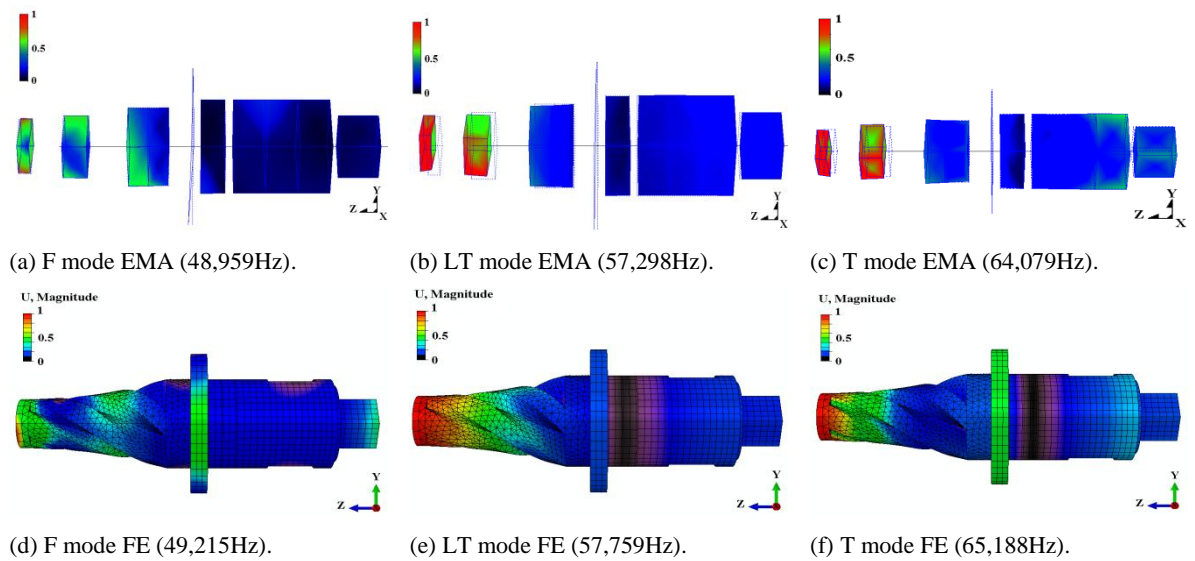
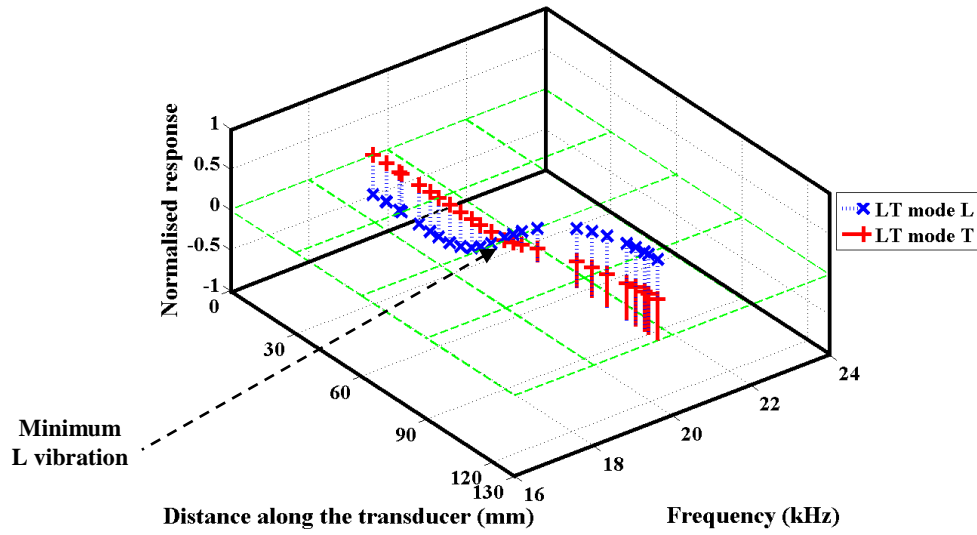


Figure 5-21 Normalised mode shapes of EMA and FE for transducer 2.

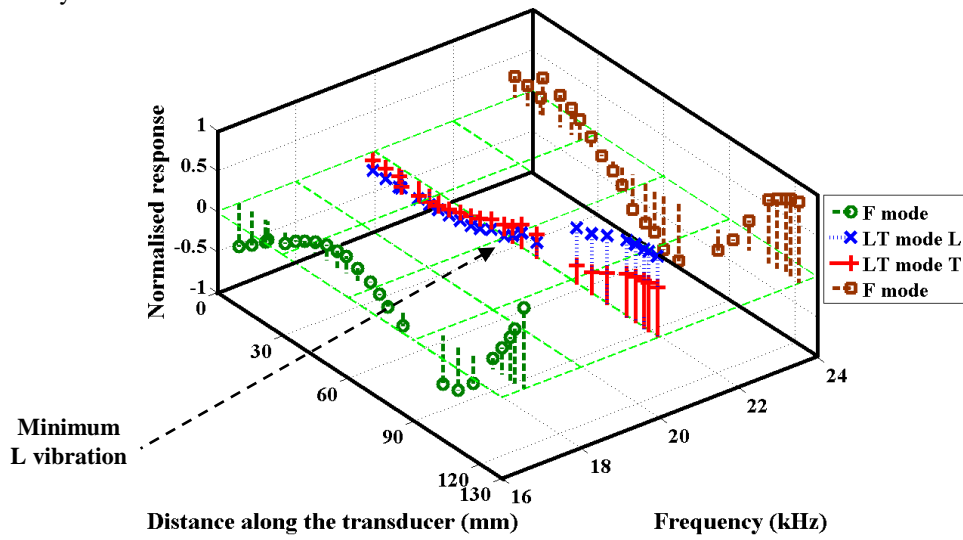
5.5 Evaluation of the analytical model for transducer 1

It is possible to calculate the vibration response distribution along the transducer structure by using the analytical model findings. The amplitude response of the analytical model was calculated from the loop current in each region of the equivalent network, which was presented in section 4.6. The loop currents represent the mechanical velocity at each regional surface. An interpolation calculation was then used to yield the velocity and

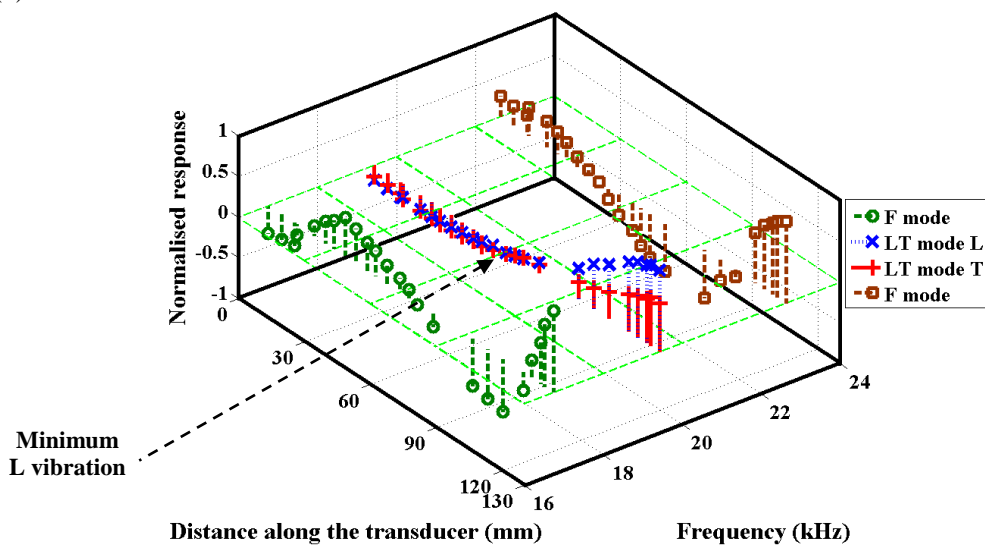
subsequent displacement at specified grid points along the length of the transducer. The combination of L and T amplitude response for the LT mode of the analytical model are presented in Figure 5-22. These results show good correlation with the FE and EMA results in terms of resonance frequency, location of nodal plane, torsionality and the amplitude response distribution. The results suggest that analytical model can serve as an easy tool for predicting the mode shape and confirming the FE findings prior to fabrication. Also, for all predicted and measured results, the position of L vibrational nodal plane of the LT mode are located in very close agreement; thus analytical model can help to identify the securing region of the transducer with confidence prior to fabrication. It should be noted that the nodal planes of the L and T vibrations coincide in the analytical model results, whilst there is slight separation between them in the FE and EMA results. This variation is due to the factor of wave reflection in these results, producing a combination of the L and T vibrations in the piezoelectric stack and the back mass of the transducer. This reflection is not considered in the analytical model.



(a) Analytical model



(b) FE model



(c) Experimental measurements.

Figure 5-22 Normalised amplitude for (a) analytical model L-T mode, (b) FE model L-T, T and F modes, and (c) experimental measurement of L-T, T and F modes.

5.6 Power harmonic analysis

A frequency sweep method consisting of a constant voltage signal was used to excite the fabricated transducers within a narrowband frequency range. This method excites the transducers over a short period of time at each specified frequency through a burst of a finite number of cycles. An upward sweep technique of the burst signal was used which includes a time delay between each frequency sweep to ensure minimum increase in temperature within the piezoceramics components during the excitation and so to avoid frequency shifts associated with increased temperature. The signal, which was set in the Labview software as RMS voltage, was generated by a function generator, Agilent 3322A, and magnified by a power amplifier, ETS Solutions HFVA-62, before exciting the transducers. A 3D LDV was used to measure the velocity response at a circumferential point on the output surface of each transducer (point 1 in Figure 5-17). National Instruments data acquisition hardware and interface in conjunction with Labview software was used to coordinate the experiment and data collection. Also, an oscilloscope, Tektronix DPO 7054, was used to view the current and voltage responses. A set of data for current, voltage, power and response amplitude were measured during the steady state vibration as shown in Figure 5-23.

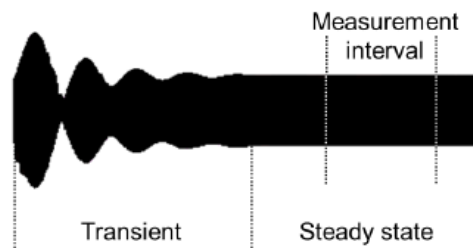


Figure 5-23 Burst response of current [68].

The measurement data of transducer 1 is presented in Figure 5-24, for excitation levels which fall within the range of 5-70V_{rms}. In general a slight shifting of resonance frequency can be noted when the excitation levels are increased. This can be related to the temperature increase within piezoceramic elements that alters their properties. As the swept frequency approached the resonance condition, a drop in the input voltage was observed. This occurred because the transducer was connected in parallel to the amplifier, where its input voltage is equal to the amplifier excitation voltage minus the voltage in the internal resistance of the amplifier. This internal voltage increases with the rise of excitation as more current passes towards the transducer, so that the difference between the

input and excitation voltages is increased at higher excitation. In these figures, the electrical input power is calculated by the RMS of the input currents and voltages.

The measured L and T responses were used to extract the torsionality over the specified range of frequency. The torsionality showed an approximately constant value of 0.55 for different levels of excitation, which is an advantage of this design approach. This value is less than the predicted torsionality, of 0.64, which can be related to the approximation in modelling methods and the consideration of the tangential component as a torsional component in the measurement technique which is discussed in section 5.1. The linear reduction of torsionality across the frequency range through resonance is related to the vibrational behaviour of the transducer structure when excited at frequencies away from the resonance frequency. Also, the slight drop in torsionality at resonance conditions with relatively high excitation can be related to the shifting effect of the resonance frequency.

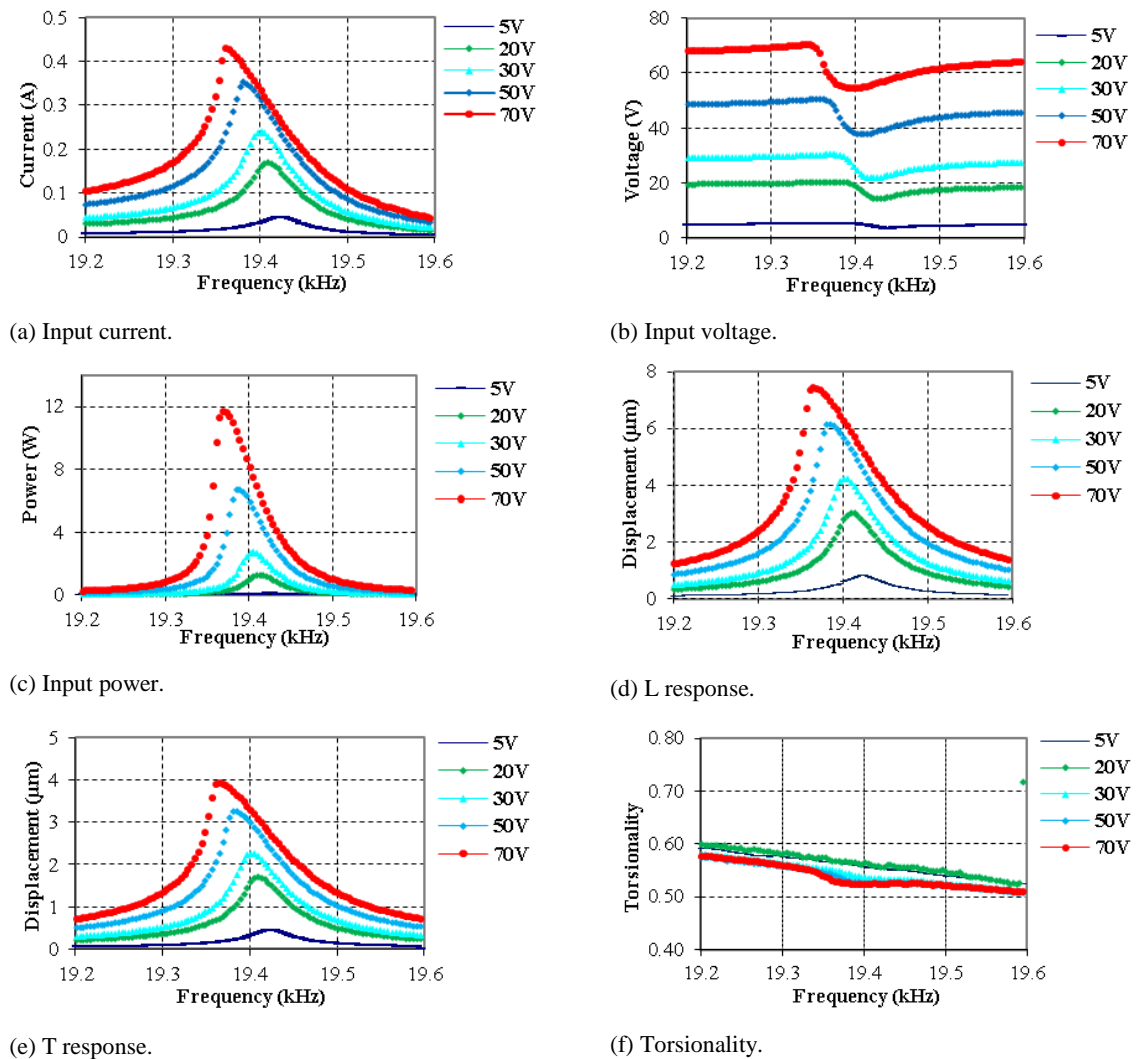


Figure 5-24 Experimental harmonic analysis data for transducer 1.

A similar test setup was used for transducer 2 and the extracted data is presented in Figure 5-25. There are similarities in response behaviour between these two transducers which can be considered the mark of the success of the scaling approach that was used for this transducer. The approximate value of torsionality over the excitation levels is 0.72. This value is higher than the torsionality of transducer 1, which suggests that the modelling approach in estimating the torsionality in the size scaling study is not highly accurate. However, the higher torsionality is desirable in such a design and therefore is considered an advantage for small sized transducers.

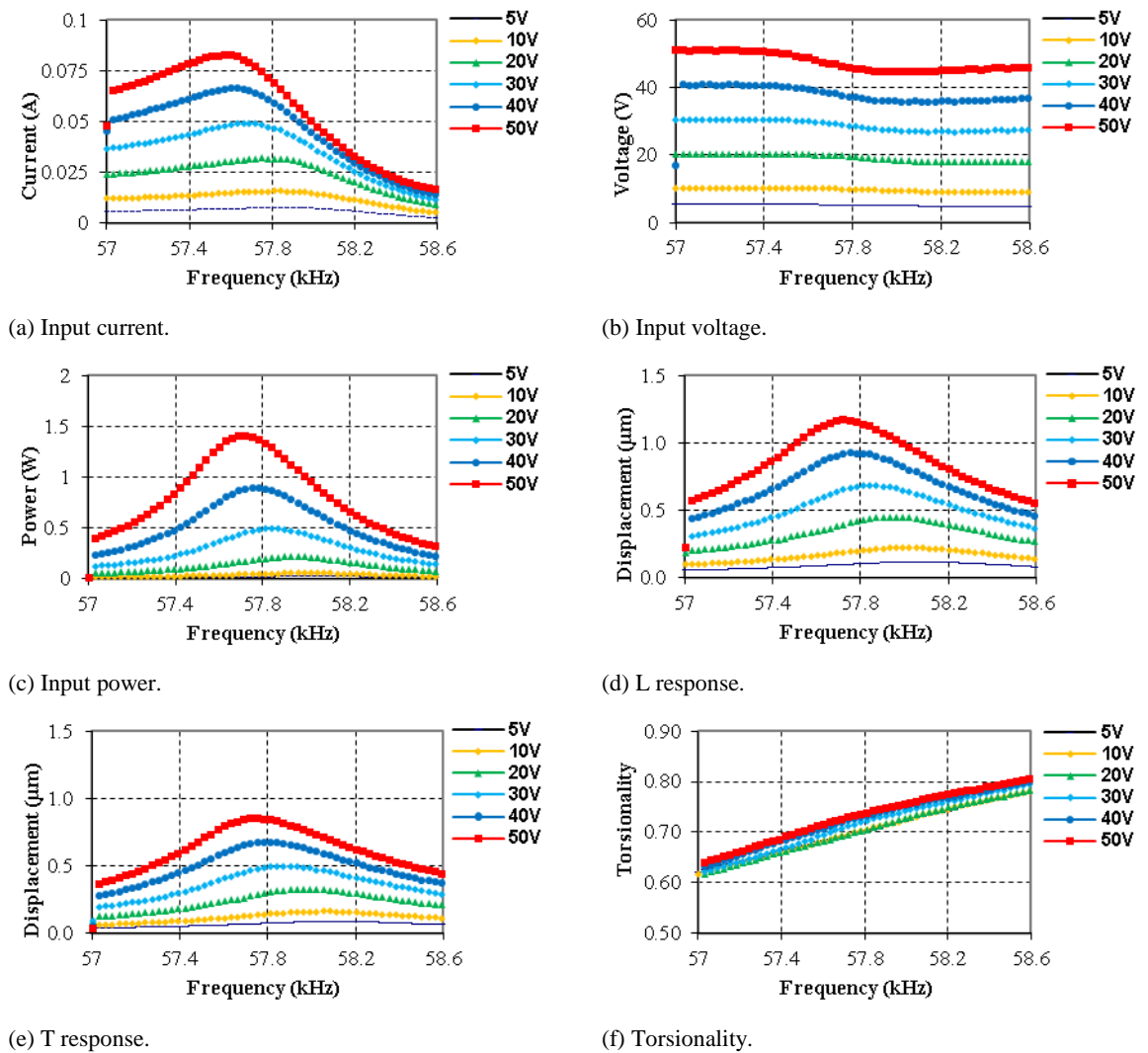


Figure 5-25 Experimental harmonic analysis data of transducer 2.

5.7 Evaluation of the analytical model

The peak values of input electrical current and power calculated by the analytical model are compared to the experimental results for transducers 1 and 2, as shown in Figures 5.26 and 5.27, respectively. In general, there is a linear relationship and excellent correlation between predicted and measured data at low excitation levels. However, the results show divergence at higher excitation where the experimental results being consistency lower. The divergence can be explained by the fact that a reduction in measured current results from a non-linear increase in mechanical and dielectric losses at higher excitation as well as due to the changes in piezoceramic properties at elevated temperatures. These results suggest that the analytical model can predict the electrical behaviour of the transducer accurately at lower excitation levels when the piezoelectric linear behaviour is dominant, whilst at higher excitation levels the non-linear behaviour is influential. These effects can also be seen clearly in the power curves where the results of input power of the analytical model and experimental measurements are plotted for the same range of excitation.

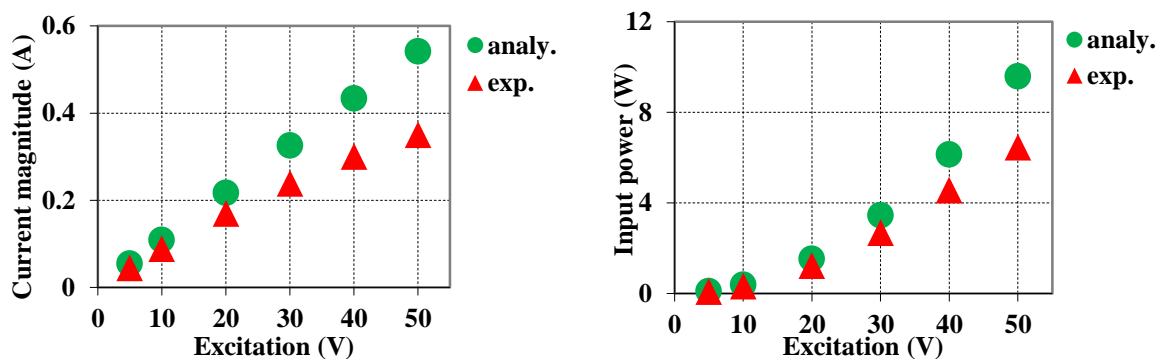


Figure 5-26 Input current (left) and power (right) at different excitation levels for transducer 1.

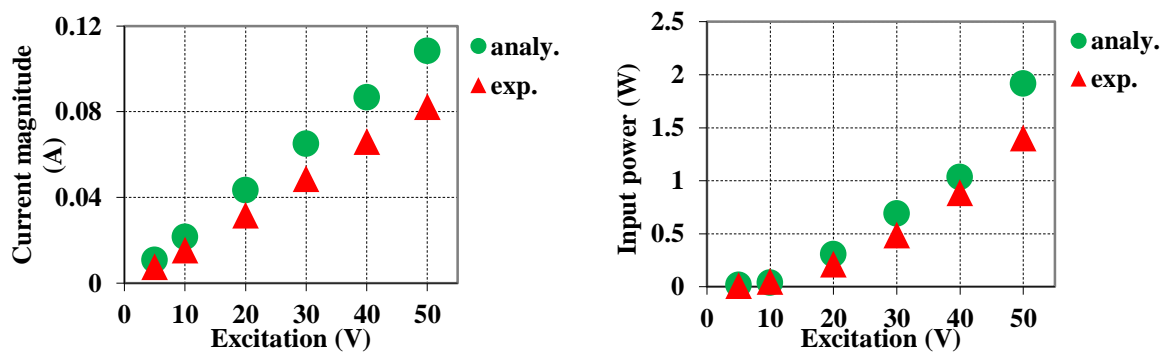


Figure 5-27 Input current (left) and power (right) at different excitation levels for transducer 2.

5.8 Dynamic evaluation of the analytical and FE models

Linear dynamic behaviour through the FE model of an LT transducer was predicted by simulating different levels of potential difference across the piezoceramic rings in a steady state dynamic analysis step. The peaks of the response amplitude for L and T vibration, and therefore the torsionality, were then calculated at a circumferential point on the output surface. In this model, Rayleigh global (structural) damping is utilised. It has two damping constants, α and β , which can be related to the damping ratio, ξ , by the following expression:

$$[C] = \alpha[M] + \beta[K] \quad 5.4$$

$$\xi = \frac{\alpha}{2\omega} + \frac{\beta\omega}{2} \quad 5.5$$

where $[C]$, $[M]$ and $[K]$ are the structure damping matrix, structure mass matrix and structure stiffness matrix, respectively, ξ is the damping ratio and ω is the angular excitation frequency. The α component of the expression relates to viscous damping and its influence decreases as the frequency of vibration increases, whilst the β component is the hysteresis or stiffness damping component and its influence increases as the frequency increases. Therefore, at frequencies of concern in ultrasonic devices, the value of the α component is found to be insignificant and can be classified as negligible. When harmonic excitation is considered, the β component can be modelled as a function of angular modal resonance ω_r and mechanical quality factor Q_m of the structure damping, as follows [84];

$$\beta = \frac{1}{\omega_r Q_m} \quad 5.6$$

The value of Q_m can be determined experimentally by using the half power bandwidth formula for frequency response curves where the curves of Figures 5-21d and 5.22d were used to calculate the mechanical quality factor for transducers 1 and 2, respectively [147].

The peaks of the response amplitude of the predicted model and the experimental measurements are plotted for different levels of excitation, as shown in Figures 5-28 and 5-29 for transducer 1 and transducer 2, respectively. The analytical and FE model calculations show a linear trend but slightly divergent for increasing excitation levels. There is good correlation between the mathematical and the experimental data, particularly at low excitation. However, experimental results exhibit a nonlinear response at higher excitation levels due to the relative motion between the real transducer components and the nonlinear relationship between the strain and electrical field in the piezoceramics. For transducer1, the torsionality calculated from the analytical model results is 0.65 across the

entire range of excitation levels, which is highly consistent with the original design stage FE model prediction of 0.64. The torsionality calculated from experimental response data is about 10% lower than these predictions but is also nearly constant across the excitation level range. For transducer 2, similar behaviour of response amplitudes can be noted. However the torsionality from experimental results is 0.72 across the excitation levels, this is higher than the mathematical prediction, which relates to the uncertainty in the mathematical model for a size scaling approach.

The similarity in response and power behaviour for these two different size LT transducers suggests that the scaling size method can provide different transducers which fit a wide range of ultrasonic applications with similar performance characteristics.

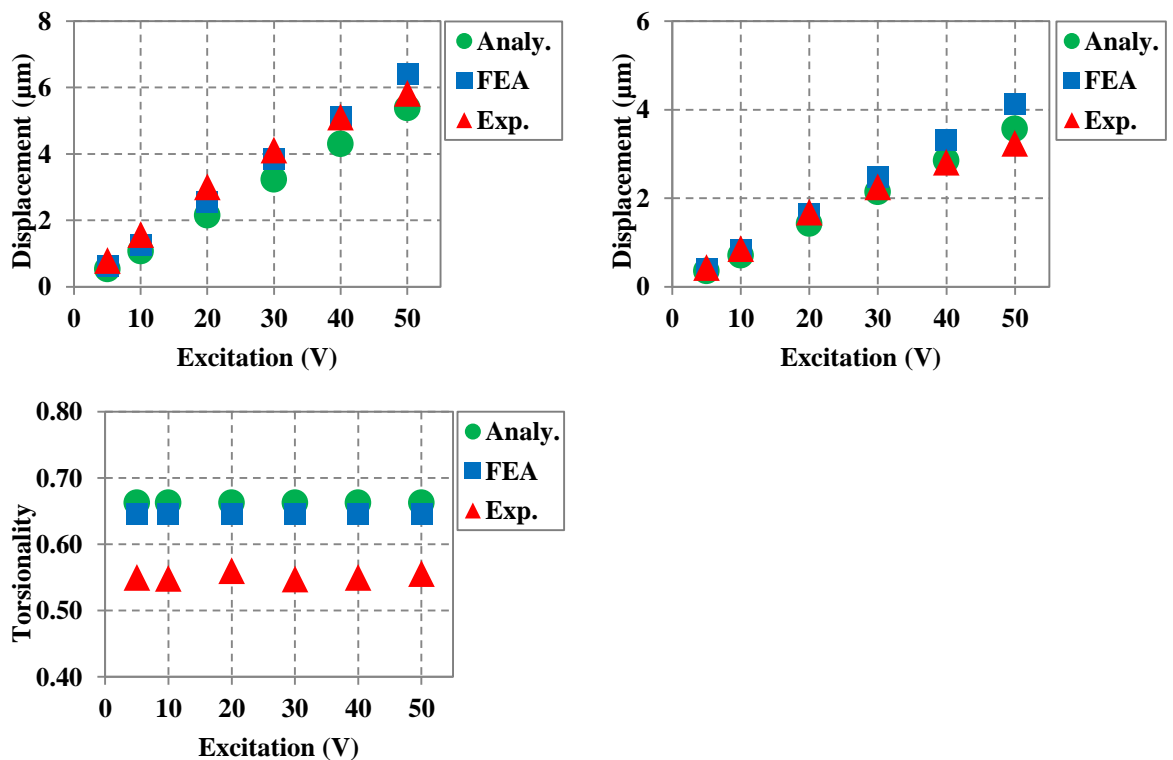


Figure 5-28 Peaks response of (a) L (b) T and (c) torsionality for varied excitation for transducer 1.

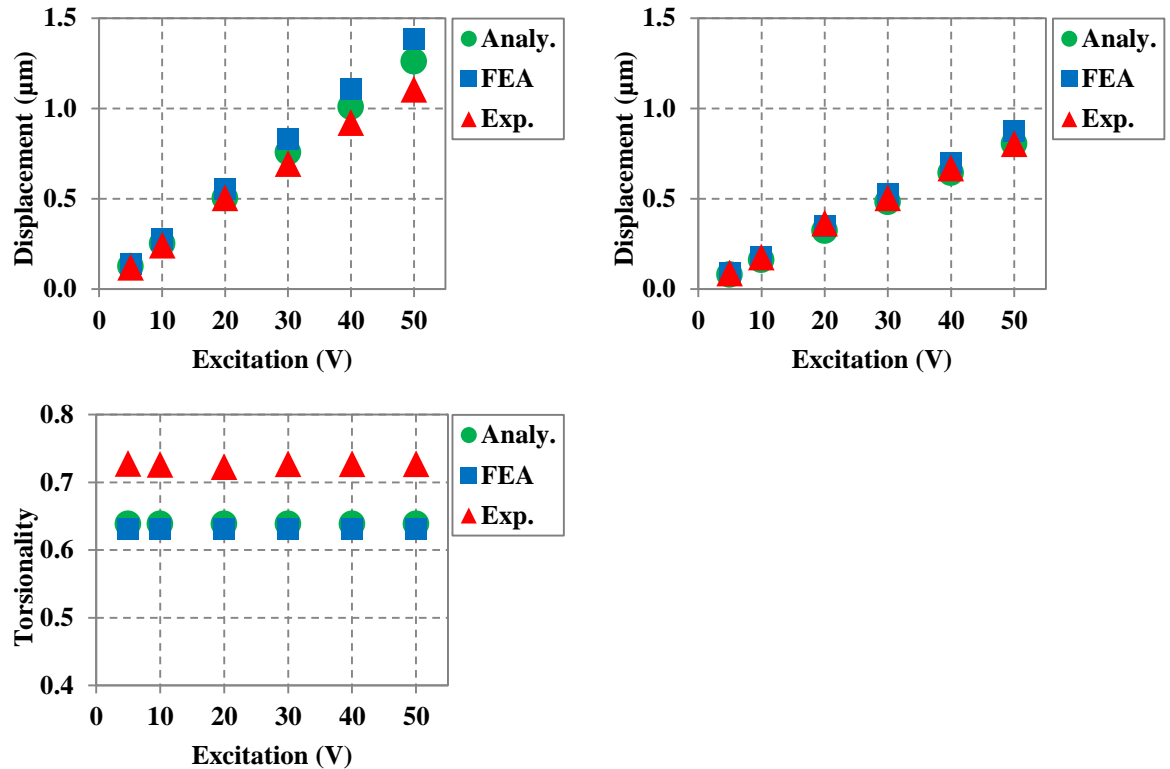


Figure 5-29 Peaks response of (a) L (b) T and (c) torsionality for varied excitation for transducer 2.

5.9 Summary

Fabrication steps and an experimental testing process for different sizes of LT transducers have been presented in detail. The fabrication process is classified into manufacturing and assembly steps of the transducer parts, which showed significant influence on the performance of the fabricated prototypes. The testing process included electrical impedance analysis to extract and validate the electromechanical parameters, experimental modal analysis to extract and validate the modal parameters, and power harmonic analysis to characterise and validate the transducer performance at different levels of excitation.

The electrical impedance analysis demonstrated the accuracy of the analytical model for electrical impedance spectra, phase difference and resonance and anti-resonance frequencies of the desired LT mode. The EMA results showed high correlation with the FE model in terms of calculating the modal parameters and locating the nodal plane along the transducer structure. The results also revealed that the frequency spacing between the LT and unwanted surrounding modes is sufficient to prevent modal coupling during transducer operation. Furthermore, the analytical prediction is extended to calculate the distribution of response amplitude along the transducer structure which is also validated with high

correlation by the EMA. The results suggest that, for future designs of LT transducers, it is possible to validate the FE findings of the mode shapes and location of the nodal plane of the desired LT mode by analytical modelling prior to fabrication.

The accuracy of predicting the linear dynamic behaviour of LT transducers at low excitation levels is confirmed by the harmonic analysis. This analysis was initially used to characterise the fabricated prototypes at different levels of excitation and to update the FE model for damping parameters. At relatively low levels of excitation, the high correlation between analytical and FE data for electrical current and power is mainly due to consideration of the linear loss forms in the definition of piezoelectric materials. The main variation, however, in experimental measurements at high excitation levels is related to the nonlinear behaviour of piezoceramic components due to increase in temperature. Overall, the results suggest that the combination of FE and analytical model can provide accurate predictions for different parameters of LT transducers. In addition, the size scaling study proved a significant feature of this design approach which can allow design of different sizes with similar performance characteristics.

Chapter 6 Case study: design of LT ultrasonic drill

6.1 Introduction

The combination of longitudinal and torsional vibration is considered an essential improvement in ultrasonic drilling. As discussed in Chapter 2, incorporating the torsional vibration into a longitudinal ultrasonic drill can increase the drilling rate by 10 times. Therefore, the developed approach of generating in LT mode is utilised in this chapter to design a novel LT ultrasonic drill. The design of transducer 2, which is discussed in chapter 5, is modified to an LT drill by increasing the number of piezoceramic components to four so as to increase the output power. In addition, the twist angle of slots is changed to 240° , which is the value of producing maximum torsionality as predicated in Figure 3.16d of section 3.6. The diameter of the fixture flange is increased and a new fabricated plastic housing is used to secure the transducer. Finally, a new exponential horn is designed, to be used as a drill bit with its first longitudinal mode set to resonate at the frequency of the LT mode of the modified transducer. The L resonance mode of the horn will amplify the L response of the LT transducer with no equivalent amplification for the T response; therefore, the torsionality at the output face of the drill will be degraded. However, this reduction in torsionality can be calculated and separated from any other possible reduction which may occur due to the change in operating conditions.

A design procedure, similar to that used for transducers 1 and 2 in Chapter 5, was employed to design the LT drill. The FE model was used first to model the initial design, predict its modal parameters, and estimate the linear response amplitudes and torsionality for different levels of excitation. The analytical model was then used to predict the electro-mechanical parameters and the electrical impedance spectrum for the optimum FE model. Finally, the drill model was fabricated and tested for electrical impedance analysis, EMA, and power harmonic analysis, with different boundary conditions (free and loaded) set to evaluate the drill performance. The response and torsionality near the output surface were used as evaluation criteria in this study. Therefore, the main focus of this chapter is on

describing the design methodology adopted in the work to design an LT drill which can be tested under different operating conditions.

6.2 FE model of LT drill

The exponential horn was modelled from titanium alloy Ti-6-4, as shown in Figure 6-1, where the L mode resonates at 52,171Hz and the amplification (gain) of the vibration amplitude is 2.3. Therefore, the torsionality of the LT transducer was expected to be reduced to 0.43 of its value when the horn is connected. The complete FE model of the LT drill is presented in Figure 6-2, in which a section of the housing frame is removed to show the inside parts. An eigenmode extraction procedure was executed to examine the mode shapes, the natural frequencies of the tuned mode and some surrounding modes, the torsionality and the location of the L nodal plane along the drill. The predicted modes of vibration are listed in

Table 6.1, it can be noted that one of the surrounding modes (7F) is very close to the LT mode. These modes, however, may not all be (physically) real. This aspect is related to the approximation in finite element methods which can give good estimation of lower modes of vibration but a progressively less accurate estimate for the higher modes [148]. Finally, the torsionality at the output face of the drill is calculated as 0.55 and the location of the flange is adjusted to be close to the L nodal plane of the model.

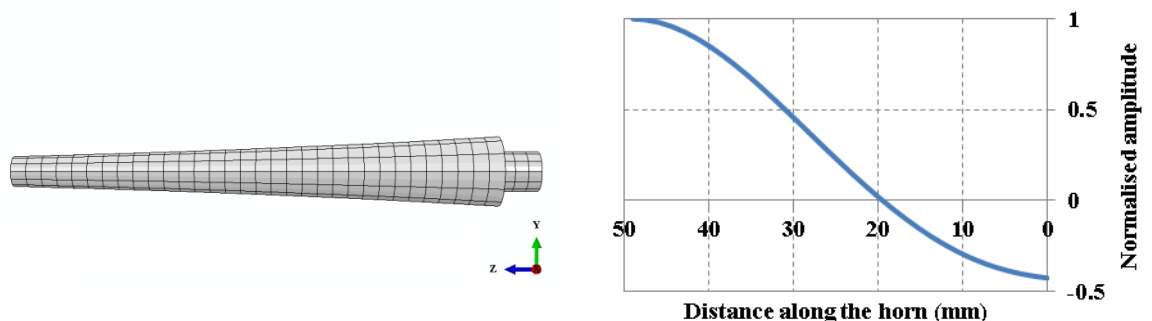


Figure 6-1 FE model of the horn (left) and the normalised distribution of vibration amplitude along the horn (right).

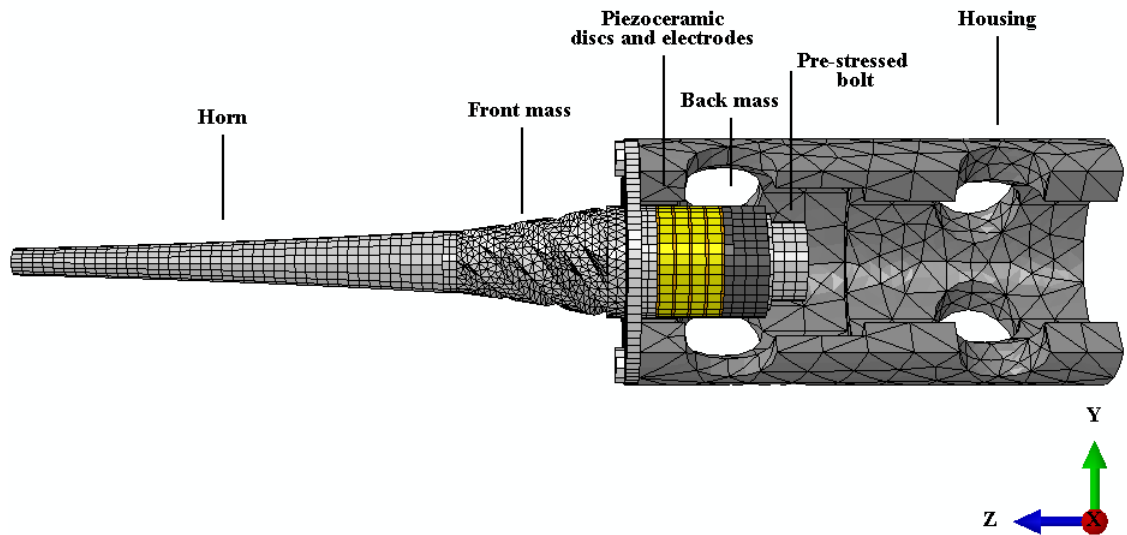


Figure 6-2 FE model of LT drill.

Table 6.1 FE predicting of modes of vibration for LT drill.

No.	Mode of vibration	Resonance frequency (Hz)
1	6F	37,274
2	2T	38,166
3	7F	50,318
4	LT	50,942
5	8F	56,404
6	3T	57,652

6.3 Analytical model of LT drill

The equivalent electrical network of an LT transducer, which is presented in Chapter 4, is extended to represent the LT drill model. This can be achieved by adding two additional circuits (region 7) to the right end to represent the horn, as shown in Figure 6-3. The first circuit is equivalent to the L modal behaviour of the horn which is added to the L branch of the network whilst the second circuit represents the T behaviour of the horn which is added to the T branch of the network. The impedance components of these two circuits were calculated by using the set of Equations 4.75 and 4.76 in Chapter 4. The equivalent network was then worked out to calculate the electrical impedance spectrum of the drill.

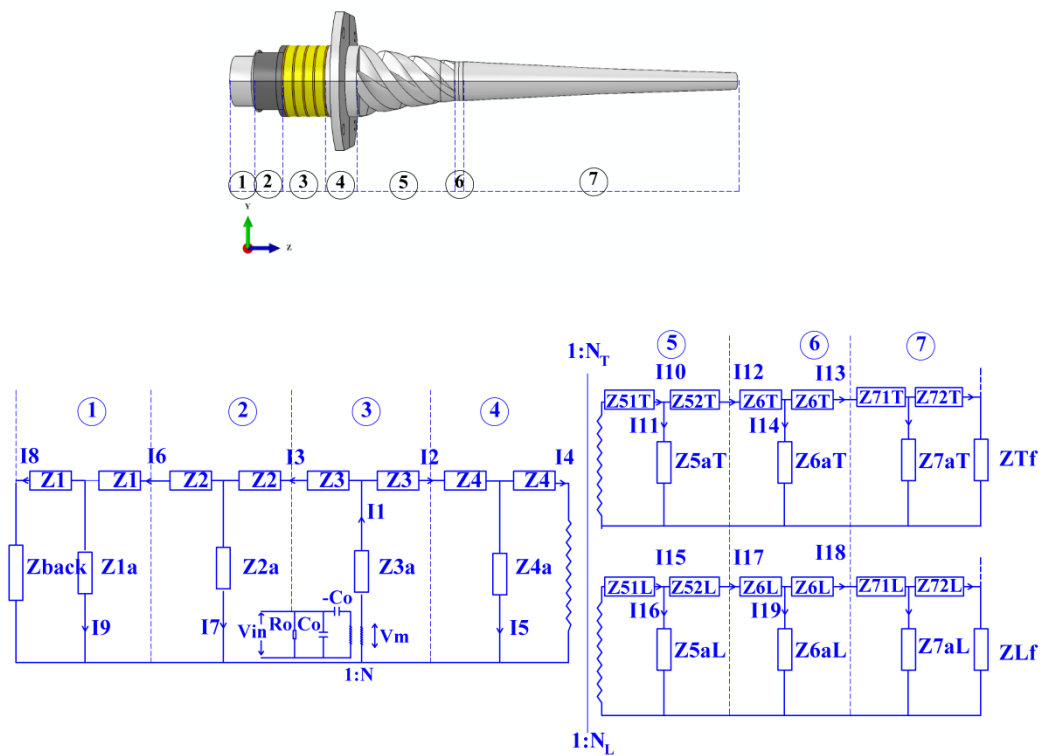


Figure 6-3 Equivalent electrical network for LT drill.

6.4 Evaluation the analytical model of LT drill

The fabricated LT drill, which is shown in Figure 6-4, has a total length of 90mm and an outer diameter of 3mm. The extended conductors of the copper electrodes were soldered to electrical wires and a layer of silicone rubber insulation was used to prevent electrical short between these conductors. The experimental data of the electrical impedance spectrum and phase difference were used to validate the analytical calculations as presented in Figure 6-5. The analytical model can predict the electrical behaviour of the drill with acceptable correlation. Although the real drill shows slightly lower overall electrical impedance than the analytical model, this may be related to the effect of copper electrodes which, for simplicity sake, were not considered in the analytical model. Also, the additional insulation layer can add some stiffness to the real drill, which shows slightly higher resonance frequency than the analytical model. This comparison suggests that the analytical model can be developed so as to be used successfully in the design of different arrangements for LT systems, such as an electrical circuit connection, which is necessary to match the LT drill with other electrical devices.



Figure 6-4 Fabricated LT drill.

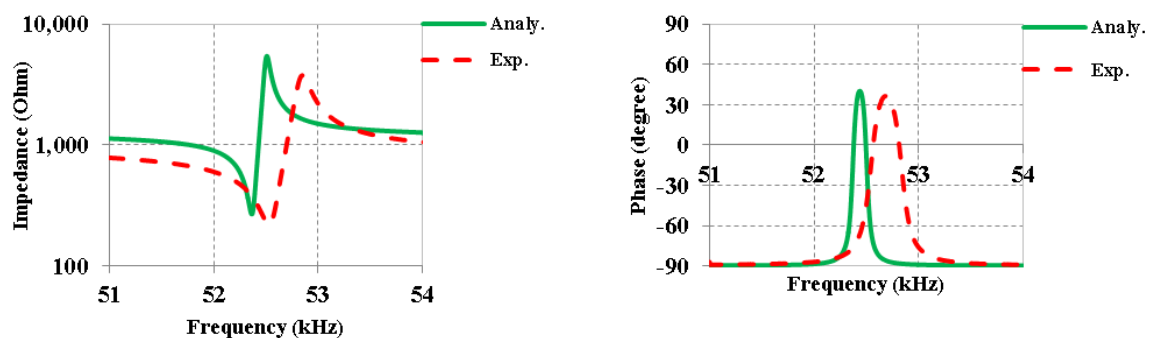


Figure 6-5 Electrical impedance spectrum (left) and phase difference (right) of analytical and experimental analysis.

6.5 Evaluation of the FE model of the LT drill

The accurate estimation of modal parameters of the LT drill was implemented by EMA techniques from a grid of measurement points. The results of overlaid modal peaks for broad-band excitation are presented in Figure 6-6. The extracted resonance frequencies and mode shapes of the desired and two surrounding modes of vibration are shown in Figure 6-7. These results show that not all predicated FE modes, listed in Table 6.1 were excited as the nearest F and T modes are at 39,466Hz and 56,659Hz respectively. These measurements provide the sufficient frequency spacing between the tuned LT mode and the neighbouring F and T modes of 24% and 9%, respectively. The separation between the LT and T mode is less than the minimum required separation of 10% as mentioned in section 3.3.1. However, the possible interaction between these modes can lead to increase the torsionality which is desirable in ultrasonic drilling. Good correlation can also be seen between the mode shapes of the FE predictions and the EMA results whilst the percentage differences between the resonance frequencies for F, LT and T modes were 5%, 2% and 1.7%, respectively.

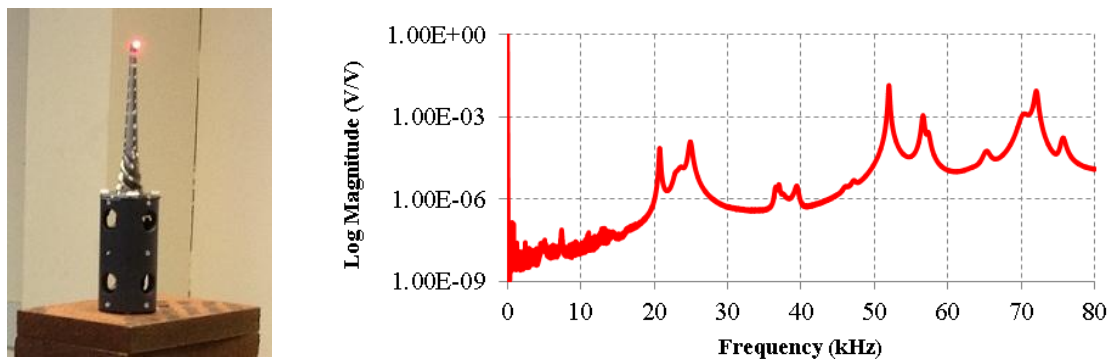


Figure 6-6 EMA testing of LT drill (left) and modal peaks function (right).

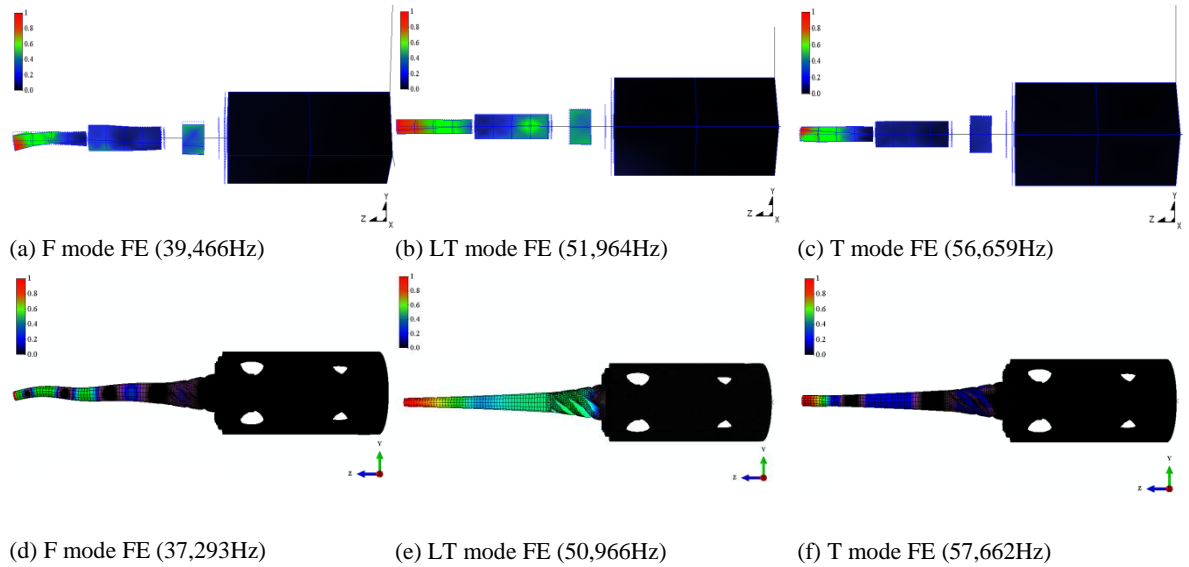


Figure 6-7 Normalised mode shapes of EMA (upper) and FE (lower) of LT drill.

6.6 Power harmonic characterisation

6.6.1 Free boundary condition

The technique of frequency sweep excitation using a burst signal, which is explained in section 5.3.3, was used to experimentally characterise the LT drill. The drill was tested first without the horn and with only the LT transducer, to characterise the response and the torsionality at the output surface at different levels of excitation. The LT transducer, which was tested under free boundary conditions, was secured to a sliding frame and the measured peaks of L and T responses were plotted, with the torsionality, as shown in Figure 6-8. An approximate linear trend of response across the entire excitation range can be noted, producing an average torsionality of 0.8. This ratio can be regarded as an indicator of the accurate modelling using this approach, as discussed in section 3.6. The horn was then (mechanically) connected to the transducer and a similar test was repeated, with the data measured at the output face of the horn and plotted against excitation level, as shown in Figure 6-9. In these results, the response-excitation linear trend no longer exists and torsionality, which is reduced by less than half, shows a gradual increase as the excitation level increases. This behaviour can be related to the amplification of the L response in the horn, which exhibits a linear excitation-response relationship up to a limit (about $4\mu\text{m}$ amplitude) where the nonlinear behaviour become dominant due to the influence of issues such as elevated temperature.

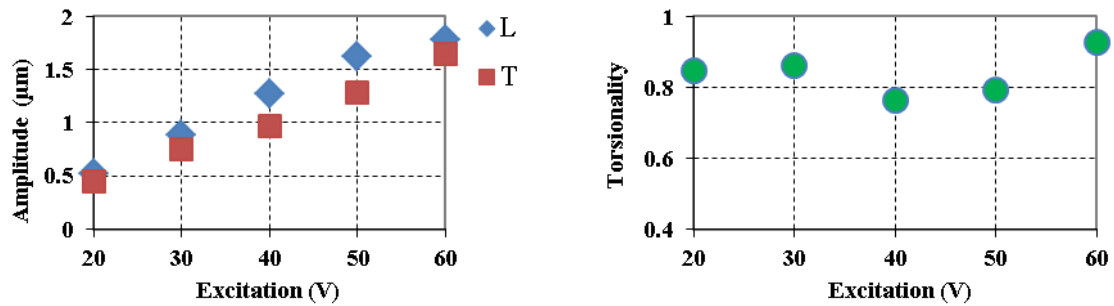


Figure 6-8 Peaks amplitude of L and T responses (left) and torsionality (right) for LT transducer (without horn).

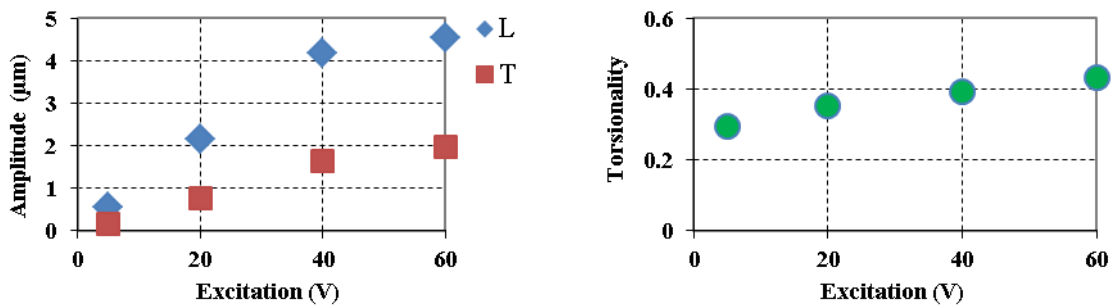


Figure 6-9 Peaks amplitude of L and T responses (left) and torsionality (right) for LT drill (with horn).

6.6.2 Load boundary condition

In order to investigate the effects of loading on the response and torsionality of the LT drill, the output face of the drill was contacted against two different materials, Sherwood sandstone and a bone surrogate material (a polymer foam), with compression loads of 5, 10 and 20N. The burst sine excitation technique at different voltage levels, 20, 40 and 60V, was used to excite the drill and the 3D LDV was utilised to measure the response near the tip of the horn as shown in Figure 6-10. The results of sandstone material loading, which are shown in Figures 6-11 and 6-12, suggest that increasing the loading will reduce both L and T responses so that the generated torsionality is not highly affected over this range of load. Slightly different behaviour, however, can be noted with bone surrogate material loading where an improvement in torsionality was found with an increase in excitation level. The results, shown in Figures 6-13 and 6-14, suggest that, although the variation in response for different loading is less than for the case of sandstone loading, the reduction in L response with excitation can be slightly higher than that in T response and that, therefore, torsionality can be improved by increasing excitation.

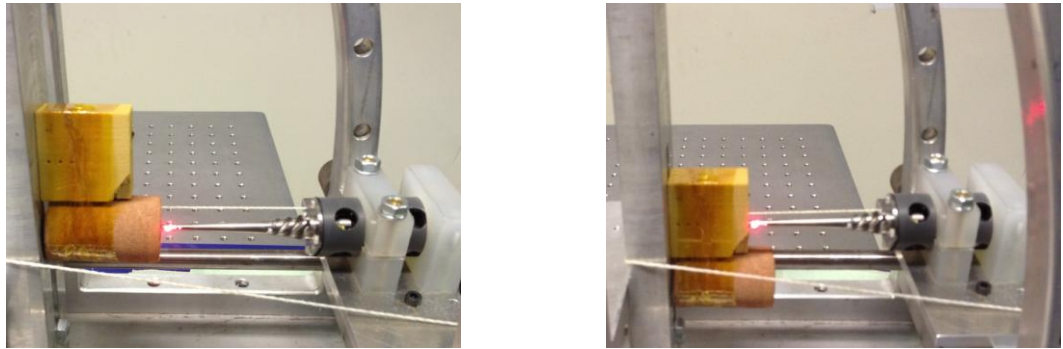


Figure 6-10 LT drill loaded to sandstone material (left) and bone surrogate material (right).

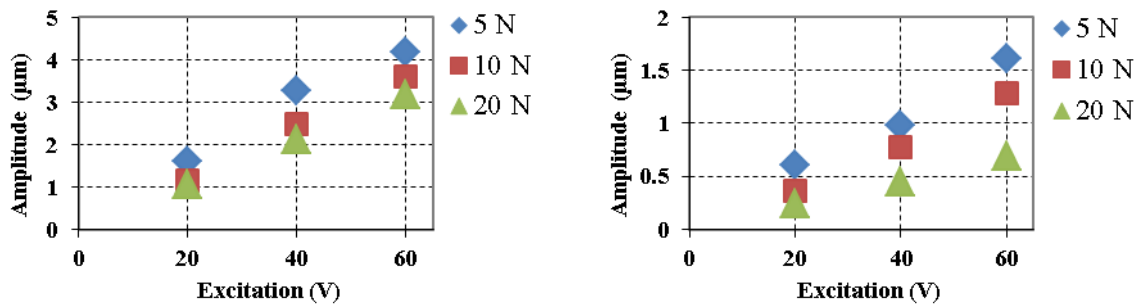


Figure 6-11 Amplitude peaks of L response (left) and T response (right) for sandstone load.

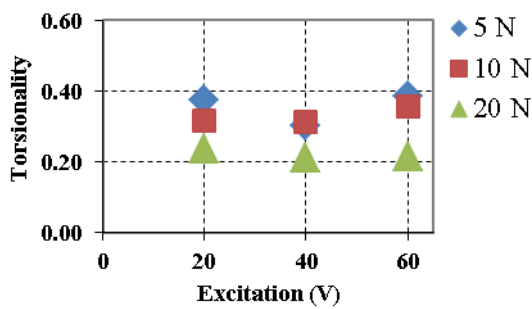


Figure 6-12 Torsionality values for sandstone load.

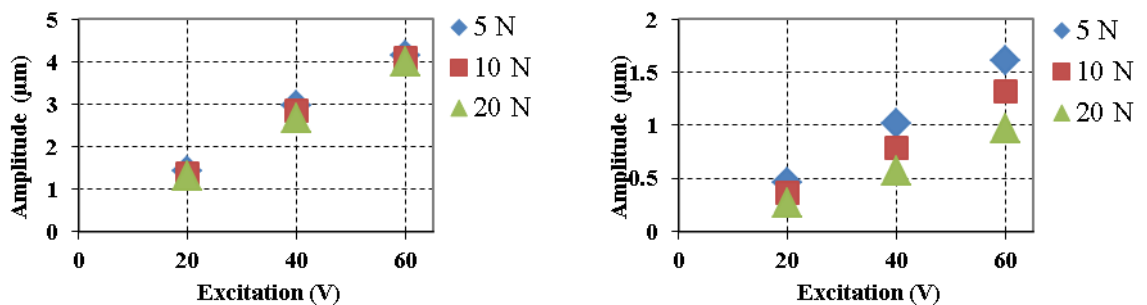


Figure 6-13 Amplitude peaks of L response (left) and T response (right) for bone surrogate load.

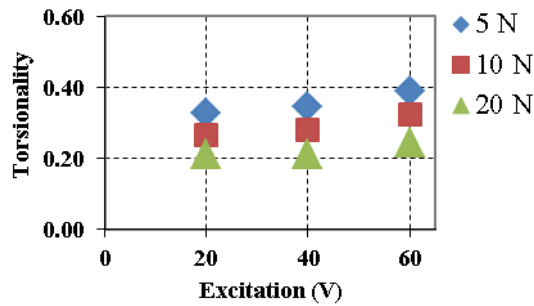


Figure 6-14 Torsionality values for bone surrogate load.

6.7 Conclusions

The methodology for designing a LT transducer was used to design an ultrasonic LT drill, for which the FE, analytical and experimental modelling procedures were combined to create and characterise the drill under different operating conditions. The effect of connecting an ultrasonic horn to the LT transducer was studied through computer modelling and experimental testing, the results of which show the accuracy of modelling prediction for response and torsionality. An assessment of the effect of loading on the response amplitude and torsionality at the output surface of the horn was also performed by using a laser vibrometer. Different arrange of loading levels were used with two different types of materials and the results showed stability, or slight improvements, in torsionality when the loading levels increased.

Chapter 7 Conclusions and suggestions for future work

7.1 Conclusions

The work presented in this Thesis outlined a designing approach for producing a longitudinal-torsional (LT) vibration in ultrasonic horns which are used as front masses for traditional Langevin transducers. The approach is based on combining the principles of two existing methods in order to simplify the design and improve the performance. Through employing the geometry modifications, it has been found that the output response and the torsionality, which is the ratio of torsional to longitudinal response at the output surface, can be highly tailored. Furthermore, the new approach has proved to be scalable for different sizes of transducer to achieve similar or better performance characteristics, an important feature that makes it applicable to a wide range of ultrasonic applications.

The development of the approach takes a number of stages. It begins with the prediction methodology of mathematical modelling and progresses through the experimental methodology of fabricating LT transducers. Mathematical modelling, which includes finite element (FE) and analytical models, is used to create, optimise and predict the performance of an initial design whilst experimental techniques, which consist of electrical impedance analysis, experimental modal analysis (EMA), and harmonic response analysis, are used to characterise the fabricated models and to validate and update the mathematical models.

The principle of this approach consists of cutting and twisting a number of slots along the axial direction of an exponential horn. This horn was used as a front mass of a longitudinal Langevin transducer on which an optimisation study by a FE model was performed by changing a number of geometric parameters to fulfil certain criteria. The geometric parameters included the shape and dimensions of slots and the angle of twist along the axial direction, whilst the optimisation criteria included the resonance frequency, output response and torsionality, frequency spacing between tuned and surrounding modes and the location of the nodal plane. The calculations showed interesting results, according to which the torsionality can reach up to 0.8 with sufficient frequency spacing between modes to prevent any possible modal coupling. Based on the initially selected size, the FE model

achieved these results at frequencies at the threshold of ultrasonics (at 20kHz). A size scale study was then performed to create differently sizes of models at higher resonance frequencies. The results of this study demonstrated the possibility for designing different sizes LT transducer which yields similar overall performance.

The optimum design was used in an analytical model study based on the equivalent circuit method to predict the electromechanical parameters which cannot be predicted in the FE model. The analytical model, which is characterised by low computing requirements, was also extended to validate some of the FE findings. These include mode shape, response and torsionality, where good correlation was achieved.

Two different sizes of the optimum transducer were fabricated and experimentally tested for validation and characterisation purposes. There was a high correlation between experimental results and analytical calculation of electrical impedance values under resonance and anti-resonance conditions but the real transducers show frequency reduction due to the reduction of front mass stiffness by slitting. However, the frequency reduction was compensated in the model by an assumption of a linear relationship between stiffness reduction and the size of the front mass. This assumption was validated by the FE model and presented high correlation in predicted resonance frequencies for differently sized models.

EMA was used to accurately estimate the modal parameters of the fabricated transducers and validate the calculations of the models. There was good correlation between predicted and measured resonance frequencies of the tuned and the surrounding modes of vibration. There was, however, lower correlation between predicted and measured frequencies for some surrounding modes, a result which may be related to slight differences in geometrical or material properties or to the interaction between parts in the mathematical models. The predicted and measured mode shapes showed good agreement where the nodal planes of these modes were located at the same place along the transducers.

A harmonic burst excitation technique was used to characterise the fabricated transducer at different levels of excitation, which proved to yield a close representation of operating conditions. A good correlation between predicted and measured amplitude peaks, of longitudinal and torsional responses at the output surface was observed at low excitation levels where the linear behaviour dominated. This correlation, however, was lower at higher excitation levels, where the effects of piezoceramic nonlinearity and structural damping become more influential.

The new approach was also employed to design a LT ultrasonic drill which was tested for unloaded and loaded conditions against different materials. The results suggest that the response can be affected by an increase in loading such that the produced torsionality can be retained or slightly improved.

7.2 Suggestions for future work

7.2.1 Design a driving system and investigate the effect of excitation method on LT drill performance

Although the developed LT drill (discussed in chapter 6) was successfully used to accomplish a real drilling process, the achieved results were not published in this work because the driving method of the drill was performed manually. This method can be used for short testing periods; however for continuous drilling, it is essential to design a driving system which has the ability to match electrical impedances of drill and power supply, track the resonance conditions and provide means of measuring all the related parameters. It is also necessary to study different excitation methods to optimise the drill performance by reducing the influence of the electrical field on the piezoceramic components. The analytical model can help to predict the electrical behaviour of the overall system (the drill and the driving system) prior to fabrication which is another advantage of this mathematical model.

7.2.2 Design of the LT drill bit

It has been shown that the designed drill bit, discussed in Chapter 6, resonates in longitudinal mode and that, therefore, it only amplifies the L response rather than the T response which degrades the output torsionality. In order to preserve the high torsionality of the LT transducer, it is important to develop a drill bit which can amplify both types of transducer response. The principles of the developed approach can be used to optimise this design by incorporating the slitting-twisting technique to produce an efficient drill bit.

7.2.3 Investigate other LT ultrasonic applications

Although ultrasonic drilling is directly related to the LT vibration, other ultrasonic applications, such as medical devices, welding and motors, can benefit from this

combination of motions. Ultrasonic welding is normally performed by a single longitudinal mode, however as earlier discussed in the literature review, incorporating other modes, such as the torsional mode, can enhance the strength and uniformity of the bonding. Furthermore, ultrasonic motors, which are characterised by high torque and low rotational speed, are widely used in different applications and therefore the developed approach can be investigated within such ultrasonic fields.

Appendix I: Publications

Journal papers

1. H. Al-Budairi, M. Lucas and P. Harkness, "A design approach for longitudinal-torsional ultrasonic transducers", *Sensors and Actuators A: Physical*, under review.

Conference papers

1. H. Al-Budairi and M. Lucas, "An analytical model of a longitudinal-torsional ultrasonic transducer", *Modern Practice in Stress and Vibration Analysis*, University of Glasgow, UK, August 2012.
2. H. Al-Budairi, M. Lucas and P. Harkness, "Optimisation of the longitudinal-torsional output of a half-wavelength Langevin transducer", *41st Ultrasonics Industry Association Symposium*, San Francisco, CA, April 2012.
3. H. Al-Budairi, P. Harkness and M. Lucas, "A strategy for delivering high torsionality in longitudinal-torsional ultrasonic devices", *Applied Mechanics and Materials*, vol. 70, (2011), pp. 339-344.
4. H. Al-Budairi, P. Harkness and M. Lucas, "A generalised approach to torsionality maximisation in longitudinal-torsional ultrasonic devices", *40th Ultrasonics Industry Association Symposium*, Glasgow, UK, May 2011.

Articles

1. H. Al-Budairi, P. Harkness and M. Lucas, "Drill Tools for Earth and Space, Design of a Novel Longitudinal-torsional Ultrasonic Transducer", *Polytec's InFocus Customer Magazine*, Issue 2, (2012), pp. 6-7.

Appendix II: References

1. O. Abramov, *High Intensity Ultrasonics Theory and Industrial Applications*, Gordon and Breach Science Publishers, 1998.
2. A. Cardoni, *Characterising the Dynamic Response of Ultrasonic Cutting Devices*, PhD Thesis, University of Glasgow, UK, 2003.
3. E. McCulloch, *Experimental and Finite Element Modelling of Ultrasonic Cutting of Food*, PhD Thesis, University of Glasgow, UK, 2008.
4. Sound Waves For Brain Waves.<http://www.biotele.com/usstim.html>, Accessed on 20th September 2012.
5. N. Mehta, *Textbook of Engineering Physics - Part II*, Asoke K. Ghosh, PHI Learning private limited, India, 2009.
6. A. Olabi and A. Grunwald, "Design and Application of Magnetostrictive Materials," *Journal of Mechanics of Materials and Structures*, vol. 29, no. 2, pp. 469-483, 2008.
7. X. Dong, J. Ou and X. Guan, "Applications of Magnetostrictive Materials in Civil Structures: A Review," *The 6th International Workshop on Advanced Smart Materials and Smart Structures Technology*, 2011.
8. <http://aml.seas.ucla.edu/research/areas/magnetostrictive/mag-composites/Magnetostriction%20and%20Magnetostrictive%20Materials.htm>, Accessed on 18th September 2012.
9. C. Rosen, B. Hiremath and R. Newnham, *Piezoelectricity*, American Institute of Physics, USA, 1992.
10. IEEE Standard on Piezoelectricity, USA, 1988.
11. MORGAN Advanced Ceramics Inc., *Piezoelectric Ceramics Properties and Applications*, UK, <http://www.morgantechnicalceramics.com/resources/piezoelectric-ceramics-properties-and-applications/>, Accessed on 8th June 2012.
12. M. Prokic, *Piezoelectric Transducers Modeling and Characterization* M.P. Interconsulting Co., Switzerland, 2004.
13. B. Fu, *Piezoelectric Actuator Design via Multiobjective Optimization Methods*, PhD Thesis, University of Paderborn, Germany, 2005.
14. G. Zhou, Y. Zhang and B. Zhang, "The Complex-mode Vibration of Ultrasonic Vibration Systems," *Ultrasonics*, vol. 40, pp. 907-911, 2002.

15. A. Cardoni, P. Harkness and M. Lucas, "Ultrasonic Rock Sampling Using Longitudinal-Torsional Vibrations," *Physics Procedia*, vol. 3, no. 1, pp. 125-134, 2010.
16. P. Harkness, A. Cardoni and M. Lucas, "Ultrasonic Rock Drilling Devices Using Longitudinal-Torsional Compound Vibration," *IEEE Proceedings of International Ultrasonics Symposium*, pp. 2088-2091, 2009.
17. A. Mitskevich, *Sources of High-intensity Ultrasound*, Edited by L. Rozenberg, Plenum Press, USA, 1969.
18. D. Wuchinich, *Longitudinal-Torsional Ultrasonic Tissue Dissection*, US Patent no. 7,762,979 B2, 2010.
19. G. Bromfield, *Ultrasonic Torsional Mode and Longitudinal-Torsional Mode Transducer System*, US Patent no. 2009/0236938A1, 2009.
20. L. Shuyu, "Study on the Longitudinal-torsional Composite Mode Exponential Ultrasonic Horns," *Ultrasonics*, vol. 34, no. 7, pp. 757-762, 1996.
21. M. Boukhny, *Torsional Ultrasonic Handpiece*, US Patent no. 6,077,285, 2000.
22. E. Eisner, "Design of Sonic Amplitude Transformers for High Magnification," *Journal of Acoustical Society of America*, vol. 35, no. 9, pp. 1367-1377, 1963.
23. B. Dubus, J. Debus, J. Decarpigny and D. Boucher, "Analysis of Mechanical Limitations of High Power Piezoelectric Transducers Using Finite Element Modelling," *Ultrasonics*, vol. 29, no. 3, pp. 201-207, 1991.
24. Y. Tomikawa, K. Adachi, M. Aoyagi, T. Sagae and T. Takano, "Some Constructions and Characteristics of Rod-type Piezoelectric Ultrasonic Motors Using Longitudinal and Torsional Vibrations," *IEEE Transaction on Ultrasonics, Ferroelectrics and Frequency Control*, vol. 39, no. 5, pp. 600-608, 1992.
25. J. Tsujino, M. Takeuchi and H. Koshisako, "Ultrasonic Rotary Motor Using a Longitudinal-torsional Vibration Converter," *IEEE Proceedings of Ultrasonics Symposium*, vol. 2, pp. 887-892, 1992.
26. J. Tsujino, "Recent Developments of Ultrasonic Welding," *IEEE Proceedings of Ultrasonic Symposium*, vol. 2, pp. 1051-1060, 1995.
27. J. Tsujino, R. Suzuki and M. Takeuchi, "Load Characteristics of Ultrasonic Rotary Motor Using a Longitudinal-torsional Vibration Converter with Diagonal Slits. Large Torque Ultrasonic Rotary Motor," *Ultrasonics*, vol. 34, pp. 265-269, 1996.
28. J. Tsujino, T. Ueoka, K. Otda and A. Fujimi, "One-dimensional Longitudinal-torsional Vibration Converter with Multiple Diagonally Slitted Parts," *Ultrasonics*, vol. 38, pp. 72-76, 2000.
29. J. Tsujino, "Ultrasonic Complex Vibration Systems and Various Applications of High Power Ultrasonics," *Proceedings of Forum Acousticum Sevilla*, vol. ULT-02-006-IP, 2002.

30. J. Tsujino, Y. Harada, S. Ihara, K. Kasahara, M. Shimizu and T. Ueoka, "Configurations of High-frequency Ultrasonics Complex Vibration Systems for Packaging in Microelectronics," *Ultrasonics*, vol. 42, pp. 125-129, 2004.
31. J. Tsujino, T. Sano, H. Ogata, S. Tanaka and Y. Harada, "Complex Vibration Ultrasonic Welding Systems with Large Area Welding Tips," *Ultrasonics*, vol. 40, pp. 361-364, 2002.
32. L. Shuyu, "Study on the Longitudinal-Torsional Compound Transducer with Slanting Slots," *Journal of the Acoustical Society of America*, vol. 105, no. 3, pp. 1643-1650, 1999.
33. L. Shuyu, "Analysis of the Equivalent circuit of Piezoelectric Ceramic Disk Resonators in Coupled Vibration," *Journal of Sound and Vibration*, vol. 231, no. 2, pp. 277-290, 2000.
34. L. Shuyu, "Sandwiched Piezoelectric Ultrasonic Transducers of Longitudinal-torsional Compound Vibrational Modes," *IEEE Transactions on Ultrasonics, Ferroelectrics and Frequency Control*, vol. 44, no. 6, pp. 1189-1197, 1997.
35. O. Ohnishi, O. Myohga, T. Uchikawa, M. Tamegai, T. Inoue and S. Takahashi, "Piezoelectric Ultrasonic Motor Using Longitudinal-torsional Composite Vibration of a Cylindrical Resonator," *IEEE Proceedings of Ultrasonics Symposium*, vol. 2, pp. 739-743, 1989.
36. P. Harkness, A. Cardoni and M. Lucas, "An Ultrasonic Corer for Planetary Rock Sample Retrieval," *Journal of Physics: Conference Series*, vol. 181, 2009.
37. C. Kleesattel, *Ultrasonically Driven Low-Speed Rotary Motor* US Patent no. 4,281,987, 1981.
38. J. Tsujino, "Ultrasonic Motor Using a One-Dimensional Longitudinal-torsional Vibration Converter with Diagonal Slits," *Smart materials and structures*, vol. 7, no. 3, pp. 345-351, 1998.
39. H. Al-Budairi, P. Harkness and M. Lucas, "A Strategy for Delivering High Torsionality in Longitudinal-Torsional Ultrasonic Devices," *Applied Mechanics and Materials*, vol. 70, pp. 339-344, 2011.
40. H. Al-Budairi, M. Lucas and P. Harkness, "Optimisation of the Longitudinal-torsional Output of a Half-wavelength Langevin Transducer," *41st Annual Ultrasonic Industry Association Symposium*, 2012.
41. H. Al-Budairi, P. Harkness and M. Lucas, "A Generalised Approach to Torsionality Maximisation in Longitudinal-torsional Ultrasonic Devices," *40th Annual Ultrasonic Industry Association Symposium*, 2011.
42. J. Tsujino, T. Ueoka, K. Hasegawa, Y. Fujita, T. Shiraki, T. Okada and T. Tamura, "New Methods of Ultrasonic Welding of Metal and Plastic Materials," *Ultrasonics*, vol. 34, pp. 177-185, 1996.

43. Y. Yi, R. Gausmann, W. Seemann and J. Zhong, "A Note on a Longitudinal and Torsional Type of Ultrasonic Motor with Two Stators," *Journal of Applied Mathematics and Mechanics* vol. 5, pp. 147-148, 2005.
44. Y. Bar-Cohen, X. Bao and W. Grandia, "Rotary Ultrasonic Motors Actuated By Traveling Flexural Waves," *Proceedings of the Smart Structures and Materials Symposium*, 1998.
45. Y. Yi, W. Seemann, R. Gausmann and J. Zhong, "Development and Analysis of a Longitudinal and Torsional Type Ultrasonic Motor with Two Stators," *Ultrasonics*, vol. 43, no. 8, pp. 629-634, 2005.
46. Y. Bar-Cohen, X. Bao, Z. Chang and S. Sherrit, "An Ultrasonic Sampler and Sensor Platform for In-Situ Astrobiological Exploration," *Proceedings of the SPIE smart structures and materials symposium*, 2003.
47. Y. Bar-Cohen, S. Sherrit, X. Bao and Z. Chang, "Ultrasonic/sonic sampler and sensor platform for in-situ planetary exploration," *Proceedings of International Conference on MEMS, NANO and Smart Systems*, pp. 22-31, 2003.
48. R. Neugebauer and A. Stoll, "Ultrasonic Application in Drilling," *Journal of Materials Processing Technology*, vol. 149, pp. 633-639, 2004.
49. P. Harkness, A. Cardoni and M. Lucas, "Vibration Considerations in the Design of an Ultrasonic Driller/Corer for Planetary Rock Sampling," *International Conference on Noise and Vibration Engineering*, 2008.
50. A. Anis, *Removal of Tissue*, US Patent no. 5,911,699, 1999.
51. T. Asami and H. Miura, "Longitudinal and Torsional Vibration Characteristics of hollow-type Stepped Horn for Hole Machining by Complex Ultrasonic Vibration," *Proceedings of Symposium on Ultrasonic Electronics*, vol. 31, pp. 533-534, 2010.
52. T. Asami and H. Miura, "Vibrator Development for Hole Machining by Ultrasonic Longitudinal and Torsional Vibration," *Japanese Journal of Applied Physics*, vol. 50, pp. 1-9, 2011.
53. L. Merkulov, "Design of Ultrasonic Concentrations," *Soviet Physics*, vol. 3, pp. 246-255, 1957.
54. L. Merkulov and A. Kharitonov, "Theory and Analysis of Sectional Concentrators," *Soviet Physics*, vol. 5, pp. 183-190, 1959.
55. S. Sherrit, S. Leary, B. Dolgin and Y. Bar-Cohen, "Comparison of the Mason and KLM Equivalent Circuits for Piezoelectric Resonators in the Thickness Mode," *IEEE Proceedings of Ultrasonics Symposium*, vol. 2, pp. 921-926, 1999.
56. M. Redwood, "Experiments with the Electrical Analog of a Piezoelectric Transducer," *Journal of Acoustical Society of America*, vol. 36, no. 10, pp. 1872-1880, 1964.

57. E. Sittig, "Effects of Bonding and Electrode Layers on the Transmission Parameters of Piezoelectric Transducers Used in Ultrasonic Digital Delay Lines," *IEEE Transactions on Sonics and Ultrasonics*, vol. 16, no. 1, pp. 2-9, 1969.
58. R. Krimholtz, D. Leedom and G. Matthaei, "New Equivalent Circuits for Elementary Piezoelectric Transducers," *Electronics Letters*, vol. 6, no. 13, pp. 398-399, 1970.
59. E. Neppiras, "The Pre-stressed Piezoelectric Sandwich Transducer," *Ultrasonics International Conference*, pp. 295-302, 1973.
60. F. Arnold, L. Bravo-Roger, M. Goncalves and M. Grilo, "A Simple Electric Circuit for Teaching One-Dimensional Characterization of Piezoelectric Plates," *Latin-American Journal of Physics Education*, vol. 5, no. 4, pp. 680-685, 2011.
61. C. Hutchens and S. Morris, "A Two-Dimensional Equivalent Circuit for the Tall Thin Piezoelectric Bar," *IEEE Proceeding of Ultrasonics Symposium*, pp. 671-676, 1985.
62. M. Willatzen, "Ultrasound Transducer Modeling-General Theory and Applications to Ultrasound Reciprocal Systems," *IEEE Transactions on Ultrasonics, Ferroelectrics and Frequency Control*, vol. 48, no. 1, pp. 100-112, 2001.
63. J. Kocbach, *Finite Element Modeling of Ultrasonic Piezoelectric Transducers*, PhD Thesis, University of Bergen, Norway, 2000.
64. H. Allik, K. Webman and J. Hunt, "Vibrational Response of Sonar Transducers Using Piezoelectric Finite Elements," *Journal of Acoustical Society of America*, vol. 56, pp. 1782-1791, 1974.
65. D. Ostergaard and T. Pawlak, "Three-dimensional Finite Elements for Analyzing Piezoelectric Structures," *Ultrasonics Symposium Proceeding*, pp. 639-642, 1986.
66. N. Abboud, G. Wojcik, D. Vaughan, J. Mould, D. Powell and L. Nikodym, "Finite Element Modeling for Ultrasonic Transducers," *Proceedings of the SPIE International Symposium on Medical Imaging*, vol. 3341, pp. 19-42, 1998.
67. B. Liu, *Transducers for Sound and Vibration- The Finite Element Method Based Design*, PhD Thesis, University of Denmark, Denmark, 2001.
68. A. Mathieson, *Nonlinear Characterisation of Power Ultrasonic Devices Used in Bone Surgery*, PhD Thesis, University of Glasgow, UK, 2012.
69. H. Hocheng and K. Kuo, "On-line Tool Wear Monitoring During Ultrasonic Machining Using Tool Resonance Frequency," *Journal of Materials Processing Technology*, vol. 123, no. 1, pp. 80-84, 2002.
70. L. STĂNĂȘEL and F. ARDELEAN, "The Parametric Design of the Ultrasonic Exponential Horns," *Nonconventional Technologies Review*, no. 4, pp. 54-58, 2010.
71. CeramTec GmbH, *Advanced Ceramics in Piezo Applications*, Germany, 2011.

72. A. Abdullah, M. Shahini and A. Pak, "An Approach to Design a High Power Piezoelectric Ultrasonic Transducer," *Journal of Electroceramics*, vol. 22, no. 4, pp. 369-382, 2009.
73. M. Radmanović and D. Mančić, *Design and Modelling of the Power Ultrasonic Transducers*, Faculty of Electronics in Niš, Serbia, 2004.
74. <http://www.americanpiezo.com/knowledge-center/piezo-theory/piezoelectric-constants.html>, Accessed on 8th June 2012.
75. Physik Instrumente Ltd., *Data Piezoceramic Materials (PZT), temperature Coefficients*, Germany, 2011.
76. <http://www.matweb.com/>, Accessed on 7th June 2012.
77. BS EN 1002-1 Metallic Materials-Tensile Testing, British Standards Institution, UK, 2001.
78. Hibbitt, Karleson & Sorensen, Inc., *ABAQUS User's Manual Version 6.10*, 2011.
79. http://www.efunda.com/formulae/solid_mechanics/mat_mechanics/hooke_orthotropic.cfm, Accessed on 11th June 2012.
80. J. Engblom, *Stress and Failure Analysis of Laminated Composite Structures*, Florida Institute of Technology, S-6001, USA, 2002.
81. PIEZO SYSTEMS, INC., *Introduction to Piezoelectricity-Catalog #8*, USA, 2011.
82. https://www.sharcnet.ca/Software/Fluent13/help/ans_thry/thy_coup2.html, Accessed on 20th July 2012.
83. J. Sheehan, "Fundamentals of Transduction Workshop," *40th Annual Ultrasonic Industry Association Symposium*, 2010.
84. G. Nader, E. Silva and J. Adamowski, "Effective Damping Value of Piezoelectric Transducer Determined by Experimental Techniques and Numerical Analysis," *ABCM symposium series in mechatronics*, vol. 1, pp. 271-279, 2004.
85. R. Holland and E. EerNisse, "Accurate Measurement of Coefficients in a Ferroelectric Ceramic," *IEEE Transactions on Sonics and Ultrasonics*, vol. 16, no. 4, pp. 173-181, 1969.
86. P. Selva, O. Cherrier, V. Budinger, F. Lachaud and J. Morlier, "Smart EMI Monitoring of Thin Composite Structures," *16th International Conference on Composite Structures*, 2011.
87. F. Arnold, "Resonance Frequencies of the Multilayered Piezotransducers," *The Journal of the Acoustical Society of America*, vol. 123, no. 5, p 3641, 2008.
88. L. Shuyu and T. Hua, "Study on the Sandwich Piezoelectric Ceramic Ultrasonic Transducer in Thickness Vibration," *Smart materials and structures*, vol. 17, no. 1, pp. 1-9, 2008.
89. D. Dragan, D. Mančić and G. Stančić, "New Three-dimensional Matrix Models of the Ultrasonic Sandwich Transducers," *Journal of Sandwich Structures and Materials*, vol. 12, no. 1, pp. 63-80, 2010.

90. L. Ostrovsky and A. Potapov, *Modulated Waves: Theory and Applications*, The Johns Hopkins University Press, USA, 1999.
91. H. Kolsky, "Stress Waves in Solids," *Journal of Sound and Vibration*, vol. 1, no. 1, pp. 88-110, 1964.
92. K. Graff, *Wave Motion in Elastic Solids*, Dover Publications Inc., USA, 1991.
93. B. Michel, "Characterization of Piezoceramics," *IEEE Transactions on Ultrasonics, Ferroelectrics and Frequency Control*, vol. 38, no. 6, pp. 603-617, 1991.
94. D. Mančić and M. Radmanović, "Piezoceramic Ring Loaded on Each Face: a Three-Dimensional Approach," *Electronic Journal of Technical Acoustics*, vol. 2, pp. 1.1-1.7, 2002.
95. F. Feng, J. Shen and J. Deng, "A 2D Equivalent Circuit of Piezoelectric Ceramic Ring for Transducer Design," *Ultrasonics*, vol. 44, pp. e723-e726, 2006.
96. L. Shuyu, "Study on the Equivalent Circuit and Coupled Vibration For the Longitudinally Polarized Piezoelectric Ceramic Hollow Cylinders," *Journal of Sound and Vibration*, vol. 275, pp. 859-875, 2004.
97. A. Iula, N. Lamberti and M. Pappalardo, "An Approximated 3-D Model of Cylinder-shaped Piezoceramic Elements for Transducer Design," *IEEE Transactions on Ultrasonics, Ferroelectrics and Frequency Control*, vol. 45, no. 4, pp. 1056-1064, 1998.
98. A. Iula, N. Lamberti, R. Carotenuto and M. Pappalardo, "A 3-D Model of the Classical Langevin Transducer," *IEEE Proceeding of Ultrasonics Symposium*, vol. 2, pp. 987-990, 1997.
99. D. Powell, G. Hayward and R. Ting, "Unidimensional Modeling of Multi-layered Piezoelectric Transducer Structures," *IEEE Transactions on Ultrasonics, Ferroelectrics and Frequency Control*, vol. 45, no. 3, pp. 667-677, 1998.
100. W. Mason, *Electromechanical Transducers and Wave Filters*, D. Van Nostrand Co., 1948.
101. A. Ballato, "Modeling Piezoelectric and Piezomagnetic Devices and Structures via Equivalent Networks," *IEEE Transactions on Ultrasonics, Ferroelectrics and Frequency Control*, vol. 48, no. 5, pp. 1189-1240, 2001.
102. P. Hagedorn and A. DasGupta, *Vibrations and Waves in Continuous Mechanical Systems*, John Wiley & Sons, Ltd, Chichester, UK, 2007.
103. R. Mahdavejad, "Finite Element Dimensional Design and Modeling of an Ultrasonic Transducer," *Iranian Journal of Science & Technology - Transaction B: Engineering*, vol. 29, 2005.
104. A. Mohammed, "Equivalent Circuits of Solid Horns Undergoing Longitudinal Vibrations," *Journal of Acoustical Society of America*, vol. 38, no. 5, pp. 862-866, 1964.
105. P. Edmonds, *Ultrasonics*, Academic Press, USA, 1981.

106. F. Arnold, L. Bravo-Roger, M. Goncalves and M. Grilo, "The Study of Piezoelectric Devices with Thevenin's Theorem," *IEEE proceedings of Global Engineering Education Conference*, pp. 846-849, 2011.
107. D. Ensminger and F. Stulen, *Ultrasonics: Data, Equations, and Their Practical Uses*, Taylor & Francis Group, USA, 2009.
108. S. Sherrit, P. Dolgin and Y. Bar-Cohen, "Modeling of Horns for Sonic/Ultrasonic Applications," *IEEE Proceedings of Ultrasonics Symposium*, vol. 1, pp. 647-651, 1999.
109. W. Mason, *Piezoelectric Crystals and thier Application in Ultrasonics*, D. van Nostrand Co. Inc., USA, 1950.
110. F. Arnold and S. Mühlen, "The Influence of the Thickness of Non-Piezoelectric Pieces on Pre-Stressed Piezotransducers," *Ultrasonics*, vol. 41, no. 3, pp. 191-196, 2003.
111. L. Shuyu, "Study of the Sandwiched Piezoelectric Ultrasonic Torsional Transducer," *Ultrasonics*, vol. 32, no. 6, pp. 461-465, 1994.
112. H. Yihua and H. Wei, "Modeling and Analysis of Circular Flexural-Vibration-Mode Piezoelectric Transformer," *IEEE Transactions on Ultrasonics, Ferroelectrics and Frequency Control*, vol. 57, no. 12, pp. 2764-2771, 2010.
113. J. Soderkvist, "Electric Equivalent Circuit for Flexural Vibrations in Piezoelectric Materials," *IEEE Transactions on Ultrasonics, Ferroelectrics and Frequency Control*, vol. 37, no. 6, pp. 577-586, 1990.
114. M. Castillo, P. Acevedo and E. Moreno, "KLM Model for Lossy Piezoelectric Transducers," *Ultrasonics*, vol. 41, no. 8, pp. 671-679, 2003.
115. M. O'Donnell, L. Busse and J. Miller, *1. Piezoelectric Transducers*, Edited by D. Peter, Academic Press, 1981.
116. T. Li, Y. Chen and J. Ma, "Development of a Miniaturized Piezoelectric Ultrasonic Transducer," *IEEE Transactions on Ultrasonics, Ferroelectrics and Frequency Control*, vol. 56, no. 3, pp. 649-659, 2009.
117. <http://www.mathportal.org/formulas/integrals/rational.php>, Accessed on 5th June 2012.
118. W. Beyer, *CRC Standard Mathematical Tables*, CRC Press, 1984.
119. L. Shuyu, "Effect of Electric Load Impedances on the Performance of Sandwich Piezoelectric Transducers," *IEEE Transactions on Ultrasonics, Ferroelectrics and Frequency Control*, vol. 51, no. 10, pp. 1280-1286, 2004.
120. L. Shuyu, "Analysis of Multifrequency Langevin Composite Ultrasonic Transducers," *IEEE Transactions on Ultrasonics, Ferroelectrics and Frequency Control*, vol. 56, no. 9, pp. 1990-1998, 2009.

121. R. Dahiya, M. Valle and L. Lorenzelli, "SPICE Model for Lossy Piezoelectric Polymers," *IEEE Transactions on Ultrasonics, Ferroelectrics and Frequency Control*, vol. 56, no. 2, pp. 387-395, 2009.
122. R. Holland, "Representation of Dielectric, Elastic, and Piezoelectric Losses by Complex Coefficients," *IEEE Transactions on Sonics and Ultrasonics*, vol. SU-14, no. 1, pp. 18-20, 1967.
123. L. Shuyu and Z. Fucheng, "Study of Vibrational Characteristics for Piezoelectric Sandwich Ultrasonic Transducers," *Ultrasonics*, vol. 32, no. 1, pp. 39-42, 1994.
124. T. Royston and B. Houston, "Modeling and Measurement of Nonlinear Dynamic Behavior in Piezoelectric Ceramics with Application to 1-3 Composites," *The Journal of the Acoustical Society of America*, vol. 104, no. 5, pp. 2814-2827, 1998.
125. D. Hall, "Review Nonlinearity in Piezoelectric Ceramics," *Journal of Materials Science*, vol. 36, no. 19, pp. 4575-4601, 2001.
126. K. Wing, H. Chan and C. Choy, "Evaluation of the Material Parameters of Piezoelectric Materials by Various Methods," *IEEE Transactions on Ultrasonics, Ferroelectrics and Frequency Control*, vol. 44, no. 4, pp. 733-742, 1997.
127. S. Sherrit, H. Wiederick, B. Mukherjee and M. Sayer, "An Accurate Equivalent Circuit for the Unloaded Piezoelectric Vibrator in the Thickness Mode," *Journal of Physics D: Applied Physics*, vol. 30, no. 16, pp. 2354-2363, 1997.
128. T. Jordan and Z. Ounaies, *Piezoelectric Ceramics Characterization*, National Aeronautics and Space Administration (NASA), 2001.
129. F. Arnold and S. Mühlen, "The Mechanical Pre-stressing in Ultrasonic Piezotransducers," *Ultrasonics*, vol. 39, no. 1, pp. 7-11, 2001.
130. F. Arnold and S. Mühlen, "The Resonance Frequencies on Mechanically Pre-stressed Ultrasonic Piezotransducers," *Ultrasonics*, vol. 39, no. 1, pp. 1-5, 2001.
131. Q. Zhang and Z. Jianzhong, "Electromechanical Properties of Lead Zirconate Titanate Piezoceramics Under the Influence of Mechanical Stresses," *IEEE Transactions on Ultrasonics, Ferroelectrics and Frequency Control*, vol. 46, no. 6, pp. 1518-1526, 1999.
132. L. Shuyu, "Load Characteristics of High Power Sandwich Piezoelectric Ultrasonic Transducers," *Ultrasonics*, vol. 43, no. 5, pp. 365-373, 2005.
133. APC International, Ltd., *Piezoelectric Ceramics: Principles and Applications*, USA, 2002.
134. C. Fung, *Ultrasonic Transducer Equipped with a Magnetolectric Sensor for Weld Quality Monitoring*, MSc. Thesis, The Hong Kong Polytechnic University, China, 2009.
135. CeramTec GmbH, *Materials for Power Converters*, Germany, 2011.
136. <http://www.futek.com/boltcalc.aspx?mode=metric>, Accessed on 27th July 2012.
137. <http://www.tohnichi.com/torque-technical-data.asp>, Accessed on 29th July 2012.

138. K. Budinski, "Tribological Properties of Titanium Alloys," *Wear*, vol. 151, pp. 203-217, 1991.
139. www.norbar.com, Accessed on 31st July 2012.
140. <http://www.cromwell.co.uk/>, Accessed on 31st July 2012.
141. <http://www.britool-expert.co.uk/>, Accessed on 31st July 2012.
142. <http://www.fluke.com/fluke/uken/home/default>, Accessed on 31st July 2012.
143. D. DeAngelis and G. Schulze, "Optimizing Piezoelectric Ceramic Thickness in Ultrasonic Transducers," *39th Annual Ultrasonic Industry Association Symposium*, pp. 1-9, 2010.
144. K. Brown, C. Morrow, S. Durbin and A. Baca, *Guideline for Bolt Joint Design and Analysis: Version 1.0*, Sandia National Laboratories, 2008.
145. C. Rajendra, *Analysis of Bolt Torquing*, PDH Center, 2012.
146. K. Park and J. Fernández, "3D Vibration Measurement Using One Laser Scanning Vibrometer (LSV)," *2nd National Conference of Metrology Society of India*, 2012.
147. W. Davis, "Measuring Quality Factor From a Nonlinear Frequency Response With Jump Discontinuities," *Journal of Microelectromechanical Systems*, vol. 20, no. 4, pp. 968-975, 2011.
148. R. Mackie, "Improving Finite Element Predictions of Modes of Vibration," *International Journal for Numerical Methods in Engineering*, vol. 33, no. 2, pp. 333-344, 2005.